

UNIVERSITY OF TWENTE

Simulating discharges and forecasting floods using a conceptual rainfall-runoff model for the Bolivian Mamoré basin

Master thesis of Civil Engineering and Management

W.H. Maat
March 2015



UNIVERSITEIT TWENTE.

Title: Simulating discharges and forecasting floods for the Bolivian Mamoré basin

Thesis for the degree of Master of Science in Civil Engineering and Management

Author: Wouter Hendrik Maat
w.h.maat@gmail.com

Institute: University of Twente
Water Engineering and Management

Graduation committee: Dr. ir. D.C.M. Augustijn
University of Twente, Department of Water Engineering and Management

Dr. ir. M.J. Booij
University of Twente, Department of Water Engineering and Management

Date: March, 2015

Title page image: Picture of a farm in an area in Bolivia during the floods of February 2014. which slowly disappears in the water. This picture is taken on 13 February by ir. R Huting. Since that date the water rose over 40 cm.

Summary

Flood protection and awareness have continued to rise on the political agenda over the last decade accompanied by a drive to improve flood forecasts. Operational flood forecasting systems form a key part of 'preparedness' strategies for disastrous flood events by providing early warnings several days ahead giving flood forecasting services, civil protection authorities and the public adequate preparation time and thus reducing the impacts of the flooding.

The River Mamoré in Bolivia, a major tributary of the Amazon, floods annually causing considerable damage, especially to cattle ranches and villages in the area. To limit the effects of flooding in Bolivia the Bolivian Vice-Ministry for Water Management and the Dutch Embassy together initiated the program 'Vivir con el Agua' (living with water). A part of the program is to set up a Flood Early Warning System, FEWS, which will warn inhabitants of any flood danger and give them time to take measures to limit the damage. This FEWS-project in Bolivia is being carried out by the consortium including RoyalHaskoningDHV, Deltares and the local organization Centro Agua Bolivia. During the FEWS project in Bolivia the curiosity arose how a semi-distributed hydrological model like HBV will perform in forecasting the discharge in this basin area, instead of the physically-based, distributed parameter, basin hydrological model TOPOG, used in the project.

The goal of this research is to set up and evaluate the hydrological HBV-model to simulate discharges and forecast floods of the Mamoré River at the city of Trinidad, a city in Bolivia which suffer from the annual floods.

A data analysis is executed to select the meteorological stations which are used in the research to determine the input data and to determine the sub basins with corresponding discharge stations. This data analysis showed that the Mamoré basin for this study should be divided into two sub basins: upstream sub basin Grande with outlet at discharge station Abapó and downstream sub basin Mamoré with outlet at discharge station Camiaco.

In the model calibration procedure the objective function Y of sub basin Grande is a combination of the well-known Nash-Sutcliffe coefficient and Relative Volume error and the objective function of sub basin Mamoré is the Nash-Sutcliffe coefficient for high flows NS_H , both with an optimum value of 1. The parameters for which the objective functions are the most sensitive, for both sub basins separately, are used for the final calibration step to obtain the sets of the optimum parameter values.

The calibrated model is run for the validation period and sub basin Grande showed an improvement in performance in terms of the objective function with an Y value of 0.39 for the calibration period and an Y value of 0.54 for the validation period. The performance for sub basin Mamoré decreased in terms of the NS_H values from 0.72 to 0.51 for the calibration period and validation period respectively.

For flood forecasting, the optimized parameter set obtained during the calibration process is used to forecast the discharge for the validation period for 1 up to 10 days ahead, using perfect weather 'forecasts' in the absence of historical weather forecasts. By following an updating procedure the observations of the state of the basin up to the current time are used for the forecasting to improve the model prediction performance.

The forecasted discharges of 1 up to 10 days ahead performed quite well considering the overall accuracy. The NS_H values of the forecasts lie between 0.99 for one day ahead and 0.69 for 10 days ahead. These performances are an improvement compared to the performance of the simulated discharges, which had a NS_H value of 0.51.

Next to the objective function value, the evaluation of the performance of the forecasted discharges are based on contingency tables, which show the total number of hits (an event occurred and the event was forecasted), misses (an event occurred, but the event was not forecasted), false-alarms (an event did not occur, but an event was forecasted) and correct rejections (an event did not occur and an event was not forecasted) for four different events for the validation period. Two types of events are taken into account in this study for two different thresholds; a high water level threshold and a flood level threshold:

- Event type 1: *'the exceedance of a discharge threshold at time step t'*
- Event type 2: *'the exceedance of a discharge threshold at time step t, with the condition that at time step t-1 this threshold was not exceeded'.*

The accuracies A of the forecasts up to 10 days ahead ($A \geq 0.94$) are at least higher than the accuracies of the simulated discharges in forecasting event type 1 for the high water level and the flood level threshold. Accuracy A has a value between 0 and 1, with 1 as optimum value, thus the performance of the forecasts in terms of accuracy are considered as good for the event type 1.

The skill of the model in forecasting high water and flood levels up to 10 days ahead in terms of False-alarm rates F is better than the skill of the model in simulating high water and flood levels. Partly due to the high number of correct rejections the false-alarm rates F , which have a value between 0 and 1, of the forecasts are ≤ 0.02 . The skill of the model in forecasting high water and flood levels up to 10 days ahead in terms of hit rate H are decreasing as the forecasting days ahead are increasing. Nevertheless, hit rates H of the high water level of the forecasts up to 7 days ahead are higher than the hit rate of the simulated discharges and the hit rates H of the flood level of the forecasts up to 3 days ahead are higher than the hit rate of the simulated discharges. At least the forecasts up to 3 days ahead perform well in terms of skill for the event type 1 for both thresholds.

The reliability of the forecasts up to 10 days ahead for event type 1 in terms of the probability of a correct warning H' is high ($H' \geq 0.92$) for the high water and flood level threshold. The reliabilities of simulated discharges are 0.76 and 0.79 for the high water level and the flood level respectively. These values are much higher than the base rates, which has a value of 0.31 and 0.19 for the high water level and the flood level respectively. The reliability of the forecasts up to 10 days ahead for event type 1 in terms of probability of an incorrect non-warning (miss rate F'), decreases sharply as the forecasting days ahead are increasing for the high water and flood level thresholds. This is not directly visible in the miss rate F' , because the number of correct rejections is high.

The contingency tables of event type 2 show that the performance of the forecasts is very poor for the high water and flood level thresholds. Event type 2 is the start of a high water or flood period. In the validation period, 6 high water periods and 2 flood periods occurred. Out of all the 80 events (2 events for flood threshold plus 6 events for high water threshold times 10 forecasts) the model was able to forecast 2 events and missed 78 events. Due to the small number of event (and thus the small

number of hits and misses) and the large number of correct rejections the evaluation in terms of accuracy, skill and reliability is not meaningful.

In conclusion, the overall accuracy of the forecasts increase as the prediction days decrease and is higher than accuracy of the simulated discharges. The accuracy, skill and reliability of the forecasts up to 3 days ahead of event type 1 are higher than the simulated discharges for both the high water and flood level. However, as a decision maker, you are also interested in ability of a model to forecast the start of a high water or flood level threshold exceedance, event type 2. This to give a high water or flood warning to the people in the area, so they are able to evacuate and limit the flood damage. Unfortunately, the model is barely able to forecast and simulate events of type 2 for both high water and flood level thresholds.

Preface

In this document I present the findings of my Master's thesis, the final product of my master Civil Engineering and Management, with a specialization in Water Engineering and Management, at the University of Twente. The goal of this research was to set up a hydrological model to simulate and forecast discharges of the Mamoré River in Bolivia. From the first steps towards a research proposal till now, I have learned a lot. I improved my modelling and analytical skills and I am more experienced in software programs Matlab and QGIS.

First of all, I would also like to thank Ric of Royal HaskoningDHV and my UT supervisors Denie and Martijn. Ric, thank you for making this research possible by initiating the research subject and providing literature of the study area and the input data of the model. Denie and Martijn, thanks for your critical and detailed feedback on my work and for providing me the motivation with fresh ideas during each meeting we had. Martijn, you always advised me when I had trouble with the HBV model or Matlab and you gave me useful tips for relevant literature. Denie, you helped me to keep the big picture in mind by proposing critical questions during our meetings and in your feedback.

Further, I would like to thank my former roommate Wouter Knoben for supplying the Matlab scripts of the HBV model and helping me out with the set up. Besides Wouter, I would like to thank all my present and former roommates of the WEM graduation room for the motivation, lunch walks, inspiration, feedback and discussions.

My final word of thanks I would like to give to my girlfriend Pauline and my parents. I am thankful for their support, their listening, their belief in me, their patience and their love. Without you, it would have been much more difficult to complete this master thesis and my education as a whole. Thank you all very much!

Wouter Maat

Enschede, March 2015

Contents

Summary	4
Preface.....	8
Contents	10
List of Tables.....	12
List of Figures.....	14
1 Introduction.....	18
1.1 Background.....	18
1.2 Problem description	18
1.3 Objective and research questions	19
1.4 Research model and reading guide	20
2 Study area and data.....	22
2.1 Study area.....	22
2.2 Data availability for calibration and validation period	24
2.2.1 Meteorological input data.....	24
2.2.2 Discharge stations	25
3 Methodology	28
3.1 HBV model.....	28
3.1.1 Model structure and applications	28
3.1.2 Model routines	29
3.1.3 Model parameters.....	31
3.1.4 Connection sub basins.....	32
3.1.5 Reservoir.....	34
3.2 Calibration and validation	35
3.2.1 Selection of parameter ranges	36
3.2.2 Calibration and validation period.....	36
3.2.3 Selection of objective functions	37
3.2.4 Selection of calibration parameters	39
3.2.5 Validation procedure.....	40
3.3 Forecasting	40
3.3.1 Updating.....	40
3.3.2 Evaluation of forecasting.....	42
4 Results & Discussion.....	46
4.1 First calibration step.....	46

4.2	Sensitivity analysis	48
4.3	Final calibration step	50
4.4	Validation	55
4.5	Forecasting	57
4.5.1	Reference run	57
4.5.2	Forecasting	59
5	Conclusions and recommendations	64
5.1	Conclusions.....	64
5.2	Recommendations.....	66
	References.....	70
	Appendix A: Data analysis	74
	Discharge stations	74
	Meteorological stations.....	76
	Appendix B: Areal mean precipitation: 4 different approaches	78
	1. +10%/ 100m - approach	78
	2. Correction factor per sub basin - approach	79
	3. Correction factor per Thiessen polygon – approach	79
	4. No correction factor - approach.....	80
	From 3 to 2 sub basins.....	81
	Appendix C.....	82

List of Tables

- Table 2.1: Areas of the sub-basins and the cumulative area of the total study area [QGIS data provided by Centro Agua Bolivia; Rodal, 2008]
- Table 3.1: Overview of the eight model parameters with their descriptions and units.
- Table 3.2: Ranges of the model parameters which are used in calibration process. Source: ¹Demirel et al.(2013), ²Uhlenbrook et al. (1999), ³Deckers et al. (2010), ⁴Lidén and Harlin (2000), ⁵Knoben (2014). The range values with * are adjusted values of that source.
- Table 3.3: Two-by-two contingency table for the assessment of a threshold based forecasts
- Table 4.1: Number of runs of the total of 100,000 runs, which satisfy criterion (1) an objective function value of the above 0 and (2) both criterion (1) and a k_{F-eff} value larger than the k_s -value. Between brackets the corresponding percentages of the total number of runs.
- Table 4.2: Results of the parameter ranges of 1st calibration of Grande for parameters sets with a Y -value >0 and >0.2 .
- Table 4.3: Results of the parameter ranges of 1st calibration of Mamore for parameters sets with a NS_H -value >0 and >0.5 .
- Table 4.4: Parameter values of the optimum parameter set after the 1st calibration and the corresponding objective function values of Grande and Mamoré.
- Table 4.5: Parameter values of the optimum parameter sets after the calibration and the corresponding objective function values of Grande and Mamoré.
- Table 4.6: Values of the objective functions of Mamore with simulated discharge of Grande as input into the Mamore basin.
- Table 4.7: Results Validation of Grande and Mamoré basins.
- Table 4.8: Logarithmic equation of the trendlines of figure 20, figure 21 and figure 22 with the corresponding value of R-squared.
- Table 4.9: Results of the updating procedure of forecasted discharges 1 to 10 days ahead in terms of objective functions with as reference the not-updated simulated discharge.
- Table 4.10: Contingency tables (with number of hits h , number of misses m , number of false-alarms f and number of correct rejections c) of the 1 up to 10 days ahead forecasted discharges and the reference simulated discharges and their accuracy A , hit rates H , false-alarm rates F , hit ratios H' , miss rate F' and the base rate B of the event type 1 with threshold of $3,000 \text{ m}^3/\text{s}$ for the validation period.
- Table 4.11: Contingency tables (with number of hits h , number of misses m , number of false-alarms f and number of correct rejections c) of the 1 up to 10 days ahead forecasted discharges and the reference simulated discharges and their accuracy A , hit rates H , false-alarm rates F , hit ratios H' , miss rate F' and the base rate B of the event type 1 with threshold of $3,900 \text{ m}^3/\text{s}$ for the validation period.
- Table 4.12: Contingency tables (with number of hits h , number of misses m , number of false-alarms f and number of correct rejections c) of the 1 up to 10 days ahead forecasted discharges and the reference simulated discharges and their accuracy A , hit rates H , false-alarm rates F , hit ratios H' , miss rate F' and the base rate B of the event type 2 with threshold of $3,000 \text{ m}^3/\text{s}$ for the validation period.
- Table 4.13: Contingency tables (with number of hits h , number of misses m , number of false-alarms f and number of correct rejections c) of the 1 up to 10 days ahead forecasted

discharges and the reference simulated discharges and their accuracy A , hit rates H , false-alarm rates F , hit ratios H' , miss rate F' and the base rate B of the event type 2 with threshold of $3,900 \text{ m}^3/\text{s}$ for the validation period.

Table A.1: Overview of the names of the discharge stations of the Mamoré River basin, their ID and the years when records were made.

List of Figures

- Figure 1.1: Map of Bolivia with the inundated area of the 2007 floods [QGIS data provided by Centro Agua Bolivia].
- Figure 1.2: Schematization of the research model of this study; step 1 is represented in blue, step 2 in green and step 3 in orange.
- Figure 2.1: Elevation map of Bolivia with the borders of the Mamoré River basin on the left and the Amazon basin with its tributaries including Madeira and Mamoré on the right [QGIS data provided by Centro Agua Bolivia].
- Figure 2.2: Average daily mean temperature and monthly mean precipitation by month measured from 1972-1996 for Trinidad [Centro de Investigaciones Fitosociológicas, 2012]
- Figure 2.3: Annual mean temperature zones of the Mamoré River basin the Mamoré [QGIS data provided by Centro Agua Bolivia].
- Figure 2.4: Annual mean precipitation lines of River basin [QGIS data provided by Centro Agua Bolivia].
- Figure 2.5: The locations of the major basin areas of Bolivia with the Mamoré River basin as a sub basin of the Amazon basin and the Mamoré River with its main tributaries [QGIS data provided by Centro Agua Bolivia].
- Figure 2.6: Climate classification of Bolivia according to Köppen-Geiger [Peel et al.,2007]
- Figure 2.7: Map of the Mamoré River basin, Mamoré River and tributaries, sub basins and their discharge stations, Meteorological measuring stations and the main cities of Bolivia.
- Figure 3.1: Schematization of the HBV model used in this study with in red the eight model parameters, the arrows represent the fluxes, the three black outlined boxes represent the three model routines used in this study. The two green boxes are the model input and the red box is the model output.
- Figure 3.2: Correlation between observed discharge of Grande and Mamoré with in red the highest correlation with a lag time of 17 days.
- Figure 3.3: 'Water Displacement' of the Mamoré river with on the horizontal axis distance [km] and on the vertical axis time [days] [source: Rodal, 2008].
- Figure 3.4: Map of total basin Mamoré, with the sub basin Mamoré, sub basin Grande, trace of the river main Mamoré and main river Grande.
- Figure 3.5: Hydrographs of the calibration and validation period of sub basins Grande and Mamoré.
- Figure 4.1: Scatter plot of Y -values as a function of parameter values for the Grande for the 1st calibration step. Only Y -values above 0 are shown.
- Figure 4.2: Scatter plot of NS_H values as a function of parameter values for the Mamoré for the 1st calibration step. Only Y -values above 0 are shown.
- Figure 4.3: Hydrograph of the observed (green) and simulated (blue) discharge after the 1st calibration.
- Figure 4.4: Hydrograph of Mamore of the observed discharge, simulated discharge, observed discharge of Grande and storage of the reservoir after the first calibration.
- Figure 4.5: Results of the sensitivity analysis of the 8 parameters of sub basin Grande.
- Figure 4.6: Results of the sensitivity analysis of the 8 parameters of sub basin Mamore.
- Figure 4.7: Scatter plot of Y -values as a function of parameter values for the Grande for the final calibration step. Only Y -values above 0 are shown.
- Figure 4.8: Scatter plot of NS_H values as a function of parameter values for the Mamoré for the final calibration step. Only NS_H -values above 0 are shown.
- Figure 4.9: Hydrograph of the observed Q_{obs} and simulated discharge Q_{sim} of Grande after the final calibration.
- Figure 4.10: Hydrograph of Mamore of the observed discharge, simulated discharge, observed discharge of Grande and storage of the reservoir after the calibration.

- Figure 4.11: Hydrograph of Mamore of the observed discharge, simulated discharge, simulated discharge of Grande and storage of the reservoir after the calibration.
- Figure 4.12: Hydrograph of the discharge of sub basin Grande after validation.
- Figure 4.13: Hydrograph of Mamore of the observed discharge, simulated discharge, simulated discharge of Grande and storage of the reservoir after the validation.
- Figure 4.14: The fractions of fast runoff q_f of the discharge q_{simM} to the discharge q_{simM} for each time step (blue dots) and the trendline in black through those points.
- Figure 4.15: The fractions of slow runoff q_s of the discharge q_{simM} to the discharge q_{simM} for each time step (blue dots) and the trendline in black through those points.
- Figure 4.16: The fractions of outflow of the reservoir q_R of the discharge q_{simM} to the discharge q_{simM} for each time step (blue dots) and the trendline in black through those points.
- Figure 4.17: Results of the updating procedure with forecasted discharges of 3, 6 and 10 days ahead.
- Figure A.1: Map of the Mamoré River basin, the Mamoré River, the inundated area of the 2007 floods and the locations of the discharge stations and main cities of Bolivia [QGIS data provided by Centro Agua Bolivia].
- Figure A.2: Map of Bolivia with the Mamoré River basin, Mamoré River, sub basins and their discharge stations and main cities of Bolivia. The pink area is the sub basin Grande with discharge station Apabo, the yellow area is sub basin Ichilo with discharge station Puerto Villarroel and the purple area is sub basin Rio Mamore with discharge station Camiaco.
- Figure A.3: Map of Mamoré River basin, Mamoré River, the locations of the discharge stations of the three sub basins, the locations of the hydrological stations in Bolivia and the main cities of Bolivia [QGIS data provided by Centro Agua Bolivia].

1 Introduction

This chapter introduces the topic of flood forecasting and hydrological modelling and gives an overview of this study. Section 1.1 presents some background of flood forecasting. Section 1.2 describes the flood problem in Bolivia and introduces the hydrological model used in this research. Section 1.3 defines the research goal and the research questions of this study. The research strategy and the research model are presented in Section 1.4 presents the research strategy, the research model and an overview of the research that counts as reading guide of this report.

1.1 Background

Flood protection and awareness have continued to rise on the political agenda over the last decade accompanied by a drive to improve flood forecasts. Operational flood forecasting systems form a key part of ‘preparedness’ strategies for disastrous flood events by providing early warnings several days ahead [De Roo et al., 2003; Patrick, 2002; Werner, 2005] giving flood forecasting services, civil protection authorities and the public adequate preparation time and thus reducing the impacts of the flooding [Penning-Rowsell et al., 2000; Cloke et al., 2009].

1.2 Problem description

The River Mamoré in Bolivia, a major tributary of the Amazon, floods annually causing considerable damage, especially to cattle ranches and villages in the area. In particular the floods of 2007 and 2008, due to heavy rains, caused a lot of damage and affected an estimated 350,000 people [Grant, 2007] and inundated $62.7 \cdot 10^3 \text{ km}^2$, see figure 1.1, of the area of the Mamoré River basin [Ministerio de Desarrollo Rural Agropecuario y Medio Ambiente, 2007]. More recently, in February 2014 a major flood occurred in the largest department of Bolivia, Beni, in the North of Bolivia.

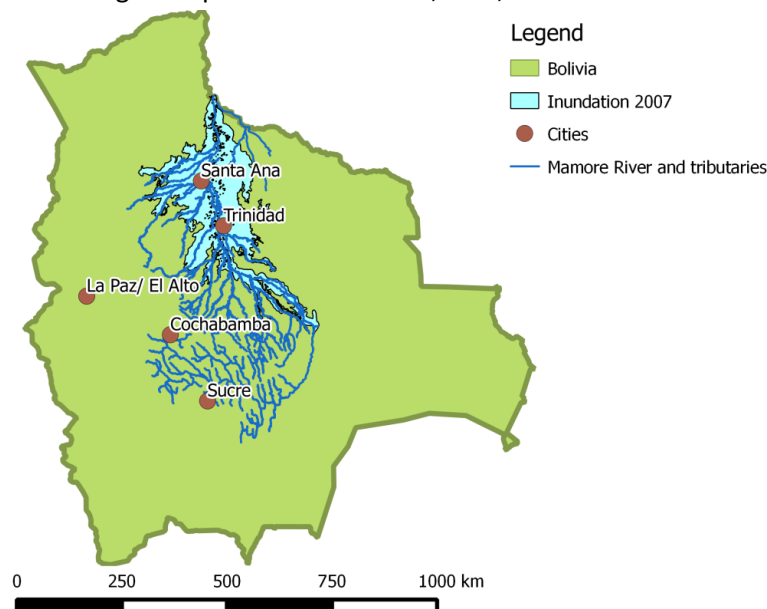


Figure 1.1: Map of Bolivia with the inundated area of the 2007 floods [QGIS data provided by Centro Agua Bolivia].

To limit the effects of flooding in Bolivia the Bolivian Vice-Minister for Water Management and the Dutch Embassy together initiated the program ‘Vivir con el Agua’ (living with water). A part of the program is to set up a Flood Early Warning System (FEWS) which will warn inhabitants of any flood

danger and give them time to take measures to limit the damage. A FEWS is a complex system which can be described, following The United Nations Office for Disaster Risk Reduction [UNISDR, 2007], as:

The set of capacities needed to generate and disseminate timely and meaningful flood warning information to enable individuals, communities and organizations threatened by a hazard to prepare and to act appropriately and in sufficient time to reduce the possibility of harm or loss.

FEWS is more than a forecasting tool and although FEWS evaluations have focused on the accuracy of hazard predictions, many researchers have recently argued that FEWS's success should be seen in terms of the impact of flood warnings on reducing damages [Molinari et al., 2013]. In order to evaluate FEWS' capacity to reduce damages, flood forecasting systems performance must be evaluated as well, because expected damages vary along with the warning outcomes.

This FEWS-project in Bolivia has been carried out by the consortium Witteveen+Bos (secretary), Royal HaskoningDHV, Deltares and the local organization Centro Agua Bolivia. The hydrological modeling framework wFlow [Schellekens, 2013] is being used for the Mamore River Basin. The model consists of 2 modules: a distributed hydrological model and the wflow_floodmap module which generates flood maps from the output of the hydrological model. In the Mamoré River basin project the wFlow_SBM model will be used as distributed hydrological model and input for the floodmap module [Deltares, 2012]. The wFlow_SBM is based on the hydrological tool TOPOG [Silberstein, 1999]. TOPOG is a physically-based, distributed parameter, hydrological model. The wflow_SBM model is used to simulate discharges at several locations of the river Rhine [Schellekens, 2013].

During the FEWS project in Bolivia the curiosity arose how a semi-distributed hydrological model like HBV [Lindström et al, 1997] will perform in forecasting the discharge in this basin area. Partly due to the knowledge of and experience with the HBV-model within the Water Engineering and Management department of the University of Twente, the decision was made to use the HBV model for forecasting discharges in the Mamoré River basin as well.

The HBV-model is a conceptual rainfall-runoff (CRR) model which uses daily precipitation, daily mean temperature and potential evapotranspiration as input and daily discharge as output. A large number of applications, under various physiographic and climatological conditions, has shown that its structure is very robust and surprisingly general, in spite of its relative simplicity [Seibert, 1999; Lidén et al., 2000].

CRR models are normally run with point values of precipitation as primary input data and produce mean basin values of actual evapotranspiration, soil-moisture, runoff generation etc. In regions where precipitation data series are available but runoff data are scarce, CRR models are essential tools. This is a common situation in many developing countries, countries with a large need of developing their infrastructure and water resources, like Bolivia. In the past, only for a small basin in Bolivia, Locotal, the HBV-model has been used in a study for discharge simulation [Lidén et al., 2000].

1.3 Objective and research questions

The aim of this research is *to set up and evaluate the hydrological HBV-model to simulate discharges and forecast floods of the Mamoré River at the city of Trinidad*. This to be able to warn the people in the area when Mamoré River water level will reach alarming levels at Trinidad, so the people can evacuate and take action to limit the flood damage.

To achieve the research objective the following questions need to be answered within this research:

1. *What is the best HBV configuration for the Mamoré River basin given the available data?*
2. *How well does the HBV-model perform in simulating discharges with the available data for the Mamoré River basin?*
3. *How well does the HBV model perform in forecasting floods of the Mamoré River at Trinidad?*

1.4 Research model and reading guide

To fulfil the research goal and to answer the research questions the following steps need to be executed.

Step 1: This study starts with analyses of the data and the study area. This in order to obtain the input data for the HBV model and to determine the sub basins. After these analyses, the HBV-model is set up by the selection of the model routines and connection of the sub basins. This is done with the knowledge from previous research in the literature and the provided data from the Bolivian partners within the consortium. When the HBV model is set up, the optimum parameter set values are determined for each sub basin. This is done by the execution of a calibration procedure. This procedure starts with the selection of the model parameters to be calibrated and from previous research the parameter value ranges are obtained. Then the calibration period and validation period are defined and for both sub basins separately, the objective functions are selected and the first calibration run is executed. With the outcome of the first calibration step, a sensitivity analysis is executed in order to select the parameters for which the model objective function is most sensitive. The sensitivity analysis is executed for each sub basin separately. The parameters for which the model is most sensitive are calibrated in the second and final calibration step where parameters for which the model is less sensitive have default values.

Step 2: After the final calibration step, the optimum parameter set is obtained and the model is run for the validation period in order to see how well the model performs for another period.

Step 3: When the calibration and validation procedures are finished, the forecasting procedure is executed. From the final calibration run empirical relations are obtained of the fast and slow components of the total runoff. These empirical relations are used for updating the model storages in the forecasting procedure. The results of the forecasting procedure are discussed by comparing discharges of the forecasting days 1 to 10 days ahead and by comparing them with the simulated discharges.

When the three steps are executed, conclusions are drawn and recommendations for further research are given.

The structure of the steps described above is shown in the schematization of figure 1.2.

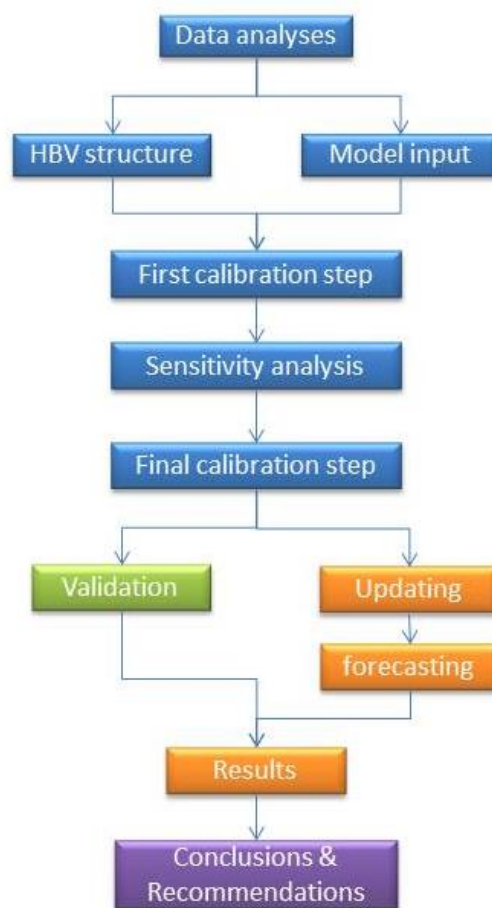


Figure 1.2: Schematization of the research model of this study; step 1 is represented in blue, step 2 in green and step 3 in orange.

Chapter 2 contains a description of the study area and a data analysis. In chapter 3 of this report the research methodology is described including the choices for the HBV model, the consecutive steps of the calibration procedure, validation and forecasting procedure. The results are presented in chapter 4 together with some discussion of the results. Finally, in chapter 5 the answers to the research questions are given by the conclusions together with recommendations for further research.

2 Study area and data

This chapter contains a description of the study area, section 2.1, and a data analysis in section 2.2.

2.1 Study area

Location and topography

The Mamoré River basin is located in Bolivia and for a small part in Brazil, within latitudes -10° to -20° S and longitudes within -62° to -66° W. The Mamoré River drains to the Madeira River, a tributary of the Amazon River, on the Brazilian-Bolivian border in the North of Bolivia. The Mamoré River basin drains an area of approximately $240 \cdot 10^3 \text{ km}^2$, which is in the same order of magnitude as the Rhine basin, covering about a quarter of the area of Bolivia. The elevation of the Mamoré River basin ranges from $\pm 4500 \text{ m}$ in the southwest at the edge of the Bolivian plateau to 110 m at the confluence with the Madeira River in the North.

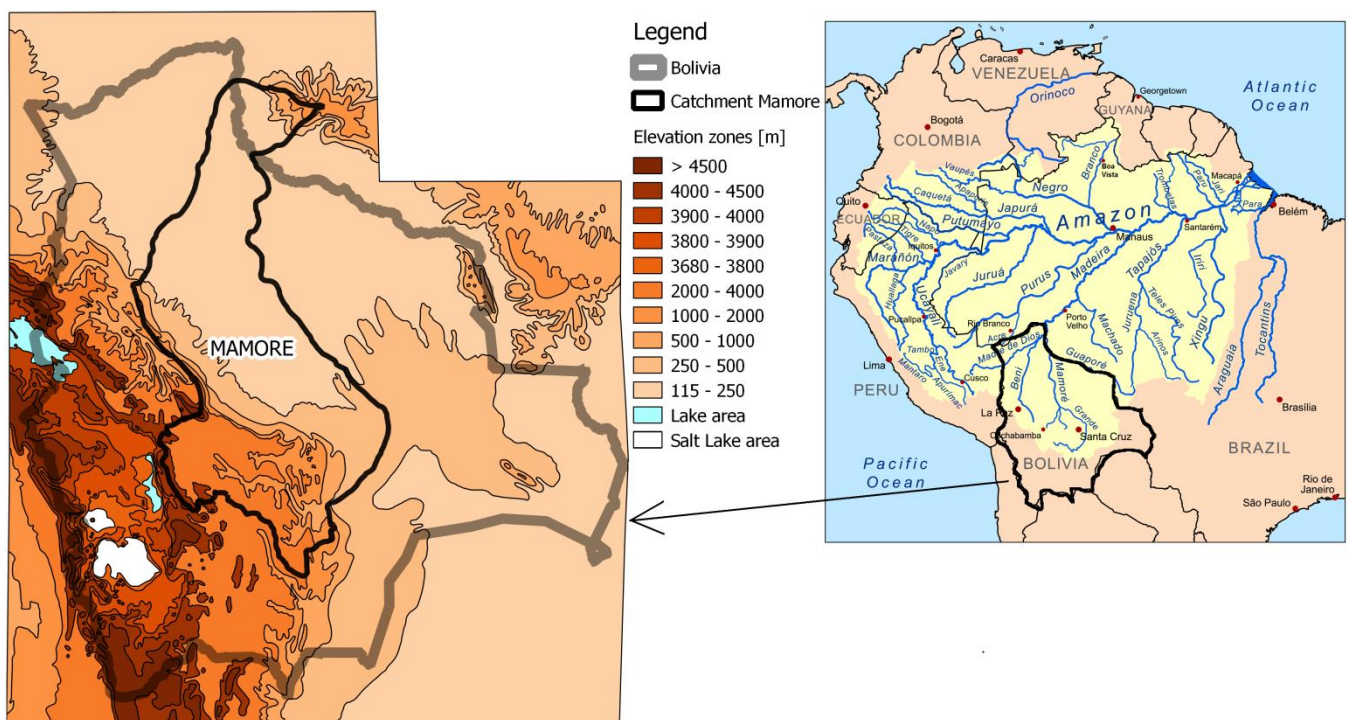


Figure 2.1: Elevation map of Bolivia with the borders of the Mamoré River basin on the left and the Amazon basin with its tributaries including Madeira and Mamoré on the right [QGIS data provided by Centro Agua Bolivia].

Climate

The climate regime in the Mamoré River basin varies from a tropical to semi-arid climate according to the Köppen-Geiger climate classification [Peel et al., 2007], see figure 2.6. One of the main cities in the basin area is Trinidad (for location, see figure 2.7) with an annual mean precipitation of 1914 mm and a mean temperature of 25.5°C . The fluctuations in temperature are low. A wet season from November till March is distinguished (see figure 2.2). The annual mean temperatures vary from 10°C in the southwest close to the plateau to 27°C in the north of the basin. With an exception of a small region near the plateau, the annual mean temperature of the basin is above 20°C , shown in figure 2.3. The annual mean precipitation varies from 500 mm/year in the south to $>5000 \text{ mm/year}$ in the middle of the basin, as seen in figure 2.4.

Hydrology

The Mamoré River basin is a sub basin of the Amazon basin. South of the Mamoré basin, the Del Plato basin is located and to the west is the Altiplano basin, see figure 2.5. Although the size of the basin is similar to the Rhine basin, the annual average discharge of the Mamoré River is over five times larger, namely $11 \cdot 10^3 \text{ m}^3/\text{s}$. The Mamoré River is a meandering river with many tributaries of which the largest one is the Rio Grande which lays in the southern part of the basin area.

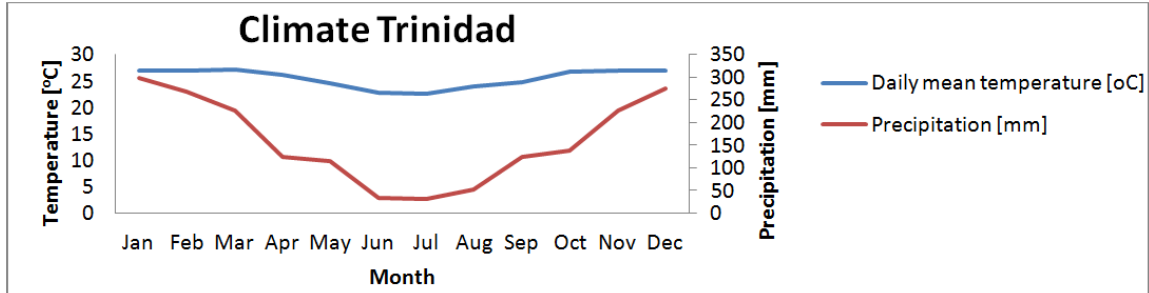


Figure 2.2: Average daily mean temperature and monthly mean precipitation for the period 1972-1996 for Trinidad [Centro de Investigaciones Fitosociológicas, 2012]

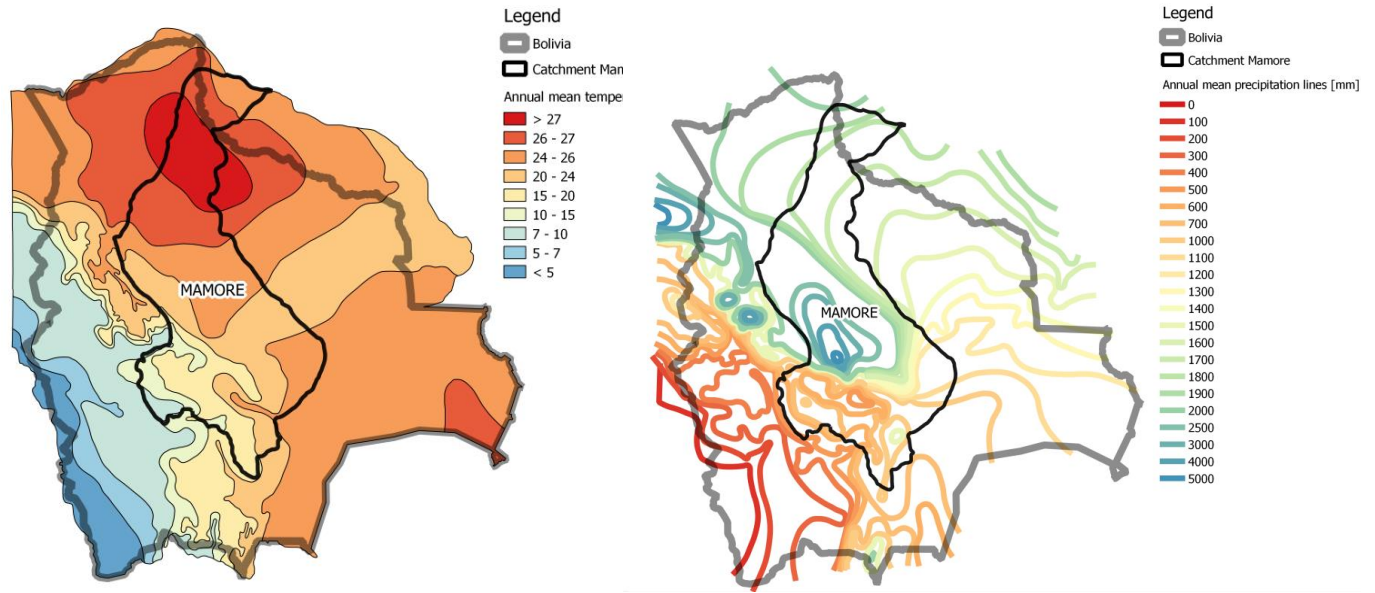


Figure 2.3: Annual mean temperature zones of the Mamoré River basin [QGIS data provided by Centro Agua Bolivia].

Figure 2.4: Annual mean precipitation lines of River Mamoré basin [QGIS data provided by Centro Agua Bolivia].

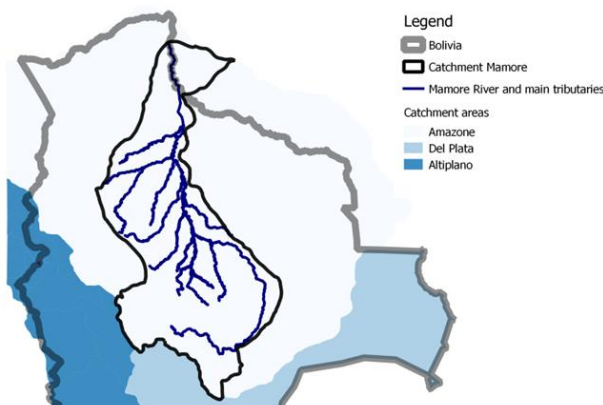


Figure 2.5: The locations of the major catchment areas of Bolivia with the Mamoré River basin as a sub basin of the Amazon basin and the Mamoré River with its main tributaries [QGIS data provided by Centro Agua Bolivia].

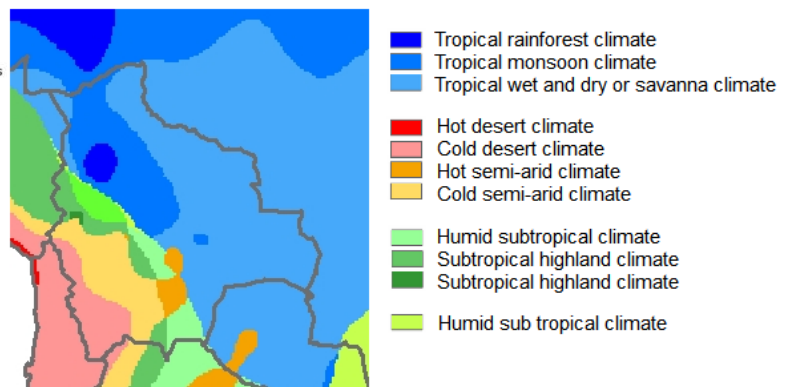


Figure 2.6: Climate classification of Bolivia according to Köppen-Geiger [Peel et al., 2007]

2.2 Data availability for calibration and validation period

Hydrological simulations and forecasts rely on observations of meteorological gauging stations within or near the basin under investigation and observations of discharge measure stations. To be able to run the HBV model in the Mamoré River basin, observed measurements of precipitation and estimates of potential evapotranspiration are necessary input variables. Observations of discharge measuring stations are necessary to compare the simulated discharges with the observed discharges for the calibration and validation procedure. The observations need to be a continuous period as long as possible to be able to define a calibration and a validation period

2.2.1 Meteorological input data

2.2.1.1 Precipitation

Daily values of precipitation have been obtained from meteorological stations within or in the vicinity of the river basin (see Appendix A) for the period of 1950 till 2013. The obtained data than have to be inter- and extrapolated on a spatial raster over the entire basin to generate a areal mean value. Given the available data, Thiessen polygons are used to obtain the areal mean value of precipitation. Appendix A shows that the meteorological stations are unevenly distributed over the basin area and section 2.1 shows that the Mamoré basin is a very diverse area concerning annual mean precipitation, elevation and climate. Therefore, an analysis is executed to find an appropriate approach to calculate the areal mean precipitation, see Appendix B.

2.2.1.2 Potential evapotranspiration

There is a wealth of methods for estimating the potential evapotranspiration et_p [mm]. Overviews of many of these methods can be found in the literature [Brutsaert, 1982; Jensen et al., 1990; Xu and Singh, 2001]. These methods can be classified into several categories, including: empirical, radiation based, temperature based, mass transfer and combination methods. The combination method [Penman, 1948] is usually considered as the most physically satisfying one by many hydrologists [Jensen et al., 1990; Shuttleworth, 1993; Beven, 2001; Lindström et al., 1997; Oudin et al., 2005]. This approach delivers a direct estimate for potential evapotranspiration, but demands detailed measurements of temperature, relative humidity, incoming global radiation, wind speed and sunshine duration [Gurtz et al., 1999]. However, data analysis shows that the meteorological stations only recorded daily temperature and precipitation, so a temperature-based method for estimating the et_p can be used in this research. Given the available data, the temperature-based Thornthwaite method to estimate et_p is used in this research and is described below.

Thornthwaite method

The Thornthwaite method [1948] is widely used for estimating potential evapotranspiration based on mean monthly temperature [Xu and Singh, 2001]. The method is based on an empirical relationship between potential evapotranspiration and the mean air temperature. While this method is not the most accurate one, and may lack theoretical basis, it can provide reasonably accurate estimates of potential evapotranspiration [Kang et al., 1999].

$$et_p = 0 \quad \text{if } T < 0^\circ\text{C} \quad (2.1)$$

$$et_p = 16L_d \left(\frac{10T_j}{I} \right)^a \quad \text{if } T \geq 0^\circ\text{C} \quad (2.2)$$

Where et_p is the monthly et_p [mm];

L_d is the daytime length, it is time from sunrise to sunset in multiples of 12 hours;

T_j is the monthly mean air temperature [°C] obtained by Thiessen polygons, using the same measuring stations used to obtain the areal mean precipitation;

$$a = 67.5 * 10^{-8}I^3 - 77.1 * 10^{-6}I^2 + 0.0179I + 0.49239;$$

and I is the annual heat index, which is computed from the monthly heat indices:

$$I = \sum_{j=1}^{12} i_j \quad (2.3)$$

Where i_j is computed as

$$i_j = \left(\frac{T_j}{5}\right)^{1.514} \quad (2.4)$$

In which i is the monthly heat index for month j ,

T_j is the mean monthly air temperature [°C] and

j is the number of months (1,...,12)

2.2.2 Discharge stations

The Mamoré River basin is a rather large basin area, so it is desirable to divide the basin into several sub basins. The Mamoré River basin can be divided into 3 sub-basins: Ichilo basin with outflow at Puerto Villarroel, Grande basin with outflow at Apabó and Rio Mamoré, with outflow at Camiaco, see Appendix A. The focus of this research is on about half the area of the Mamoré River basin ($240 * 10^3 \text{ km}^2$), see table 2.1. Data of these discharge stations is available for the period 7-8-2001 to 7-5-2009.

The city of Trinidad, which is a major city in Bolivia, was affected by the 2007 floods, see figures 2.1 and A.1. Long term data sets of observed discharges by discharge measuring stations at Trinidad are absent. Therefore, the simulation and forecasts of discharges at Camiaco, which is about 50 km upstream of the city of Trinidad, is the goal of this research.

Table 2.1: Areas of the sub-basins and the cumulative area of the total study area [QGIS data provided by Centro Agua Bolivia; Rodal, 2008]

<i>Sub basin</i>	<i>Area [$*10^3 \text{ km}^2$]</i>	<i>Area cumulative [$*10^3 \text{ km}^2$]</i>
Grande	53.3	53.3
Ichilo	7.9	7.9
Rio Mamoré	61.4	122.6

Appendix B shows an analysis to find out which approach use to determine the mean areal precipitation. This analysis showed the poor quality of the data of the sub basin Ichilo and the choice is made to redistribute the area of the Mamore river basin into two sub basins: Grande and Mamore which includes the former sub basin Ichilo, see figure 2.7.

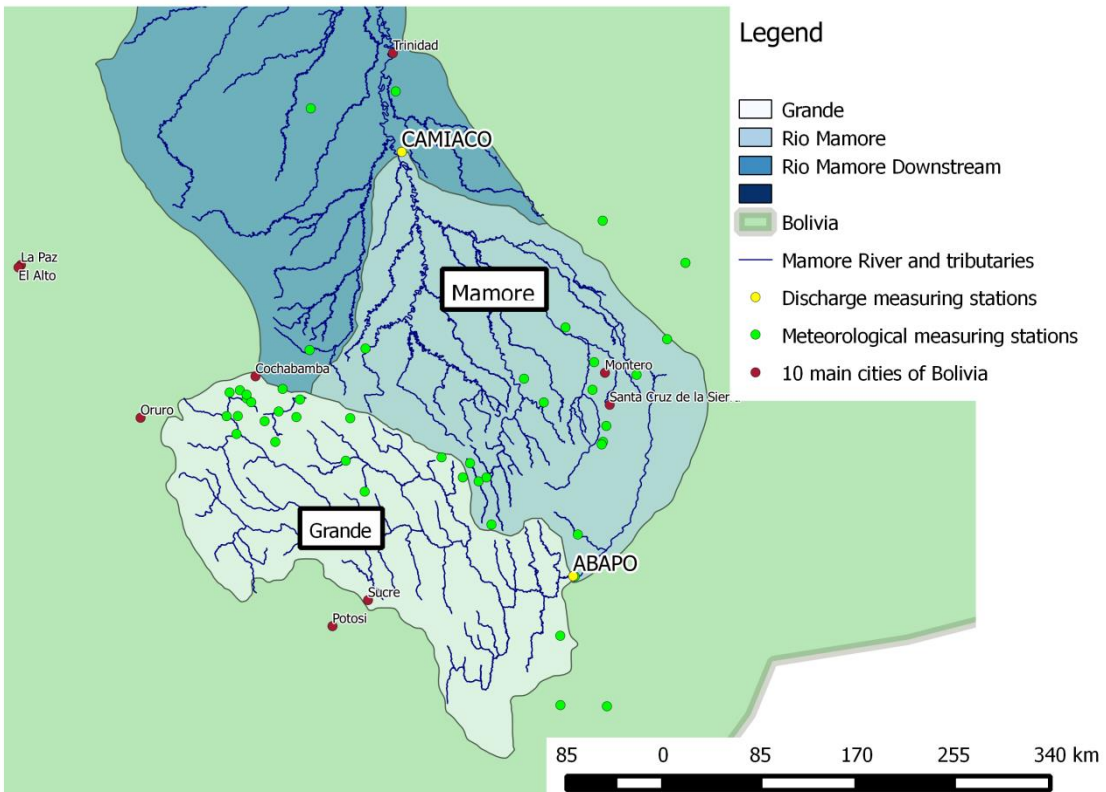


Figure 2.7: Map of the Mamoré River basin, Mamoré River and tributaries, sub basins and their discharge stations, Meteorological measuring stations and the main cities of Bolivia.

3 Methodology

This chapter describes the various steps undertaken and choices made in this study. First, in section 3.1, the hydrological model HBV is described. Section 3.2 explains the steps to be taken in the calibration and validation procedure. Finally, in section 3.3, the flood forecasting, an updating procedure and evaluation of flood forecasting are described.

3.1 HBV model

The HBV-model is introduced and briefly described by its structure and applications in section 3.1.1. In section 3.1.2. the model is described more in detail by explaining its routines. Section 3.1.3 gives an overview of the model parameter and sections 3.1.4 and 3.1.5 describe the connection of the two sub basins.

3.1.1 Model structure and applications

The hydrological model used in this study is the HBV model, developed in the early 70's of the last century by the Swedish Meteorological and Hydrological Institute (SMHI). The HBV model is named after the abbreviation of Hydrologiska Byråns Vattenbalansavdelning, a former section of the SMHI. It is a conceptual rainfall-runoff model and different model versions of HBV have been applied in more than 60 countries all over the world. It has been applied to countries with highly different climatic conditions and highly different basin area sizes [Perrin et al, 2001]. The HBV-model has also been applied in Bolivia for a small sub-basin (200 km²) of the Mamoré River basin in a study by Lidén et al. [2000].

The reasons the HBV model is chosen for this study are first because it is a proven model and has been in use for a long time. Since its development, multiple revisions and adjustments have been made resulting in the HBV-96 model [Lindström et al., 1997]. It has been applied to many basins and provided good results in most applications [Seibert, 2005]. Second, the model needs a moderate amount of input data to generate the output of the model. The input data are easily to obtain which makes this study feasible. Further, the HBV model has been applied at the University of Twente before, thus experience with the model is available [Booij, 2002; Booij & Krol, 2010; Demirel et al., 2013; Akhtar et al., 2008; Deckers et al., 2010; Knoben, 2013; Tillaart, van der, 2010].

The HBV model generates daily discharges as output and uses daily precipitation, temperature and potential evapotranspiration as input. Every time step the water balance of the basin is calculated. It is a conceptual hydrological model, which means it attempts to cover the most important runoff generating processes using a simple and robust structure, and a small number of parameters [Abebe et al., 2010]. The model parameters do not directly represent physical properties. That is why model parameters cannot be measured in the field. The model parameters, which represent some basin characteristics, are determined by calibration of the model.

The HBV model can be used as a semi-distributed or lumped model [Lidén et al., 2000; Lindström et al, 1997]. A semi-distributed model is used if a basin can be separated into a number of sub-basins with different characteristics in for example elevation and vegetation. A lumped model does not take into account the spatial variability of processes, input, boundary conditions and watershed geometric characteristics [Singh, 1995]. As a result of data analysis, see section 2.2, a semi-distributed model with two sub basins has been used in this study. The HBV version used in this study is the by Knoben [2013] adjusted version applied by Tillaart [2010], which is a Matlab implementation of the HBV-15

model developed in Fortran by Booij [2002]. Individually sub basins are modeled with the HBV-96 model [Booij, 2005]. In this study two sub basins are considered: Grande and Mamoré. Further some other adjustments made to the model are considered in section 3.1.4 and 3.1.5.

3.1.2 Model routines

In this study, the model uses three storage boxes, connected by various fluxes. These storage boxes and fluxes are described in sections 3.1.2.1 and 3.1.2.2 per routine. For each sub basin the HBV model is run separately. Model input consists of time series of daily precipitation P [mm] and daily potential evapotranspiration et_p [mm]. In this study the precipitation routine has not been taken into account, because snowfall rare phenomenon in the study area. The model calculates all fluxes and storages terms in unit [mm] with a daily time step. Model output is a time series of simulated mean daily discharge Q_{sim} [m^3/s], converted from the daily total runoff flux [mm]. The routines, fluxes, parameters, input and output of the HBV model used in this study are shown in figure 3.1 in a schematization.

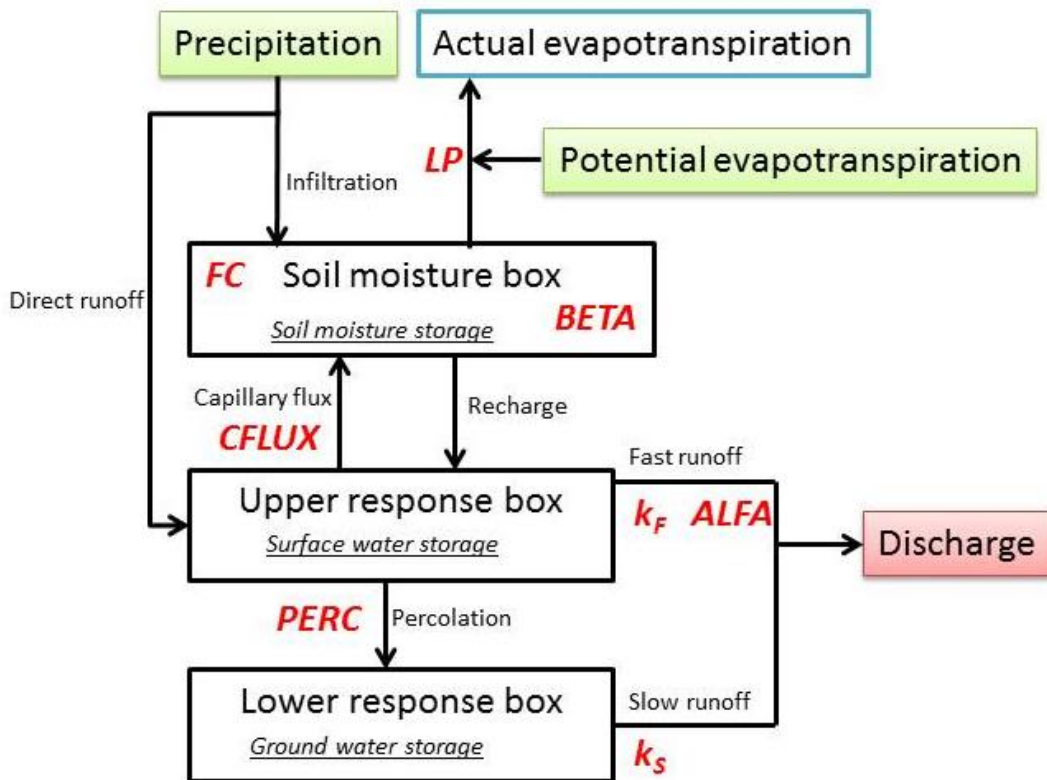


Figure 3.1: Schematization of the HBV model used in this study with in red the eight model parameters, the arrows represent the fluxes, the three black outlined boxes represent the three model routines used in this study. The two green boxes are the model input and the red box is the model output.

3.1.2.1 Soil moisture routine

The soil moisture accounting of the HBV model is based on a modification of the bucket theory in that it assumes a statistical distribution of storage capacities in a basin [Lindström et al., 1997]. This is the main part controlling runoff formation. Water enters the soil moisture routine from the precipitation P [mm] via infiltration and from the upper response box via capillary rise q_c [mm]. Water from precipitation is divided into infiltration q_{in} [mm] into the soil moisture box S_{SM} [mm] and, in case of saturation of the soil moisture box, direct runoff q_d [mm] into the upper response box:

$$q_{in}(t) = P(t) - q_d(t) \quad (3.1)$$

$$q_d(t) = q_{in}(t) + S_{SM}(t) - FC \quad (3.2)$$

Where S_{SM} [mm] is the soil moisture storage and FC [mm] is the field capacity, the maximum S_{SM} .

Capillary rise q_c [mm] from the upper response box replenishes soil moisture storage, providing that the soil moisture storage is not yet saturated:

$$q_c(t) = CFLUX * \frac{FC - S_{SM}(t)}{FC} \quad (3.3)$$

Where $CFLUX$ is the maximum rate of capillary rise [mm d⁻¹].

The soil moisture storage releases water as seepage, recharge q_r [mm], into the upper response box and actual evapotranspiration et_a [mm], which leaves the model completely:

$$q_r(t) = \left(\frac{S_{SM}(t)}{FC} \right)^{BETA} * q_{in}(t) \quad (3.4)$$

$$et_a(t) = et_p(t) * \left(\frac{S_{SM}(t)}{LP * FC} \right) \quad \text{if } S_{SM}(t) < LP * FC \quad (3.5)$$

$$et_a(t) = et_p(t) \quad \text{if } S_{SM}(t) \geq LP * FC$$

Where $BETA$ is a non-linearity parameter [-] ($BETA > 1$) and LP a factor limiting potential evapotranspiration [-] ($0 < LP < 1$).

This routine includes three parameters, $BETA$, LP and FC . The parameter $BETA$ controls the contribution to the response function or the increase in soil moisture storage from each millimeter of rainfall. The parameter LP is a soil moisture value above which evapotranspiration reaches its potential value. The parameter LP is given as a fraction of FC [Seibert, 1999]. Another parameter, $CFLUX$, is the maximum capillary flow from the upper response box to the soil moisture box.

3.1.2.2 Runoff generation routine

The runoff generation routine is the response function which transforms excess water from the soil moisture zone to runoff. The function consists of one upper, non-linear, and one lower, linear, reservoir [Lindström et al., 1997]. These are the origin of the quick and slow runoff components of the hydrograph.

Fast runoff routine

The fast runoff routine is linked to the upper response box which contains the recharge from the soil moisture box and direct runoff from precipitation and holds the surface water storage S_{SW} [mm]. Three outflows exist; capillary transport to the soil moisture box, percolation $PERC$ [mm d⁻¹] into the lower response box and fast runoff of the model q_f [mm]:

$$q_f(t) = k_f * S_{SW}(t)^{1+ALFA} \quad (3.6)$$

Where k_f is the fast runoff parameter [d⁻¹] and $ALFA$ is a non-linearity parameter [-]

PERC is not expressed as equation, but rather calibrated as a model parameter.

Slow runoff routine

The slow runoff routine is linked to the lower response box which contains the ground water storage S_{GW} [mm]. The ground water storage receives water via percolation and has a single outflow as slow runoff q_s [mm]:

$$q_s(t) = k_s * S_{GW}(t) \quad (3.7)$$

Slow runoff and fast runoff together constitute the total runoff q_t [mm] of the model:

$$q_t(t) = q_f(t) + q_s(t) \quad (3.8)$$

The runoff routine has two recession coefficients, namely k_f and k_s , a measure for non-linearity of slow flow in the upper response box *ALFA* and a percolation rate *PERC* from the upper to the lower response box.

3.1.2.3 Changes in storage

The storage terms are updated based on daily fluxes. Safeguards are included for cases where total outflow fluxes exceed the total of current storage and inflow fluxes. In such a case the storage term is set at zero and outflow flux is equal to storage + inflow fluxes, rather than letting it reach physically impossible negative storage values, which also prevents numerical issues in the model equations.

Soil moisture storage:

$$S_{SM}(t + 1) = S_{SM}(t) + q_{in}(t) + q_c(t) - q_r(t) - et_a(t) \quad (3.9)$$

Surface water storage:

$$S_{SW}(t + 1) = S_{SW}(t) + q_d(t) + q_r(t) - PERC - q_f(t) - q_c(t) \quad (3.10)$$

Ground water storage:

$$S_{GW}(t + 1) = S_{GW}(t) + PERC - q_s(t) \quad (3.11)$$

3.1.3 Model parameters

The HBV model used in this study includes eight model parameters, as seen in figure 3.1 and described in the previous sections. An overview of the model parameters, their descriptions and units is shown in table 3.1.

Table 3.1: Overview of the eight model parameters with their descriptions and units.

<i>Parameter</i>	<i>Description</i>	<i>Unit</i>
FC	Field capacity, maximum soil moisture storage	[mm]
BETA	Non-linearity parameter	[-]
LP	Factor limiting actual evapotranspiration	[-]
ALFA	Non linearity parameter	[-]
k_F	Fast runoff coefficient	[d ⁻¹]
k_S	Slow runoff coefficient	[d ⁻¹]
PERC	Rate of percolation	[mm d ⁻¹]
CFLUX	Rate of capillary rise	[mm d ⁻¹]

3.1.4 Connection sub basins

The observed discharge at Camiaco, the outflow of sub basin Mamoré, is the discharge generated in both sub basins. The discharge from the upstream basin Grande flows into the downstream basin at Abapó and then flows approximately 850 kilometers through sub basin Mamoré before it reaches the point of outflow at Camiaco. In order to calibrate the sub basin Mamoré, the discharge of the Grande basin, Q_g , needs to be subtracted from the observed discharge at Camiaco, Q_{obsM} , to obtain the discharge generated in the Mamoré basin itself. Therefore the travel time of the discharge of Grande through the Mamoré basin needs to be determined. Because not enough information is available to calculate the travel time, it is found by using the Pearson's correlation coefficient.

3.1.4.1 Pearson's correlation coefficient

The Pearson's correlation coefficient R is a measure of the strength and direction of a linear relationship between two variables giving a value between +1 and -1 inclusive, where 1 is total positive correlation, 0 is no correlation, and -1 is total negative correlation. R is defined as the covariance of the variables divided by the product of their standard deviations and the formula for R is:

$$R = \frac{\sum \left((Q_{obs,G(t-\Delta t)} - \overline{Q_{obs,G}}) (Q_{obs,M(t)} - \overline{Q_{obs,M}}) \right)}{\sqrt{\sum \left((Q_{obs,G(t-\Delta t)} - \overline{Q_{obs,G}})^2 \right) \sum \left((Q_{obs,M(t)} - \overline{Q_{obs,M}})^2 \right)}} \quad (3.12)$$

for $\Delta t = 0, 1, 2, \dots, 40$

with:

$Q_{obs,G(t)}$ is the observed mean daily discharge of sub basin Grande of time step t [m³/s]

$Q_{obs,M(t)}$ is the observed mean daily discharge of sub basin Mamoré of time step t [m³/s]

$\overline{Q_{obs,G}}$ is the average mean daily discharge of sub basin Grande [m³/s]

$\overline{Q_{obs,M}}$ is the average mean daily discharge of sub basin Mamoré [m³/s]

Δt is the lag time [day]

The correlation between the discharge of the Grande and the discharge of the Mamoré is determined for the period for which discharge data are available. The correlation coefficients for a lag time of 0 to 40 days are calculated and presented in figure 3.2.

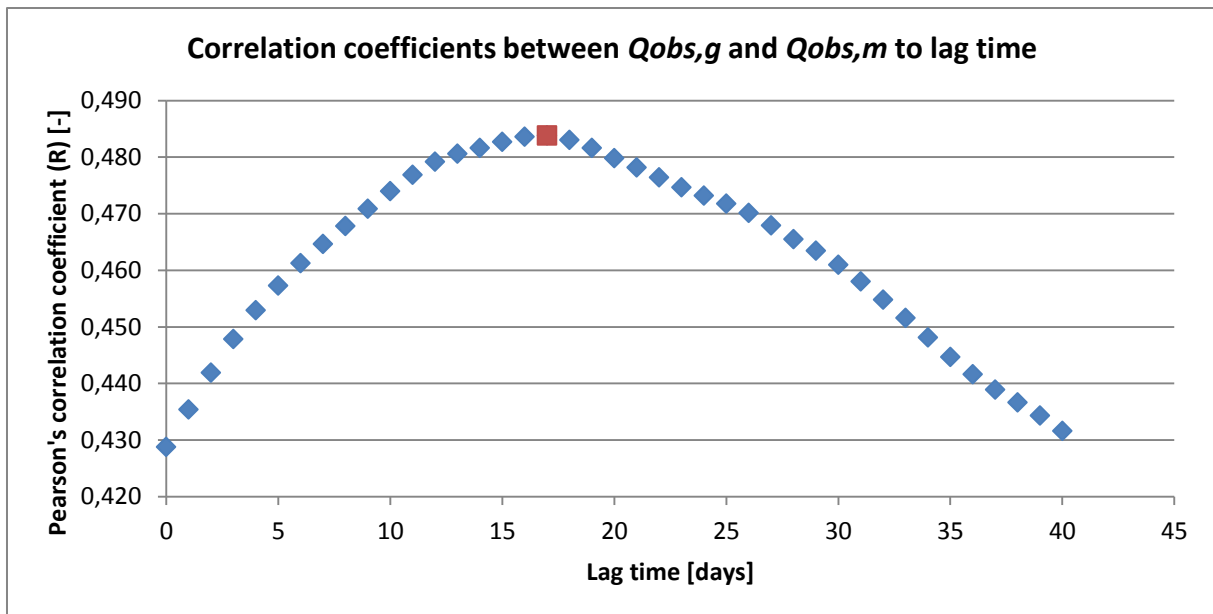


Figure 3.2: Correlation between observed discharge of Grande and Mamoré with in red the highest correlation with a lag time of 17 days.

The optimum correlation coefficient is 0.484 corresponding to a lag time of 17 days, but the range of R is small. The assumption is made that peaks at Abapo show up at Camicao with floods in Mamoré. This correlation may be weak or peaks of Abapo may be completely dampened.

This lag time corresponds to a mean velocity of 0.6 m/s over the length of 850 kilometers.

The route of the runoff from Abapo (point of outflow of sub basin Grande) to Camiaco (point of outflow of sub basin Mamoré) can be divided into two parts: tributary Grande and Rio Mamoré. Figure 3.3 is a figure provided by the Bolivian partners of RHDHV. It shows the travel time of the main river Rio Mamoré. The Rio Mamoré part of the route is from Grande to Sécure. The travel time is 1.28 days, over a distance is 95 km, giving a mean velocity of 0.86 m/s and is of the same magnitude as the 0.6 m/s mentioned before.



Figure 3.3: 'Water Displacement' of the Mamoré river with on the horizontal axis distance [km] and on the vertical axis time [days] [source: Rodal, 2008].

3.1.5 Reservoir

When looking at the hydrograph of the discharges of both sub basins, figure 3.5, it can be observed that the peak discharges of sub basin Grande exceeds the peak discharges of the outflow of the total basin. This looks controversial, but an explanation of this phenomenon can be that inundations take place within the sub basin Mamoré. In this study the assumption is made that this phenomenon occurs and this assumption is supported by inundation maps of floods in the past, like the 2007 floods, see figure A.1. Therefore, a reservoir is added to the HBV model in sub basin Mamoré, to deal with the floods within the sub basin Mamoré due to the contribution of the discharge from sub basin Grande. When the discharge of the Grande exceeds a certain value, Q_{gmax} , the surplus flows into the reservoir. The value of Q_{gmax} is based on the information provided by the Bolivian partners of RHDHV. The value of Q_{gmax} is determined to be $1.0 \cdot 10^3 \text{ m}^3/\text{s}$, which is the total capacity of the whole tributary Grande of the Mamoré river. River Grande originates in sub basin Grande and flows at Abapo into sub basin Mamoré and is there connected to the Mamoré River at last, see figure 3.6. The assumption is made that inundations occur in the sub basin Mamoré of tributary Grande.

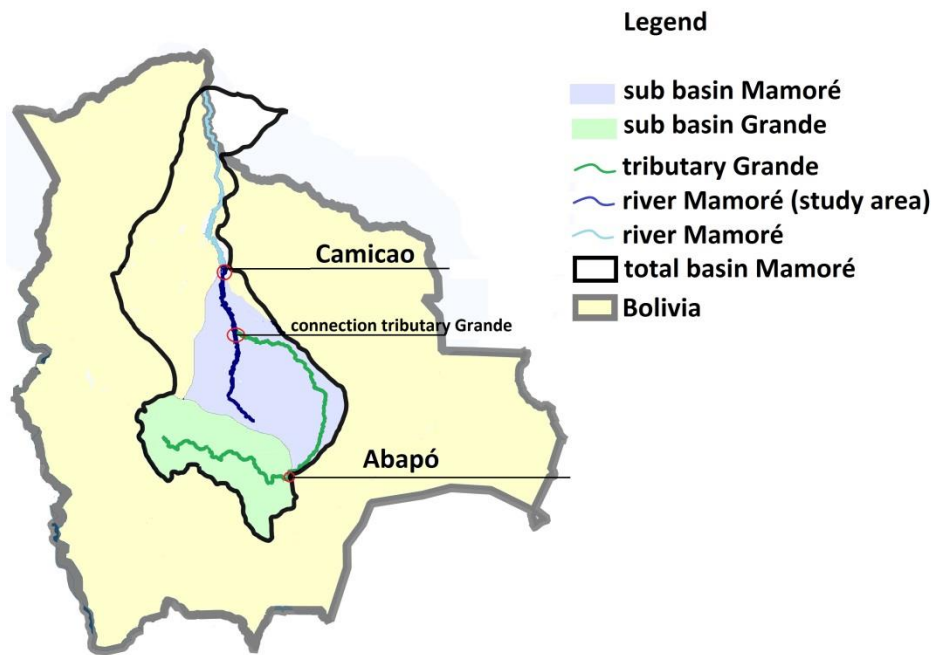


Figure 3.4 Map of total basin Mamoré, with the sub basin Mamoré, sub basin Grande, trace of the river main Mamoré and main river Grande.

If the discharge of the Grande is below Q_{gmax} , the reservoir will empty. The assumption is made that the reservoir outflow, $q_R(t)$ behaves similar to the fast runoff component of the HBV model: q_f . Thus a non-linear dependency with storage. Therefore, the formula of $q_R(t)$ is similar to the equation of q_f and is as follows:

$$q_R(t) = S_R(t)^{1+ALFA} * k_f \quad (3.13)$$

With the same values

q_R is outflow of the reservoir [mm]

S_R is storage in the reservoir [mm]

$ALFA$ is the nonlinearity parameter [-]

k_f is the fast runoff coefficient of the fast runoff [-]

t is the time [days]

3.2 Calibration and validation

To make a hydrological model ready to use in practice for a specific application, calibration of the model should be performed. Calibration is the process of searching for a parameter set which closely simulates the behaviour of the basin [Madsen et al, 2002]. The goal of the calibration procedure is to adjust the model parameters to decrease the difference between e.g. observed and simulated values of discharge for a certain period in time [Viviroli et al, 2009].

The procedure to find the optimum parameter set in this study is Monte Carlo Simulation (MCS). MCS is a technique in which, through numerous model simulations, a best objective function value is sought by using randomly generated parameter values within a pre-defined model parameter range. Important aspects of MCS are the determination of prior parameter ranges (see section 3.2.1), the

determination of the calibration period (see section 3.2.2), the selection of the objective function(s) (see section 3.2.3), the selection of calibration parameters (see section 3.2.4) and the validation (see section 3.2.5)

To be certain that the entire model parameter space is examined and to permit statistical treatment of the results, a sufficient number of runs should be executed [Booij & Krol, 2010]. The number of model simulations carried out in this study is 100,000. This number is limited because of the time consuming characteristics of this procedure. Shrestha et al. [2009] found that in case of using MCS for a HBV model with nine parameters, 10,000 simulations is a reasonable number for stable convergence of the MCS.

Advantages of using MCS are that it is an easily understood and flexible method, which is very flexible and it can easily be extended and developed as required. Disadvantage of using MCS are that it is a time consuming process, compared to other methods and the calibration with other methods can be done more efficiently.

3.2.1 Selection of parameter ranges

Because the model parameters are not directly measurable, the first part of the calibration process is to estimate ranges of possible values for these parameters based on prior research. These estimated ranges of the model parameters are shown in table 3.2.

Table 3.2: Ranges of the model parameters which are used in calibration process. Source: ¹Demirel et al.(2013), ²Uhlenbrook et al. (1999), ³Deckers et al. (2010), ⁴Lidén and Harlin (2000), ⁵Knoben (2014). The range values with * are adjusted values of that source.

Parameter	Range		Unit
	MIN	MAX	
¹ FC	100	800	[mm]
² BETA	1	5	[-]
¹ LP	0.1	0.9*	[-]
³ ALFA	0*	2*	[-]
^{2,4} k _F	0.0005	0.1	[d ⁻¹]
^{2,4} k _S	0.0005	0.1	[d ⁻¹]
¹ PERC	0	6	[mm d ⁻¹]
⁵ CFLUX	0	4	[mm d ⁻¹]

3.2.2 Calibration and validation period

The available discharge and climate data for this basin have been analyzed during the data analysis, see section 2.2. In this analysis it has been determined that the total time period considered in this research is from 7-8-2002 till 7-5-2009. This time period is limited by the data of the discharge gauging stations. The period shows seven hydrological years, where the first four years (7-8-2002 to 7-8-2006) are used for the calibration and the last three years (8-8-2006 to 7-5-2009) are used for the validation of the model, see the figure below.

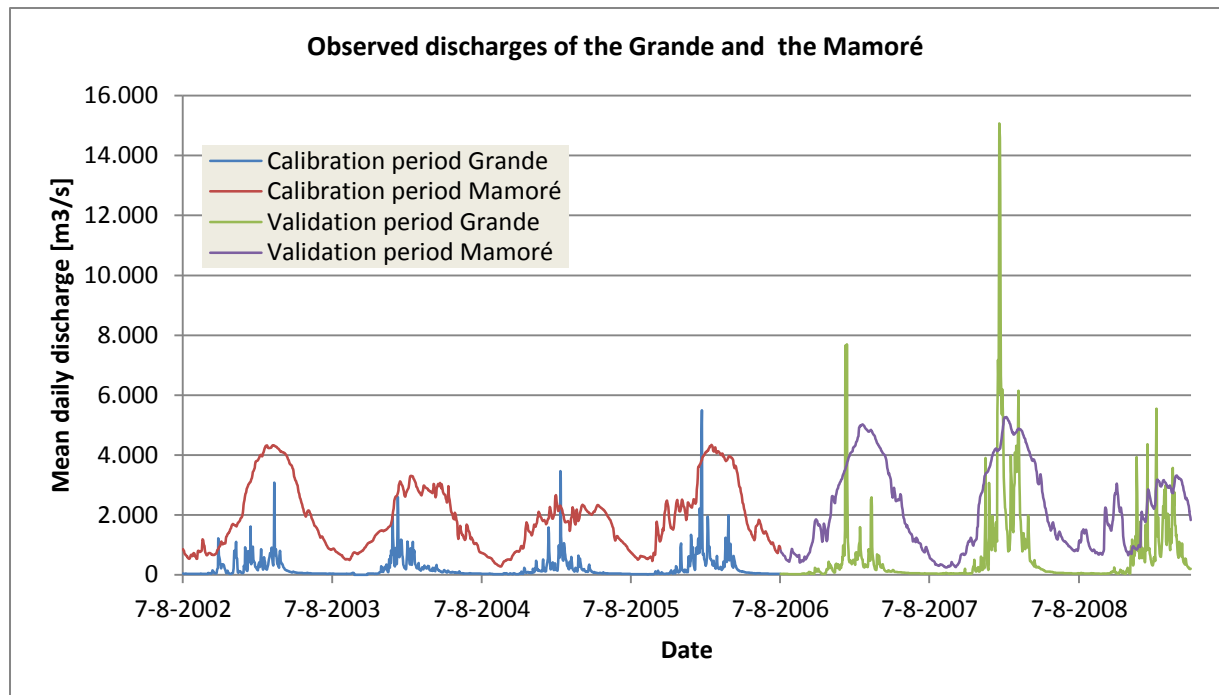


Figure 3.5: Hydrographs of the calibration and validation period of sub basins Grande and Mamoré.

Because climatic data are available before this period, a warm up period of approximately 1.5 years is used from 1-1-2001 to the start of the calibration period. The warm up period of the validation is also from 1-1-2001 to the start of the validation period. This is a total warm up period of approximately 5.5 years.

3.2.3 Selection of objective functions

For a proper evaluation of the calibrated model, it is necessary to translate the overall calibration objective into more operational terms: objective functions [Madsen, 2000]. The following four objectives are usually considered: (1) a good water balance, (2) a good overall agreement of the shape of the hydrograph, (3) a good agreement of the peak flows with respect to timing, rate and volume and (4) a good agreement for low flows. Since in the research the objective of model calibration is to forecast floods adequately, a good agreement of low flows is less important and therefore not taken into account. Examples of objective functions related to the objectives of Madsen are given below:

3.2.3.1.1 Relative Volume Error [Madsen, 2000]

With respect to the objective 'a good water balance', the Relative Volume Error (R_{VE}) is a commonly used objective function. Equation 3.14 represents R_{VE} and is shown below:

$$R_{VE} = \frac{\sum_{i=1}^n Q_{sim,i} - \sum_{i=1}^n Q_{obs,i}}{\sum_{i=1}^n Q_{obs,i}} \quad (3.14)$$

Where Q_{sim} stands for simulated discharge, Q_{obs} for observed discharge, i for the time step and n for the total number of time steps used during calibration. The value of R_{VE} can vary between $-\infty$ and ∞ . The model performs best when a value of 0 is generated since no difference between total simulated and observed discharge occurs.

3.2.3.1.2 Nash-Sutcliffe Coefficient [Nash and Sutcliffe, 1970]

Regarding the objective ‘good overall agreement of the hydrograph’, the Nash-Sutcliffe coefficient (NS) is the most widely used objective function in rainfall-runoff modeling. The Nash-Sutcliffe coefficient is shown below in equation 3.15:

$$NS = 1 - \frac{\sum_{i=1}^n (Q_{obs,i} - Q_{sim,i})^2}{\sum_{i=1}^n (Q_{obs,i} - \overline{Q_{obs}})^2} \quad (3.15)$$

Where $\overline{Q_{obs}}$ represents the mean of the observed discharges and the other variables as defined before. It should be noted that NS emphasizes high flows because of the squaring of the difference with $Q_{obs,i}$. The value of this objective function can vary between $-\infty$ and 1, and the best model performance is when a value of 1 is generated. When a NS -value below 0 is generated, the mean observed discharge performs better compared to the simulated discharge, so in such a case the model should not be used.

3.2.3.1.3 Nash-Sutcliffe coefficient for high flows (NS_H) [Deckers, 2006]

With respect to the objective ‘a good agreement of the peak flows with respect to timing, rate and volume’ several objective functions are used in the literature. One of them is the Nash-Sutcliffe coefficient for high flows and is described below.

$$NS_H = 1 - \frac{\sum_{i \text{ } Q_{obs}(t_i) \geq Q_{high}} (Q_{obs,i} - Q_{sim,i})^2}{\sum_{i \text{ } Q_{obs}(t_i) \geq Q_{high}} (Q_{obs,i} - \overline{Q_{high,obs,i}})^2} \quad (3.16)$$

The Nash-Sutcliffe coefficient for high flows is defined as the Nash Sutcliffe coefficient [Nash and Sutcliffe, 1970] but for discharge values above a selected high discharge threshold Q_{high} . Where $\overline{Q_{high,obs,i}}$ is the mean observed daily discharge above Q_{high} . The value of NS_H can, like NS , vary between $-\infty$ and 1, and has an optimum value of 1. The thresholds Q_{high} for sub basin Grande and Mamoré used in this study are 500 m³/s and 1,500 m³/s respectively. These values are derived from the hydrographs of both basins, see figure 3.5, in a way that for each meteorological year the peak flows of the wet seasons are part of the calculation of NS_H .

In this research two different objective functions are used in the calibration process; one for the calibration of sub basin Grande and one for sub basin Mamore.

For the upstream sub basin Grande it is preferred that the HBV model simulates the discharge as accurate as possible compared to the observed discharge over the entire time period, because the outflow of the upstream basin is the inflow into the downstream basin. Thus, the objectives for the upstream sub basin are a good water balance and a good overall agreement of the shape of the hydrograph. Therefore, a multiple objective function Y is used. Y is a function which combines the objective functions R_{VE} and NS . The combined objective function Y is defined as [Akhtar et al., 2009]:

$$Y = \frac{NS}{1 + |RVE|} \quad (3.17)$$

The optimum value of NS is 1 and R_{VE} has an optimum value of 0. This makes that the optimum value of Y is 1.

The downstream sub basin Mamoré has a different objective function compared to the upstream sub basin Grande. The objective for this sub basin is to find a good agreement of high flows with respect to timing, rate and volume and therefore NS_H has been selected.

3.2.4 Selection of calibration parameters

Some parameters have a larger influence on the objective function and thus the model performance than other parameters. That is why these parameters need more attention in the calibration procedure. The calibration process is executed in two calibration steps: the first calibration and the final calibration.

In the first calibration, eight model parameters are used to optimize the model for each sub basin separately. This is done by two MCSs: one for sub basin Grande and one for sub basin Mamoré, with 100,000 runs each. Downstream sub basin Mamoré has to deal with the inflow of the discharge of upstream sub basin Grande. In order to calibrate sub basin Mamoré independently of the simulation of Grande, the observed discharge of Grande is used as the inflow into sub basin Mamoré, with a delay of 17 days (section 3.1.4), during the calibration process.

In order to make the simulations realistic, the following selection of parameter sets is made. As mentioned before in section 3.1.2, the runoff generation routine of the HBV model consists of two components: fast runoff and slow runoff, which are generated in the fast and slow response box, respectively. The amount of fast runoff depends on the storage of the fast response box and two model parameters, k_F and $ALFA$. The amount of slow runoff depends on the storage of the slow response box and one model parameter, k_S . By executing a Monte Carlo Simulation the random chosen values of the parameters of the model can be generated in a way that the slow runoff will flow faster than the fast runoff and have a larger contribution during floods. Realistically, the slow runoff coefficient, k_S , needs to be smaller than the so called 'effective fast runoff coefficient', k_{F-eff} .

The formula of the slow runoff can be rewritten into an equation for k_S :

$$q_s = S_{GW} * k_S \quad (3.18) \quad \rightarrow \quad k_S = \frac{q_s}{S_{GW}} \quad (3.19)$$

The formula of the fast runoff is:

$$q_f = S_{SW}^{1+ALFA} * k_F \quad (3.20)$$

The effective k_F , k_{F-eff} , is defined as the ratio of fast runoff q_f and surface water storage S_{SW} similar to k_S and combined with the equation 3.20 of q_f it can be rewritten as:

$$k_{F-eff} = \frac{q_f}{S_{SW}} = k_F * S_{SW}^{ALFA} \quad (3.21)$$

So, k_{F-eff} depends, besides two model parameters, on the surface water storage, S_{SW} , which varies over time. Therefore, k_{F-eff} is determined for each day the discharge is above a certain level, when the fast runoff component of the discharge should be the major contributor to the total discharge, compared to the slow runoff component. The boundary levels of the discharge of sub basin Grande and sub basin Mamoré above which k_{F-eff} is determined are 500 m³/s and 1,500 m³/s respectively. These discharge thresholds are equal to the discharge thresholds used to calculate NS_H . Then the mean value of k_{F-eff} is determined for each run of the Monte Carlo Simulation for each sub basin.

The result of MCS is a list of parameter sets with corresponding values of the objective functions and mean k_{F-eff} . The parameter sets for which the value of the mean k_{F-eff} is larger than the value of the k_s are selected for further analysis, the others are discounted.

To select the most influential parameters to be calibrated in the final calibration, a univariate sensitivity analysis is performed. This means that the values of the optimum parameter set are varied once at a time while other parameter values are kept at a constant value. The parameters are all varied with the same factor over the scaled parameter values: 0.5, 0.75, 1.25 and 1.5. Then, a selection is made of the 4 or 5 most sensitive parameters for each sub basin which are used in the final calibration. The values of the optimum parameter set from the first calibration are used in the final calibration as default values for the less sensitive parameters. After the first calibration, the parameter ranges of the best performing parameter sets are examined, to check whether the ranges tend towards a cert value and should be adapted in the final calibration.

Next the final calibration is executed and, like after the first calibration, a selection is made of the parameter sets for which the value of k_{F-eff} is larger than the value of parameter k_s .

3.2.5 Validation procedure

After the final calibration step, the validation procedure is executed. The goal of the validation procedure is to see whether the model is capable of making accurate predictions for other conditions than during the calibration period. The final calibration step results in optimum parameter sets for the objective functions for sub basin Grande and sub basin Mamoré. These parameter values are used for a period other than the calibration period, the validation period, see section 3.2.2. The evaluation of the performance of the calibrated HBV-model for the validation period is similar to the evaluation of the results of the calibration procedure.

3.3 Forecasting

In this study the focus is on flood forecasting, in order to be able to warn the people when a flood will occur. The meteorological input data in flood forecasting are usually based on ensemble weather predictions. In this study, perfect weather forecasts are used to predict floods. This means that at the forecast issue day, the precipitation and daily mean temperatures for the coming days are not based on weather forecasts, but are the measured precipitations and temperatures at the meteorological stations in the field. This, because no historical records of (ensemble) weather forecasts are available.

For flood forecasting, the optimized parameter set obtained during the calibration process, is used to forecast the discharge for the validation period for 1 up to 10 days ahead.

3.3.1 Updating

Model predictions of runoff from a basin often differ from the observations [Wöhling et al., 2006]. By following an updating procedure the observations of the state of the basin up to the current time are used to improve the model prediction performance. The most natural method of forecast updating is state correction in which a direct or related measurement of a model state is used to adjust its value so as to improve forecast performance [Moore et al., 2005]. In this study, the ground water storage and the reservoir storage are updated on the forecast issue day, based on the observed discharge of that day. First the calibrated model is run for the calibration period with its best performing parameter set and the model state is analyzed. This run is called the 'reference run' in other recent

works [Fundel and Zapp, 2011; Roulin, 2007; Roulin and Vannitsem, 2005]. Empirical relations between the simulated discharge from sub basin Mamoré and the fast runoff, slow runoff and outflow out of the reservoir for the calibration period are used to divide the observed discharge between the fast runoff, slow runoff, the reservoir outflow and the discharge originating from sub basin Grande for the validation period. Equation 3.22 shows the composition of the observed discharge at Camiaco and the empirical relations are shown in equation 3.23 to 3.25.

$$q_{sim}(t) = q_f(t) + q_s(t) + q_R(t) + q_{Grande}(t - 17) \quad (3.22)$$

With q_{obs} is the observed mean daily discharge measured at Camiaco [mm],
 q_f is the daily fast runoff from the surface water of sub basin Mamoré [mm],
 q_s is the daily slow runoff from the ground water of sub basin Mamoré [mm],
 q_R is the daily outflow of the reservoir [mm],
 q_{Grande} is the daily discharge from sub basin Grande with a maximum of q_{gMAX} , see section 3.1.5.

The functions k_{qf} , k_{qs} and k_{qR} of the relations between q_f , q_s and q_R respectively, and q_{simM} are determined with the data of the calibration period. Where q_{obsM} is the daily discharge at Camiaco minus the contribution of the outflow of sub basin Grande, which has an approximated travel time of 17 days, see section 3.1.4:

$$q_{simM}(t) = q_{sim}(t) - q_{Grande}(t - 17) \quad (3.23)$$

The fractions of q_f , q_s and q_R of q_{simM} are plotted against q_{simM} . The equations of the three trend lines through those three scatter plots are the functions k_{qf} , k_{qs} and k_{qR} which are functions of q_{obsM} . In the updating procedure, the q_f , q_s and q_R are updated by using the functions k_{qf} , k_{qs} and k_{qR} as follows:

$$q_f(t) = q_{obsM} * k_{qf} \quad (3.24)$$

$$q_s(t) = q_{obsM} * k_{qs} \quad (3.25)$$

$$q_R(t) = q_{obsM} * k_{qR} \quad (3.26)$$

With

$$q_{obsM}(t) = q_{obs}(t) - q_{Grande}(t - 17) \quad (3.27)$$

The updated q_f , q_s and q_R are used to update the surface water storage S_{sw} , ground water storage S_{GW} and reservoir storage S_R are updated as follows:

$$S_{sw}(t + 1) = \left(\frac{q_f(t)}{k_F} \right)^{(1/(1+ALFA))} \quad (3.28)$$

$$S_{GW}(t + 1) = \frac{q_s(t)}{k_S} \quad (3.29)$$

$$S_R(t + 1) = \frac{q_R(t)^{\left(\frac{1}{1+ALFA}\right)}}{k_F} \quad (3.30)$$

3.3.2 Evaluation of forecasting

A variety of verifications and skill assessments are reported in the literature to evaluate the performance of forecasting [Cloke & Pappenberger, 2008; Roulin, 2007; Bartholmes et al, 2009]. The goodness of forecasts can be evaluated against its quality: the correspondence between the forecast and observations [Murphy, 1993; Molinari et al., 2013]. Most forecast models are probabilistic, because they use meteorological ensemble forecasts for producing predictions. This study uses perfect forecasts as input of the hydrological model, and thus is deterministic. The fact that the forecasts are deterministic, the different aspects (or attributes) to describe forecast quality is limited. The aspects to describe the forecast quality used in this study are accuracy, skill and reliability.

According to Murphy [1993] these aspects are defined as:

- Accuracy: the level of agreement between the forecast and observations (the difference between the forecast and the observation is the error: the lower the errors, the greater the accuracy).
- Skill: Accuracy of forecasts of interest relative to accuracy of forecasts produced by stand of reference.
- Reliability: The average agreement between forecast values and observed values.

The overall accuracy of the forecasts in this study is described by the NS , R_{VE} , Y and NS_H . Skill measures that can be determined with a deterministic model are commonly calculated from contingency tables. Contingency tables are used to assess the performance of flood forecasts. Contingency tables can be used to estimate the utility of hydrological forecasts and indicate the forecast models ability to correctly anticipate the occurrence or non-occurrence of preselected events [Martina et al., 2005]. The four possible cases are given in a two-by-two contingency table, table 3.3.

In this study two types of events are taken into account and are defined as:

- Event type 1: *'the exceedance of a discharge threshold at time step t'*
- Event type 2: *'the exceedance of a discharge threshold at time step t, with the condition that at time step t-1 this threshold was not exceeded'*.

Appendix C shows characteristics of the Mamoré river and its tributaries. The maximum capacity of the river Mamoré at Camiaco, the point of outflow of the basin considered in this study, is $3.9 \cdot 10^3 \text{ m}^3/\text{s}$. In this study a threshold for a flood is $3.9 \cdot 10^3 \text{ m}^3/\text{s}$ at Camiaco. Next to the flood threshold, another threshold is considered in this study: high water threshold with a value of $3.0 \cdot 10^3 \text{ m}^3/\text{s}$, which is the q80 of the calibration period. Event type 1 focuses on every time step that the discharge exceeds the discharge threshold and event type 2 focuses on start of an exceedance of the discharge threshold, i.e. the beginning of a flood or high water.

Thus, four events are taken into account in this study: event type 1 with the flood threshold, event type 1 with the high water threshold, event type 2 with the flood threshold and event type 2 with the high water threshold.

Table 3.3: Two-by-two contingency table for the assessment of a threshold based forecasts

Forecasts			
Observations	Event (W)	Non-event (W')	Total
Event (E)	h	m	e
Non-Event (E')	f	c	e'
Total	w	w'	n

With a total number of n observations, one can distinguish the total number of e event occurrences and non-occurrences e' and the total number of w flood warnings and no-warnings w' . Four outcomes are possible: a hit, when an event occurred and a warning was issued; a miss, when an event occurred but no warning was issued; a false alarm, when a warning was issued, but an event did not occur; and a correct rejection, when no event occurred and no warning was issued (with h the total number of hits, m the total number of misses, f the total number of false alarms and c the total number of correct rejections).

Next to the overall accuracy of the forecast in terms of NS , R_{VE} , Y and NS_H , the accuracy A can also be determined from the contingency table by dividing the sum of the hits and correct rejections by the total observations, see eq. 3.31:

$$A = \frac{h + c}{h + c + m + f} = \frac{h + c}{n} \quad (3.31)$$

The accuracy A value is ranges from 0 to 1, with 1 as the optimum value of A .

The skill of a forecasting model can be represented on the basis of the hit rate H (eq 3.30) and the false-alarm rate F (eq 3.31) [Cloke and Pappenberger, 2009; Martina et al., 2005]. These ratios are also known as the probability of detection and the probability of false detection in other hydrological studies [Velázquez et al., 2010]. H and F indicate, respectively, the proportion of events for which a correct warning was issued and the proportion of non-events for which a false warning was issued by the forecast model. Both ratios can be easily evaluated from the contingency table [Mason, 1982; Demirel et al., 2013].

$$H = \frac{h}{h + m} = \frac{h}{e} \quad (3.32)$$

$$F = \frac{f}{c + f} = \frac{f}{e'} \quad (3.33)$$

Hit rate H and false-alarm rate F have a value ranging between 0 and 1, with 1 as the optimum value of H and 0 as the optimum value of F .

The reliability of a forecasts of a forecasting model can be represented by the hit ratio H' (eq 3.34), which should not be mistaken with the previously discussed hit rate, and conditional miss rate F' (eq 3.35) [Stephenson, 1999]. Where H' is the proportion of warnings for which an event occurred and F' is the proportion of forecasted non-events for which an event occurred. H' is the probability of a correct warning and F' is the probability of an incorrect non-warning, i.e. the probability of a miss.

$$H' = \frac{h}{h + f} = \frac{h}{w} \quad (3.34)$$

$$F' = \frac{m}{m + c} = \frac{m}{w'} \quad (3.35)$$

The hit ratio H' and miss rate F' have a value ranging between 0 and 1, with 1 as the optimum value of H' and 0 the optimum value of F' . The probability of a correct warning, F' , should be at least larger than the base rate B (eq 3.36), which is an estimate of the probability that the event will occur [Stephenson, 1999].

$$B = \frac{h + m}{h + m + f + c} = \frac{e}{n} \quad (3.36)$$

4 Results & Discussion

The HBV model is run as described in the methodology in section 3. The results of the first calibration (section 4.1), sensitivity analysis (section 4.2), final calibration (section 4.3), validation (section 4.4) and forecasting (section 4.5) are shown and discussed in this chapter.

4.1 First calibration step

First a Monte Carlo Simulation of 100,000 runs of the HBV-model is executed by varying eight parameters for both sub basins. The results of the first calibration of sub basin Grande and Mamoré are shown below. Figure 4.1 shows as a function of each parameter for the Grande the combined objective function value Y . Figure 4.2 shows as a function of each parameter for the Mamoré the combined objective function value NS_H . Only parameter sets with an objection function value above zero are shown and the results for which $k_{F\text{-eff}} < k_S$ are left out.

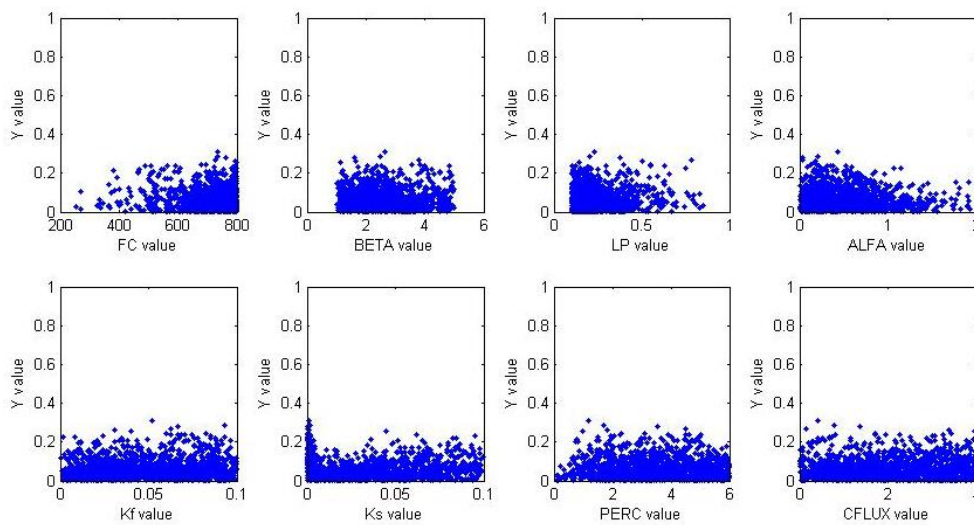


Figure 4.1: Scatter plot of Y -values as a function of parameter values for the Grande for the 1st calibration step. Only Y -values above 0 are shown.

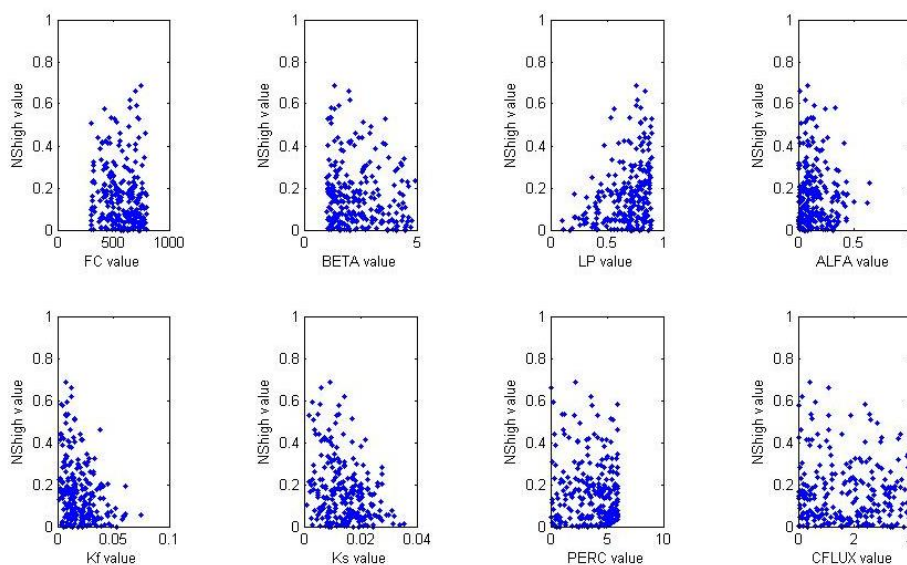


Figure 4.2: Scatter plot of NS_H values as a function of parameter values for the Mamoré for the 1st calibration step. Only Y -values above 0 are shown.

Of the 100,000 runs for both sub basins, only 1.9 % and 1.2% of the parameter sets for sub basin Grande and sub basin Mamoré respectively correspond to an objective function value above 0. Of the parameter sets which have a value above zero, the parameter sets which meet the criterion $k_{F-eff} > k_S$ are selected. This results in 1,3% and 0.2% of the 100,000 runs for Grande and Mamoré respectively, see table 4.1.

Table 4.1: Number of runs of the total of 100,000 runs, which satisfy criterion (1) an objective function value above 0 and (2) both criterion (1) and a k_{F-eff} value larger than the k_S -value. Between brackets the corresponding percentages of the total number of runs.

	Criterion 1		Criterion 2
	Objective Function		Objective function > 0 and $k_{F-eff} > k_S$
	$Y\text{-value} > 0$	$NS_H\text{-value} > 0$	
1st calibration Grande	1,881 (1.9 %)	-	1,295 (1.3%)
Final calibration Grande	30,245 (30 %)	-	30,245 (30 %)
1st calibration Mamoré	-	1,196 (1.2 %)	248 (0.25 %)
Final calibration Mamoré	-	4,068 (4.1 %)	989 (0.99 %)

Table 4.2 shows the results of the first calibration step of Grande quantitatively with the ranges of parameter values corresponding to the selection of runs with a Y-value: > 0.2 and > 0.0. Table 4.3 shows the results of the 1st calibration of Mamoré quantitatively with the ranges of parameter values corresponding to the selection of runs with a NS_H -value: > 0.5 and > 0.0. This information gives insight whether the predefined parameter ranges were wide enough and whether it should be adapted for the final calibration step, see section 4.2.

Table 4.2: Results of the parameter ranges of 1st calibration of Grande for parameters sets with a Y-value >0 and >0.2.

Parameter range:	FC	BETA	LP	ALFA	KF	KS	PERC	CFLUX
	[mm]	[-]	[-]	[-]	[d ⁻¹]	[d ⁻¹]	[mm d ⁻¹]	[mm d ⁻¹]
<i>min</i>	100	1	0.1	0	0.0005	0.0005	0	0
No. of sets <i>max</i>	800	5	0.9	2	0.1	0.1	6	4
39 <i>min [Y > 0.2]</i>	381	1.1	0.11	0.0	0.0018	0.0005	0.8	0.1
<i>max [Y > 0.2]</i>	799	4.8	0.79	1.2	0.10	0.09	5.0	4.0
1,295 <i>min [Y > 0.0]</i>	252	1.0	0.10	0.0	0.0005	0.0005	0.1	0.0
<i>max [Y > 0.0]</i>	800	5.0	0.85	1.9	0.10	0.10	6.0	4.0

Table 4.3: Results of the parameter ranges of 1st calibration of Mamore for parameters sets with a NS_H -value >0 and >0.5.

Parameter range	FC	BETA	LP	ALFA	KF	KS	PERC	CFLUX
	[mm]	[-]	[-]	[-]	[d ⁻¹]	[d ⁻¹]	[mm d ⁻¹]	[mm d ⁻¹]
<i>min</i>	100	1	0.1	0	0.0005	0.0005	0	0
No. of sets <i>max</i>	800	5	0.9	2	0.1	0.1	6	4
12 <i>min [NShigh > 0.5]</i>	304	1.0	0.54	0.02	0.0036	0.0017	0.0	0.0
<i>max [NShigh > 0.5]</i>	751	3.6	0.90	0.33	0.0157	0.0169	5.9	2.6
248 <i>min [NShigh > 0.0]</i>	301	1.0	0.11	0.00	0.0015	0.0009	0.0	0.0
<i>max [NShigh > 0.0]</i>	797	4.9	0.90	0.64	0.0751	0.0355	6.0	4.0

The values of the optimum parameter sets of sub basin Grande and Mamoré are shown in table 4.4. The objective function of sub basin Grande, Y, has a value of 0.31. The objective function of Mamoré,

NS_H , has a value of 0.69. Especially when the Y-values of both basins are compared, the discharge of sub basin Mamoré is simulated much better than of sub basin Grande.

Table 4.4: Parameter values of the optimum parameter set after the 1st calibration and the corresponding objective function values of Grande and Mamoré.

1st Calibration - optimum parameter sets								
Sub basin	FC [mm]	BETA [-]	LP [-]	ALFA [-]	KF [d ⁻¹]	KS [d ⁻¹]	PERC [mm d ⁻¹]	CFLUX [mm d ⁻¹]
Grande	733	2.62	0.229	0.431	0.0519	0.00067	1.19	0.42
Mamoré	751	1.34	0.75	0.080	0.0074	0.0091	2.21	0.43

4.2 Sensitivity analysis

The optimum parameter sets of table 4.4 of Grande and Mamoré are used to execute two sensitivity analyses. The parameters are varied one at a time and the results are shown in figure 4.5 and figure 4.6. In order to compare the parameter values with each other, the parameters are scaled i.e. the adapted value of the parameter is divided by the optimum value, see table 4.4.

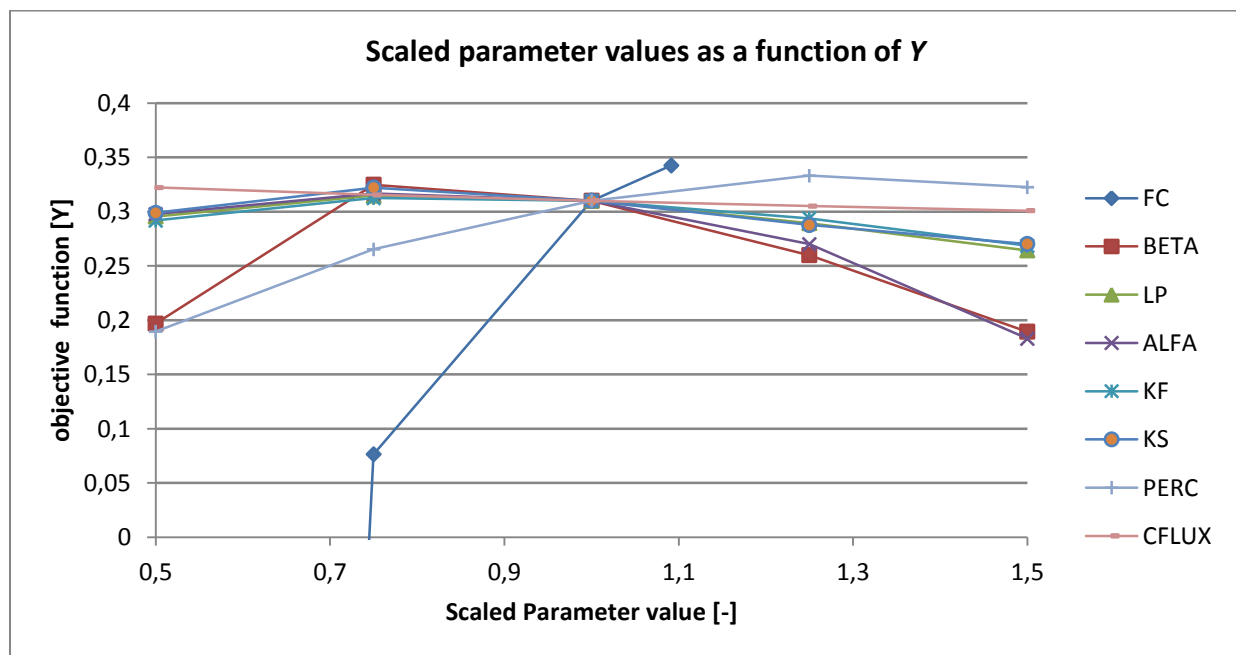


Figure 4.5: Results of the sensitivity analysis of the 8 parameters of sub basin Grande.

The sensitivity analysis in figure 4.5 shows that Y is more sensitive to the parameters *FC*, *BETA*, *ALFA* and *PERC* than the other four parameters. Thus, parameters *FC*, *BETA*, *ALFA* and *PERC* are more important, therefore, these four parameters are varied in the final calibration step. The parameter values belonging to the optimum Y-value of the 1st calibration step, are the default values of the less sensitive parameters *LP*, *k_F*, *k_S* and *CFLUX* during the final calibration step (table 4.4).

After analyzing the results presented in table 4.2, the parameter range of *FC* is adapted from 100 – 800 mm to 300-800 mm. The parameter ranges of the other three parameters are not adapted.

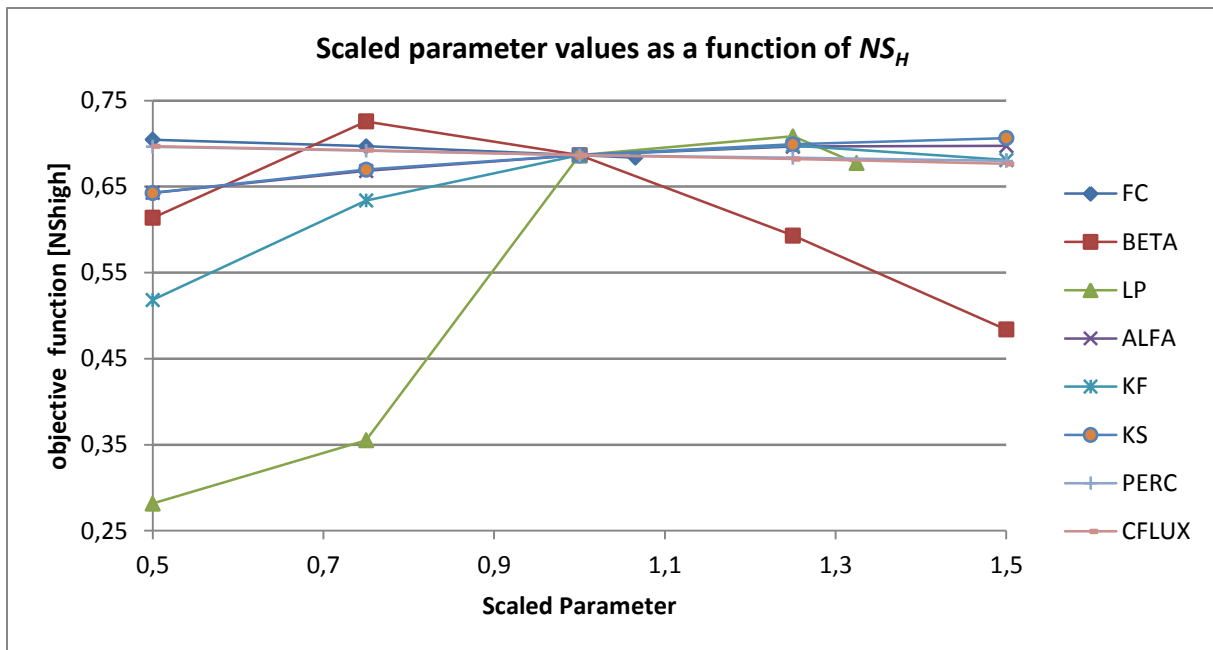


Figure 4.6: Results of the sensitivity analysis of the 8 parameters of sub basin Mamore.

The results of the sensitivity analysis of the Mamoré in figure 4.6 show that NS_H is more sensitive to the parameters *BETA*, *LP*, *ALFA*, k_F and k_S than the other three parameters. Thus, parameters *BETA*, *LP*, *ALFA*, k_F and k_S are more important and therefore, these five parameters are varied in the final calibration step. The parameter values belonging to the optimum NS_H -value of the 1st calibration step are the default values of the less sensitive parameters *FC*, *PERC* and *CFLUX* during the final calibration step (table 4.4).

The five parameters ranges of the parameters to be varied in the final calibration step for sub basin Mamoré are not adapted.

4.3 Final calibration step

Sub basin Grande is calibrated with the four parameters selected in the sensitivity analysis by executing MCS with 100,000 runs. Figure 4.7 shows as a function of each parameter for the Grande the combined objective function value Y , for parameter sets with a minimum Y -value of 0.0. Sub basin Mamoré is calibrated with the five parameters selected after the sensitivity analysis by executing MCS with 100,000 runs. Figure 4.8 shows as a function of each parameter for the Grande the combined objective function value NS_H , for parameter sets with a minimum NS_H -value of 0.0. Table 4.1 shows that of the 100,000 runs for both sub basins, 30.2 % and 4.1 % of the parameter sets for sub basin Grande and sub basin Mamoré respectively correspond to an objective function value above 0. Of the parameter sets which have a value above zero, the parameter sets which meet the criterion $k_{F-eff} > k_s$ are selected. This results in 30.2% and 0.99% of the 100,000 runs for Grande and Mamoré respectively. These percentages of the final calibration step are considerably higher, than those of the first calibration step (see table 4.1).

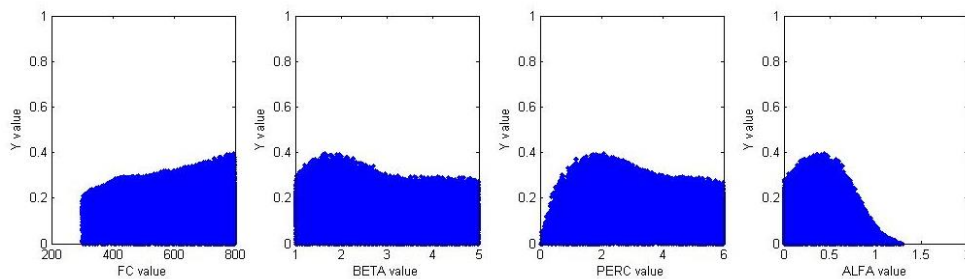


Figure 4.7 : Scatter plot of Y -values as a function of parameter values for the Grande for the final calibration step. Only Y -values above 0 are shown.

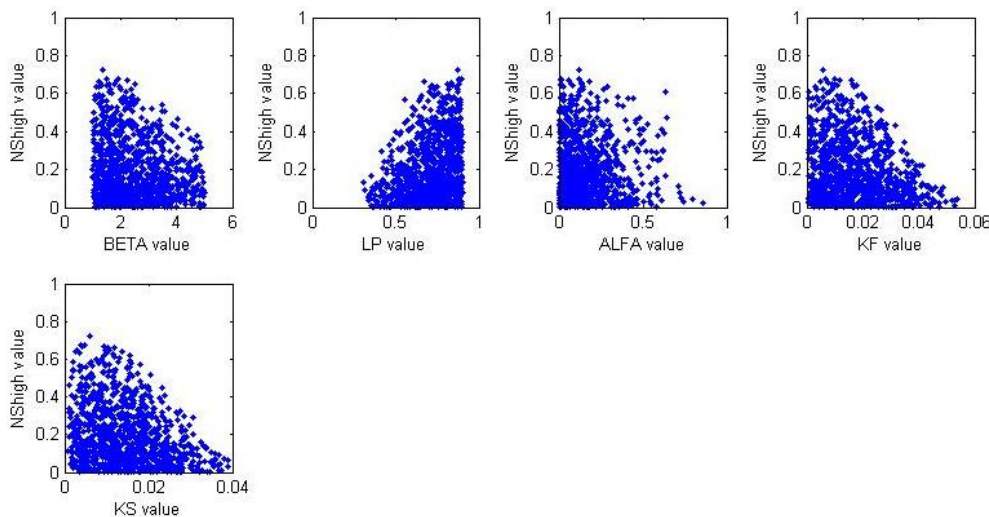


Figure 4.8: Scatter plot of NS_H values as a function of parameter values for the Mamoré for the final calibration step. Only NS_H -values above 0 are shown.

The shapes of the scatter plots of parameter $BETA$, $PERC$ and $ALFA$ of sub basin Grande (see figure 4.7) give confidence that their optimum values are actually the global optimum values. This because the scatter plot shows a curve with the highest Y -value on top of this curve. The shape of the scatter plot of parameter FC gives less confidence that the optimum parameter value is the actual optimum value. The scatter plot shows an ascending line towards the upper boundary of the parameter range

of *FC*. It seems that the parameter range of parameter *FC* for sub basin Grande (300 mm – 800 mm) of the final calibration step is too narrow. Subsequently, the upper boundary with a value of 800 mm, should have been adapted after the first calibration step to a higher value, in order to gain more confidence that the optimum value of *FC* corresponding to the highest value of the objective function is actually the optimum value.

The shapes of the scatter plot of parameter k_s , k_f and *ALFA* of sub basin Mamoré (see figure 4.8) give confidence that their optimum values set are actually the global optimum values for the same reason for parameters *BETA*, *PERC* and *ALFA* of sub basin Grande, as described above. Because the number of points in the scatter plot of sub basin Grande are a factor 7 larger than those of sub basin Mamoré, the curves of the scatter plots are less smooth for sub basin Mamoré. The shapes of the scatter plots of the parameters *LP* and *BETA* of sub basin Mamoré give less confidence that the optimum parameter value is the actual optimum value. The scatter plot of *LP* shows an ascending line and the scatter plot of *BETA* shows a descending line, which indicates that the boundaries of both parameter ranges (*LP*: 0.1 – 0.9 and *BETA*: 1 – 5) are too narrow. The upper boundary of the parameter range of *LP* and the lower boundary of the parameter range of *BETA* should have been adapted after the first calibration. But the value of *BETA* has a boundary condition that is should be >1. It seems that the parameter range of the final calibration step for *LP* is are too narrow and the parameter range for *BETA* is wide enough.

The values of the optimum parameter sets of sub basin Grande and Mamoré are shown in table 4.5. The objective function of Grande, *Y*-value, has a value of 0.39. The objective function of Mamoré, NS_H , has a value of 0.72. The objective function values of both sub basins are higher compared to the objective function values of the optimum parameter sets of the 1st calibration. The simulated discharge with the optimum parameter set for Grande and the observed discharge at Abapó for the calibration period are shown in figure 4.9. The simulated discharge with the optimum parameter set for Mamoré, the observed discharge at Camiaco, the observed discharge at Abapó and the reservoir volume are shown in figure 4.10.

Table 4.5: Parameter values of the optimum parameter sets after the final calibration step and the corresponding objective function values of Grande and Mamoré.

Final Calibration step - optimum parameter sets													
<i>Sub basin</i>	<i>FC</i> [mm]	<i>BETA</i> [-]	<i>LP</i> [-]	<i>ALFA</i> [-]	<i>KF</i> [d ⁻¹]	<i>KS</i> [d ⁻¹]	<i>PERC</i> [mm d ⁻¹]	<i>CFLUX</i> [mm d ⁻¹]	<i>KF-eff</i>	<i>NS</i>	<i>RVE</i>	<i>Y</i>	<i>NS_H</i>
Grande	795	1.65	0.23	0.43	0.052	0.00067	2.1	0.42	0,14	0.42	0.066	0.39	-
Mamoré	751	1.37	0.87	0.12	0.0059	0.0060	2.21	0.43	0.011	0.82	0.082	0.76	0.72

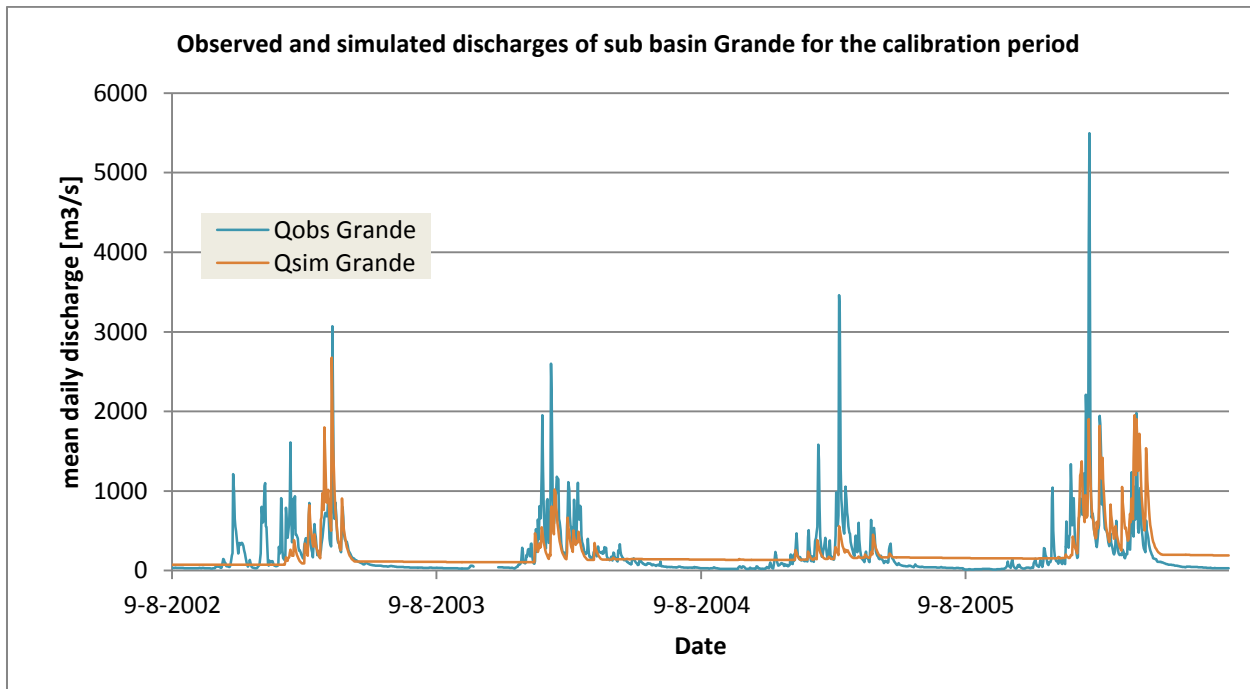


Figure 4.9: Hydrograph of the observed Q_{obs} and simulated discharge Q_{sim} of Grande after the final calibration.

The hydrographs of Q_{simG} and Q_{obsG} show four wet periods, see figure 4.9. The hydrograph of the Q_{simG} shows lower peak discharges in comparison with Q_{obsG} for the first three wet periods, but at the fourth wet period, some peaks of Q_{simG} are higher than the peaks of Q_{obsG} . These differences may be caused by the set-up of the model, where the areal mean precipitations is just based on a few meteorological stations.

In general Q_{simG} underestimates the observed discharge peaks. These underestimations may be caused by the value of parameter FC , because the model run with the optimum parameter values shows that the direct runoff, q_d , for every time step is 0. As equation 3.2 shows, the direct runoff is controlled by the soil moisture storage, the precipitation and the field capacity. Because direct runoff never occurs, the field capacity is never reached. This means that the runoff is generated through the soil moisture box into the upper and lower response box, which is a slower.

In the dry periods the Q_{simG} shows a flat hydrograph that overestimates the observed discharge. It seems that the base flow, the slow runoff, is overestimated by the model. Further, some of the observed discharge peaks are completely missed by the simulated discharge, which could be caused by the estimation of the areal mean precipitation, which differs from the actual precipitation, which can be locally variable.

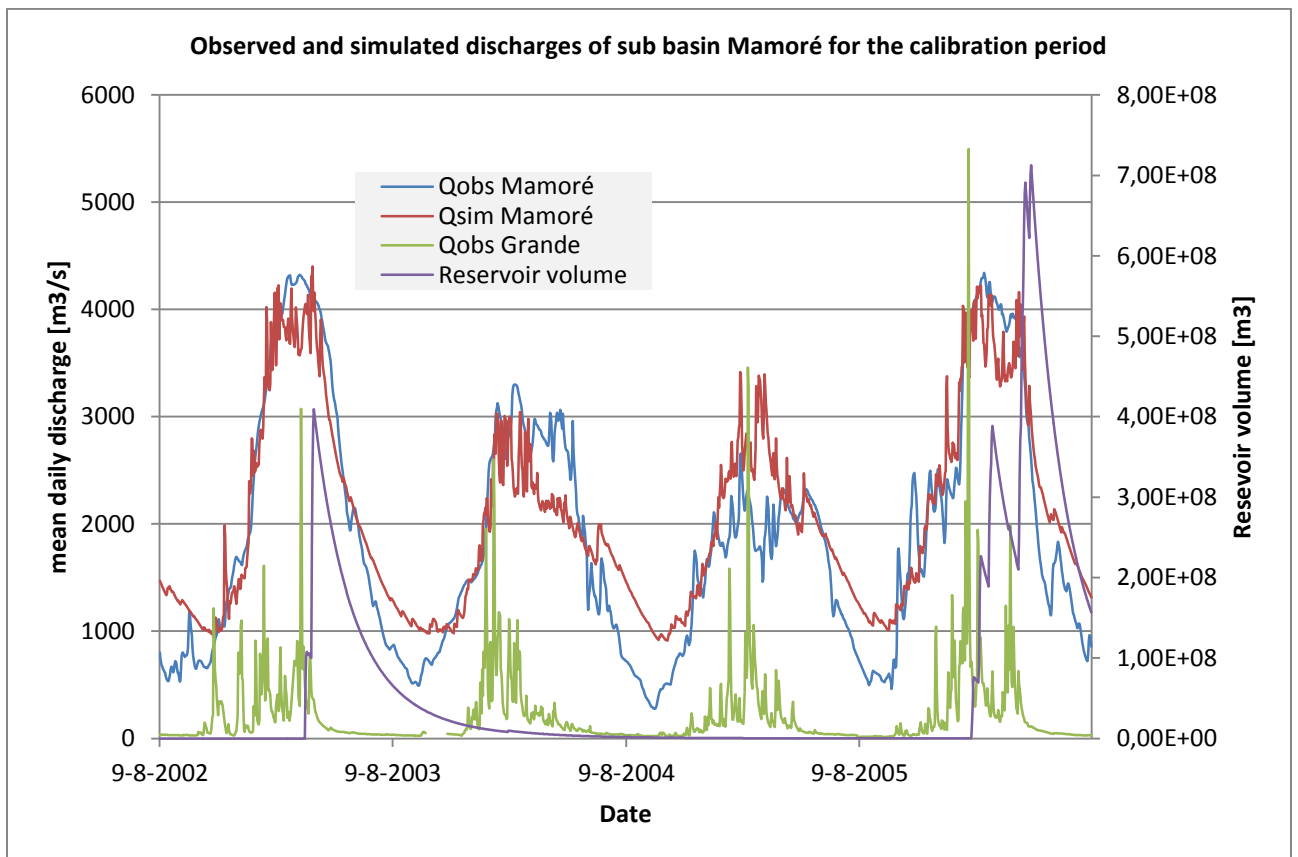


Figure 4.10: Hydrograph of Mamore of the observed discharge, simulated discharge, observed discharge of Grande and storage of the reservoir after the calibration.

The simulated discharge Q_{simM} follows the hydrograph of the observed discharge Q_{obsM} reasonably well at the rise of a high discharge peak, but underestimates the height of such a peak and at the fall of a high discharge peak the model tends to react slower than the observed discharge, see figure 4.10. The objective function of the model during the calibration was NS_H , which calculates the NS -value for all discharges above the threshold $1,500 \text{ m}^3/\text{s}$. The aim of the calibration was to simulate the periods of high water. Low water periods are less important in this study and therefore not taken into account in de calibration process. This is visible in the relatively large differences between the hydrographs of Q_{obs} Mamoré and Q_{sim} Mamoré when Q_{obs} is below the threshold $1,500 \text{ m}^3/\text{s}$.

The peaks of the observed discharge of the Grande are visible with a lag time of 17 days in the simulated discharge.

The Mamoré sub basin is also modeled with the simulated discharge of sub basin Grande as inflow instead of the observed discharge. The results in terms of the objective function are shown in the table 4.6. Notice that the values of the four objective functions show that the model performs better with the simulated discharge of the Grande than with the observed discharge.

Table 4.6: Values of the objective functions of Mamore with observed and simulated discharge of Grande as input into the Mamore basin.

	NS	RVE	Y	NS-high
Calibration run with Q_{obsG}	0.79	0.089	0.73	0.70
Calibration run with Q_{simG}	0.82	0.082	0.76	0.72

The hydrograph of the simulated discharge with the simulated discharge of the Grande as inflow and the observed discharge of Mamoré are shown in the figure 4.11 below.

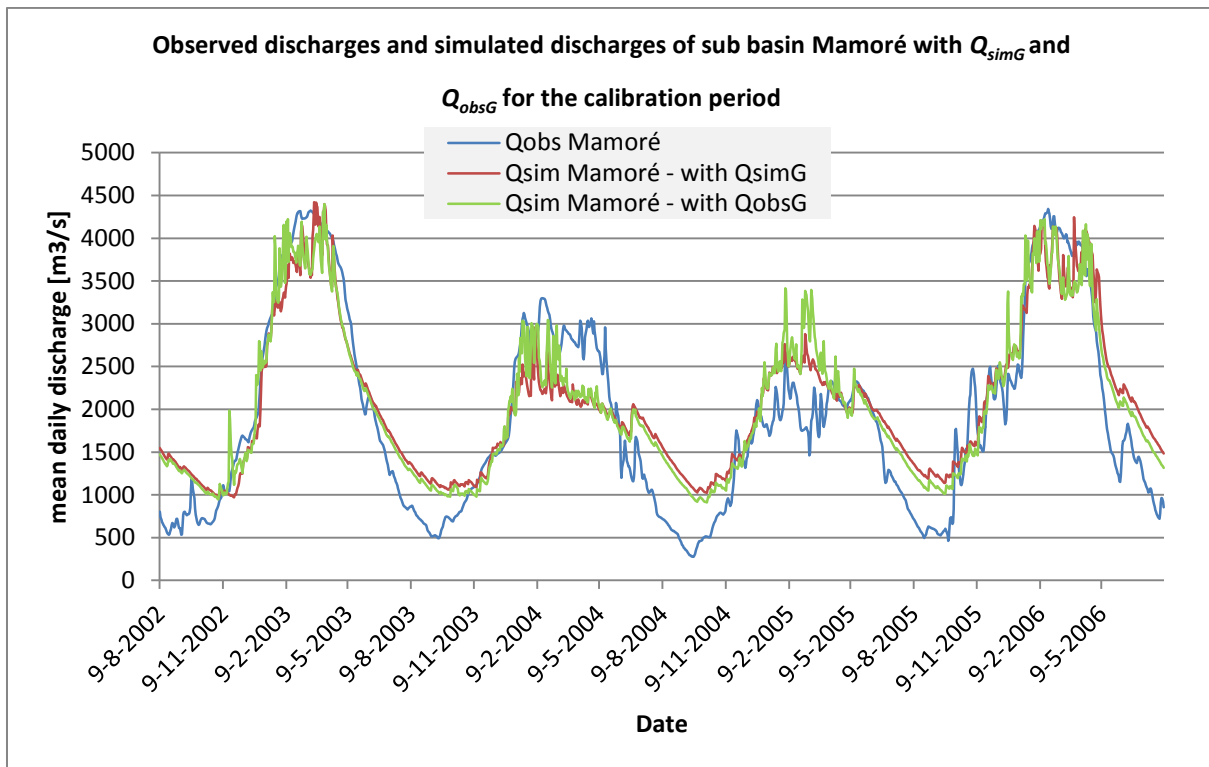


Figure 4.11: Hydrograph of Mamore of the observed discharge, simulated discharge with simulated discharge of Grande and simulated discharge with observed discharge of Grande after the calibration.

The hydrographs of Q_{sim} with Q_{obsG} as input (green line of figure 4.11) and Q_{sim} with Q_{simG} as input (red line of figure 4.11) look quite similar, with the difference that the red line is slightly fluctuating at peak discharges compared to the green line, which can be explained by fact that this are the same differences visible in the calibration of sub basin Grande, see figure 4.9.

4.4 Validation

In the validation procedure, the parameter values derived in the calibration are used to run the model for another period. The validation period follows after the calibration period from 8-8-2006 till 7-5-2009, see figure 3.5. Since the calibration of sub basin Mamoré performs better when the simulated discharge of sub basin Grande Q_{simG} is used as input, compared to the observed discharge of sub basin Grande Q_{obsG} , Q_{simG} is used as input during the validation run of sub basin Mamoré with the same lag time of 17 days as used in the calibration.

In figure 4.12 and figure 4.13 the outcome of the validation runs is shown. The blue line is the observed discharge and the red line is the simulated discharge. Figure 4.13 shows the simulated discharge of the Grande and the storage of the reservoir as well. When looking at figure 4.12, the same trend is visible as in the calibration process: in the dry periods an overestimation of the observed discharge by the model and at discharge peaks, the model is not able to simulate the height of the peaks of sub basin Grande. But in comparison to the calibration procedure in the validation period the model is able to simulate the discharge peaks in terms of timing, where in the calibration run some of the discharge peaks are missed by the model. The reason for this could be that the estimated areal mean precipitation for the validation period are estimated closer to the actual precipitation in terms of timing.

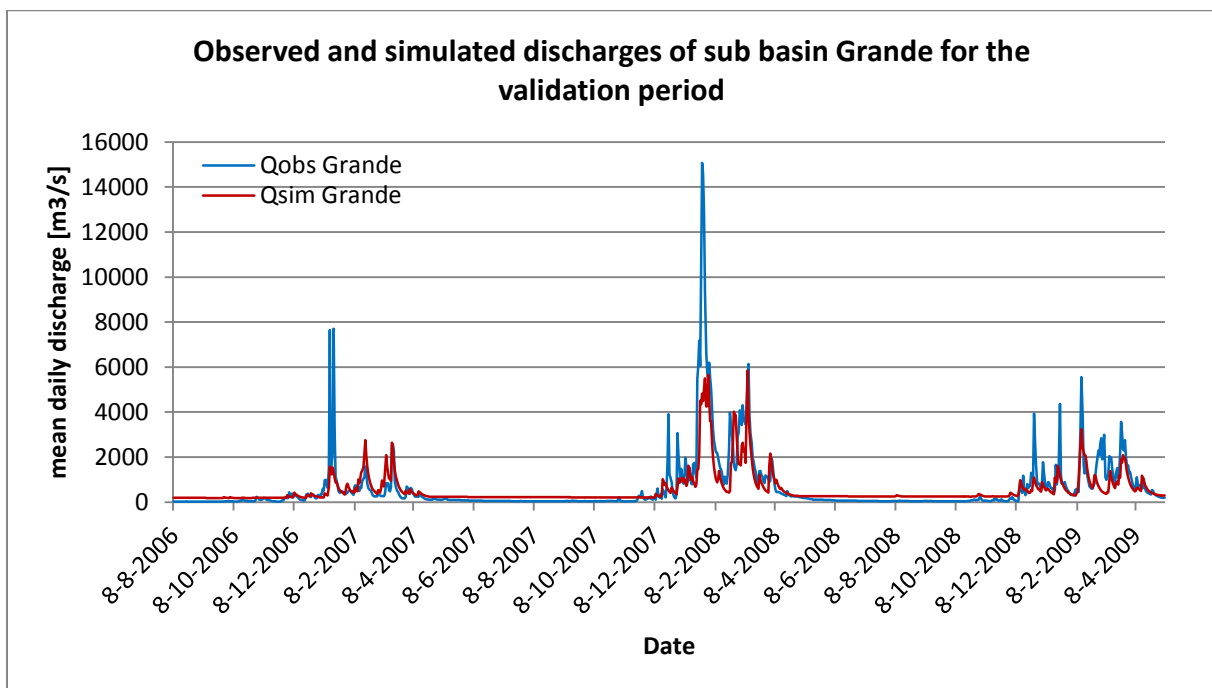


Figure 4.12: Hydrograph of the discharge of sub basin Grande after validation.

When looking at the results of the validation of sub basin Mamoré, figure 4.13, like sub basin Grande, the same trends are noticeable as in the calibration process: overestimation of the discharge after a peak discharge. The simulated discharge of the second wet period of the validation period is highly fluctuating, due to the outflow of the reservoir. Further, as opposed to the simulated discharge of the calibration period, the height of the discharge peaks are reached and especially during the second high water period, overestimated. This could be caused by the poor estimation of the areal mean precipitation and the contribution of outflow of the reservoir to the total discharge.

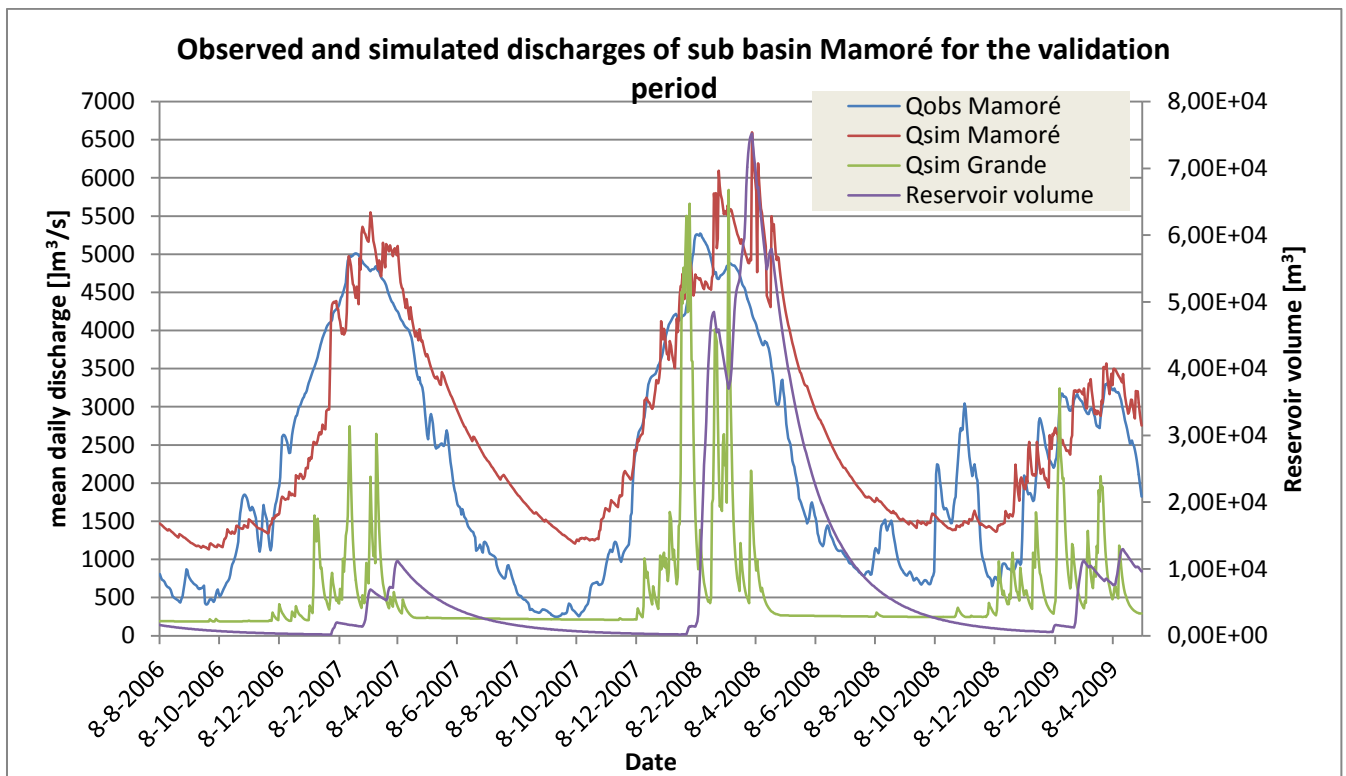


Figure 4.13: Hydrograph of Mamore of the observed discharge, simulated discharge, simulated discharge of Grande and storage of the reservoir after the validation.

Table 4.7 shows the objective functions of the calibration and validation in order to compare both periods. Notice the increase in the Y-value of sub basin Grande from 0.39 in the calibration to 0.54 in the validation. This is a surprising result, since the parameter values are optimized during the calibration procedure in order to see how well these parameter values perform for another period. The reason for this could be that the meteorological input data of the validation period are much closer to the actual meteorological input data of the calibration period. Another reason could be that observed discharge data of the calibration period is of less quality than the validation period.

The NS_H value of sub basin Mamoré decreased from 0.74 in the calibration to 0.51 in the validation. The overestimation of the simulated discharge during the second wet period could be a major contributor to this performance difference.

Table 4.7: Results Validation of Grande and Mamoré basins.

		NS	R_{VE}	Y	NS_H
Grande	Calibration	0.42	0.066	0.39	-
	Validation	0.60	-0.098	0.54	-
Mamoré	Calibration	0.79	0.089	0.73	0.72
	Validation	0.67	0.21	0.55	0.51

4.5 Forecasting

4.5.1 Reference run

The optimized parameter set obtained during the final calibration is used to run the model again for the calibration period. For each time step the fractions of fast runoff q_f , slow runoff q_s and outflow of the reservoir q_R to simulated mean daily discharge q_{simM} are determined. These fractions are plotted against the simulated daily discharge q_{simM} and shown in figure 4.14, 4.15 and 4.16. The black line in these figures is the trendline through these points.

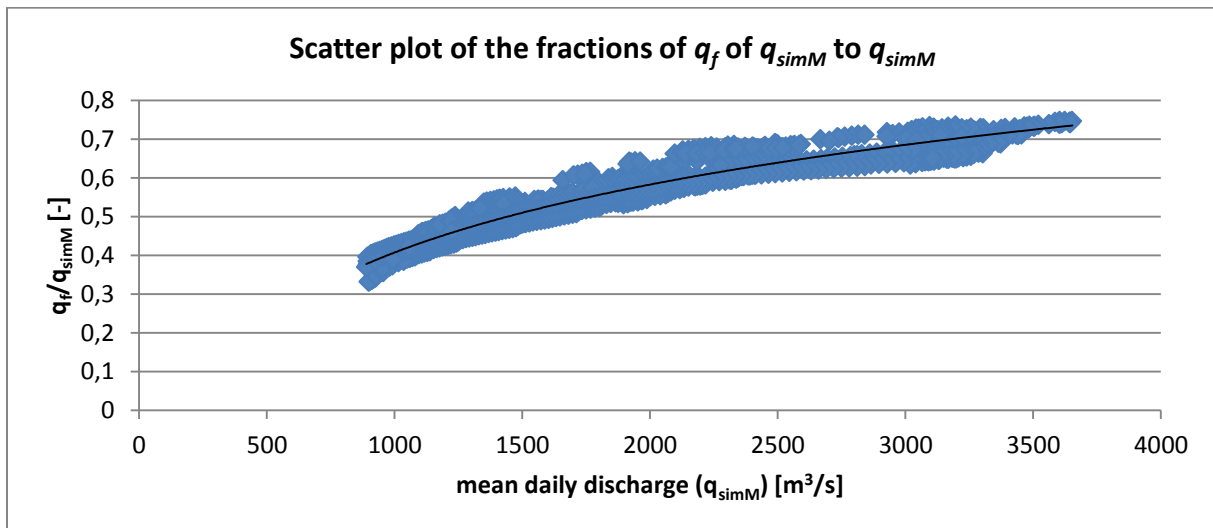


Figure 4.14: The fractions of fast runoff q_f of the discharge q_{simM} to the discharge q_{simM} for each time step (blue dots) and the trendline in black through those points.

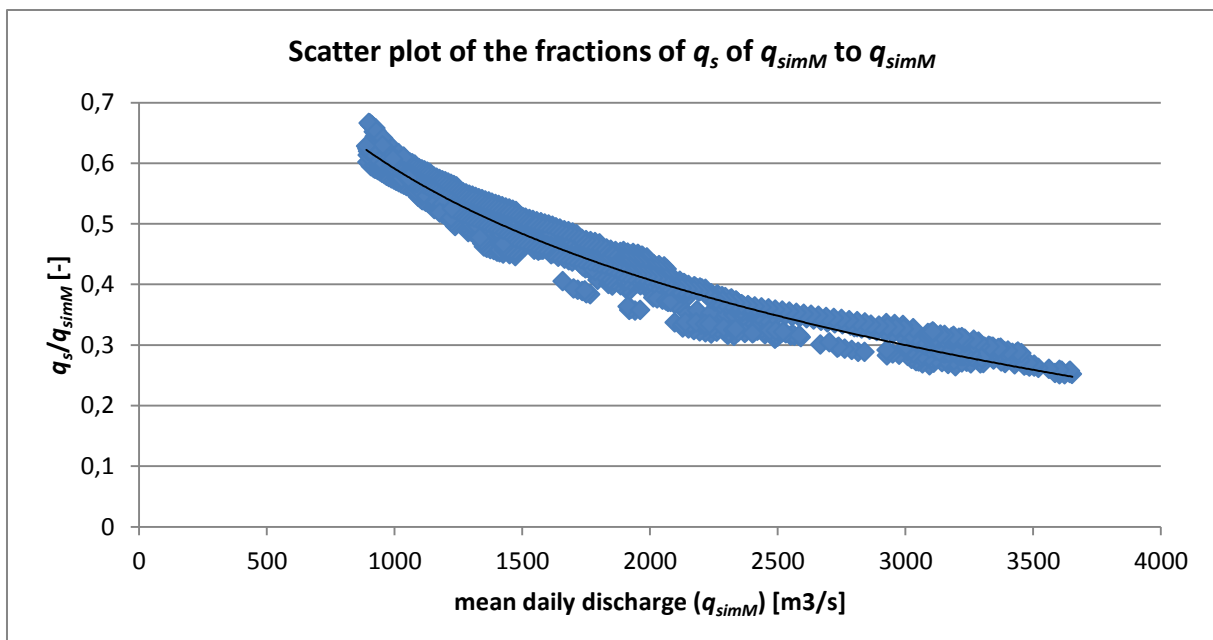


Figure 4.15: The fractions of slow runoff q_s of the discharge q_{simM} to the discharge q_{simM} for each time step (blue dots) and the trendline in black through those points.

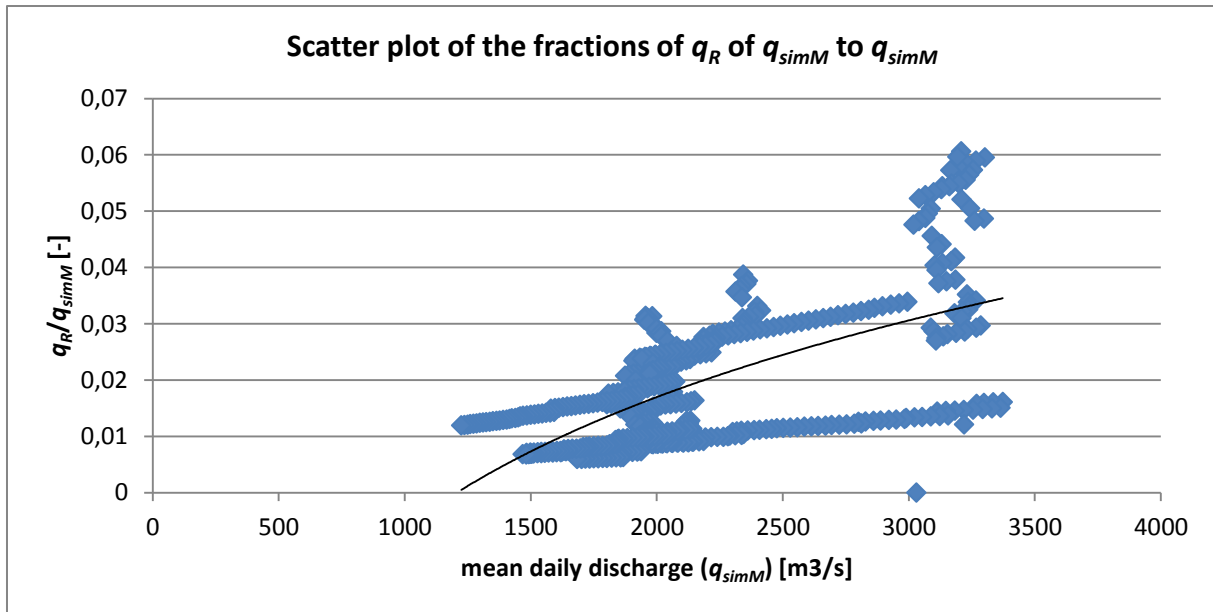


Figure 4.16: The fractions of outflow of the reservoir q_R of the discharge q_{simM} to the discharge q_{simM} for each time step (blue dots) and the trendline in black through those points.

The logarithmic relations between the fraction values and the simulated discharge are shown in table 4.8, together with the corresponding Pearson's coefficients R .

Table 4.8: Logarithmic equations of the trendlines of figure 14, figure 15 and figure 16 with the corresponding value of R .

Equation	Pearson's coefficient R
$k_{qf} = 0.25 * \ln(q_{simM}) - 1.3$	0.93
$k_{qs} = -0.27 * \ln(q_{simM}) + 2.4$	0.96
$k_{qR} = 0.033 * \ln(q_{simM}) - 0.24$	0.40

The trendlines of the fractions of fast runoff and slow runoff to the simulated discharge fit quite well, with a R value of 0.93 and 0.96 respectively. But the trendline of the fraction of outflow of the reservoir to the simulated discharge does not fit well, with a R value of 0.40. This means that there is no clear relation between the magnitude of the discharge and the fraction of the outflow of the reservoir (see also fig 4.16). Which makes sense, because the reservoir storage is controlled by the simulated discharge of Grande, which makes the outflow of the reservoir dependent of the simulated discharge of Grande, see equation 3.13 in section 3.1.5. In the calibration period the reservoir fills roughly twice at high water periods; during the first high water period of the first hydrological year and during the high water period of the fourth hydrological year. This explains the two descending lines of points of the scatter plot of figure 4.16. The randomness of the fractions of q_R to q_{simM} between $q_{simM} = 3,000 \text{ m}^3/\text{s}$ and $q_{simM} = 3,400 \text{ m}^3/\text{s}$ is caused by the refills of the reservoir in the fourth wet period, see figure 4.10. Because the fraction of q_R to q_{simM} is small (up to 6%) and thus has not a large influence on the simulated discharge. Therefore equation 5.3 is, despite its uncertainty, used in this study for updating and forecasting discharges.

The equations of k_{qf} , k_{qs} and k_{qR} of table 4.8 are used for updating as described in section 3.7, with the difference that q_{simM} is substituted for q_{obsM} .

4.5.2 Forecasting

The HBV-model is run using the updating method, described in section 3.3, and the 1 to 10 days ahead forecasted discharges are determined for the validation period with 'perfect' weather predictions. In order to observe the differences between the forecasting days, only the results of forecasted discharge of 3, 6 and 10 days ahead are shown in figure 4.17. The results in terms of accuracy are shown in table 4.9.

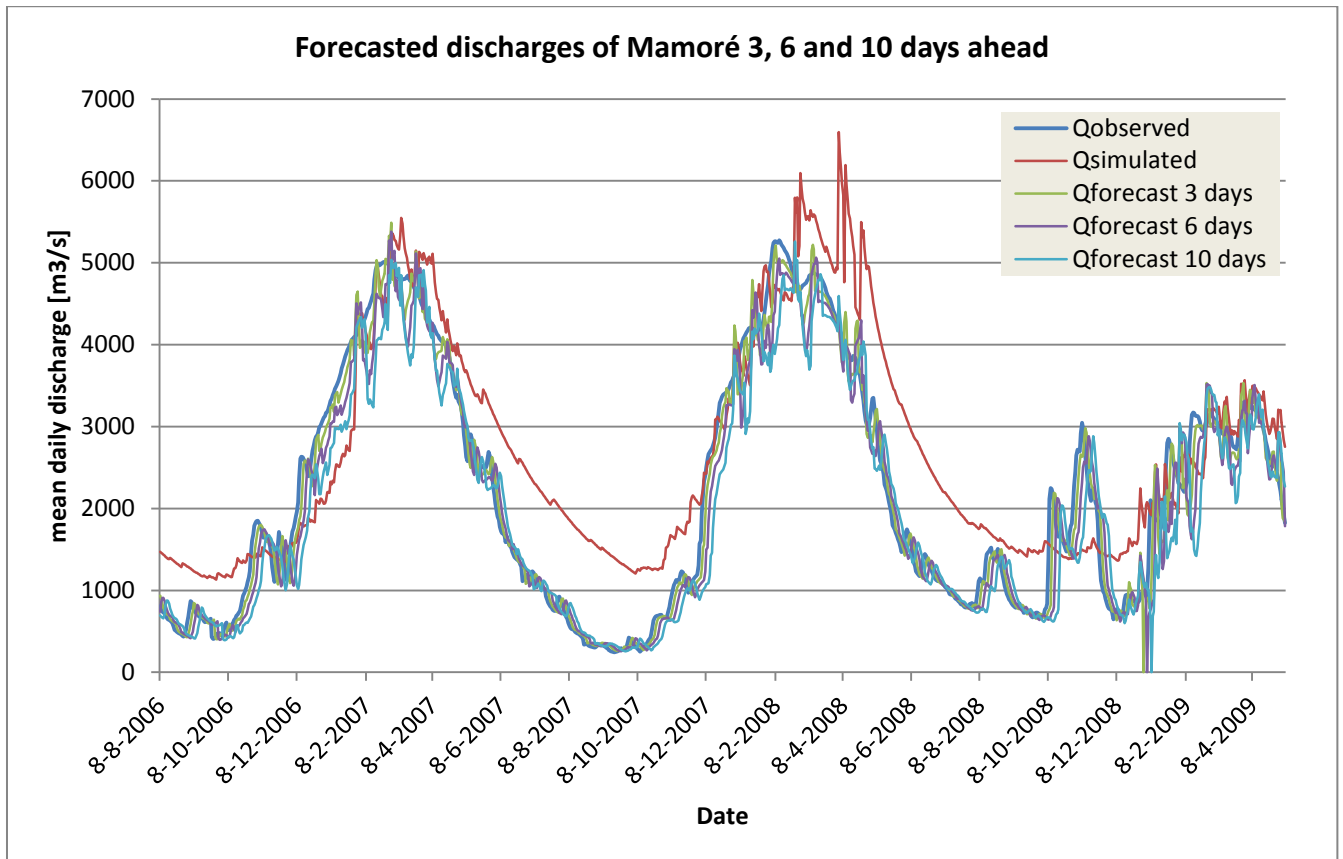


Figure 4.17: Results of the updating procedure with forecasted discharges of 3, 6 and 10 days ahead.

Table 4.9 shows that the forecasted discharges up to 10 days ahead perform better in terms of the objective functions NS , R_{VE} , Y and NS_H compared to the reference simulated discharge without reservoir updating. The more days ahead the discharges are forecasted, the less accurate they perform in terms of the values of the objective functions, which makes sense.

The hydrographs of the forecasted discharges seems to approach the observed discharge reasonably well, especially compared to the simulated discharge. The results shown in table 4.9 endorse this performance. When looked closely to figure 4.17, the hydrographs of the forecasted discharges tend to approach the observed hydrographs with a delay of the forecasting time (3, 6 and 10 days). Also the trend of the simulated discharge is visible in the corresponding forecasted discharges, as you would expect.

Table 4.9: Results of the updating procedure of forecasted discharges 1 to 10 days ahead in terms of objective functions with as reference the not-updated simulated discharge.

	NS	R_{VE}	Y	NS_H
<i>Qsim</i>	0.55	0.67	0.21	0.51
<i>Qforecast 1 day</i>	0.99	-0.01	0.99	0.99
<i>Qforecast 2 days</i>	0.98	-0.01	0.97	0.96
<i>Qforecast 3 days</i>	0.97	-0.02	0.95	0.93
<i>Qforecast 4 days</i>	0.96	-0.03	0.93	0.90
<i>Qforecast 5 days</i>	0.95	-0.04	0.91	0.86
<i>Qforecast 6 days</i>	0.94	-0.05	0.89	0.83
<i>Qforecast 7 days</i>	0.92	-0.05	0.88	0.79
<i>Qforecast 8 days</i>	0.91	-0.06	0.86	0.76
<i>Qforecast 9 days</i>	0.89	-0.07	0.84	0.72
<i>Qforecast 10 days</i>	0.88	-0.08	0.82	0.69

The results of forecasting 1 up to 10 days ahead in terms of skill are shown in contingency tables, table 4.10 to 4.13.

As mentioned before (section 3.3.2) this study takes two types of events into account:

- Event type 1: ‘the exceedance of a discharge threshold at time step t ’
- Event type 2: ‘the exceedance of a discharge threshold at time step t , with the condition that at time step $t-1$ this threshold was not exceeded’.

The contingency tables of event type 1 of the 1 to 10 days ahead forecasts, with as reference the simulated discharge without updating, are shown in table 4.10 and 4.11, together with the accuracy hit rates, false-alarm rates, miss rates, hit ratios and the base rates. Table 4.10 shows the results of the event type 1 for high water with a threshold of 3,000 m³/s and table 4.11 shows the results of the event type 1 for floods with a threshold of 3,900 m³/s as described in section 3.3.2.

Table 4.10: Contingency tables (with number of hits h , number of misses m , number of false-alarms f and number of correct rejections c) of the 1 up to 10 days ahead forecasted discharges and the reference simulated discharges and their accuracy A , hit rates H , false-alarm rates F , hit ratios H' , miss rate F' and the base rate B of the event type 1 with threshold of 3,000 m³/s for the validation period.

Event type 1 <i>High water level</i>	Contingency tables				A	H	F	H'	F'	B
	h	m	f	c						
<i>Qsim</i>	268	45	84	607	0.87	0.86	0.12	0.76	0.07	0.31
<i>Qforecast 1 day</i>	303	10	8	683	0.98	0.97	0.01	0.97	0.01	0.31
<i>Qforecast 2 days</i>	296	17	10	681	0.97	0.95	0.01	0.97	0.02	0.31
<i>Qforecast 3 days</i>	287	26	12	679	0.96	0.92	0.02	0.96	0.04	0.31
<i>Qforecast 4 days</i>	279	34	11	680	0.96	0.89	0.02	0.96	0.05	0.31
<i>Qforecast 5 days</i>	276	37	11	680	0.95	0.88	0.02	0.96	0.05	0.31
<i>Qforecast 6 days</i>	275	38	10	681	0.95	0.88	0.01	0.96	0.05	0.31
<i>Qforecast 7 days</i>	268	45	6	685	0.95	0.86	0.01	0.98	0.06	0.31
<i>Qforecast 8 days</i>	267	46	6	685	0.95	0.85	0.01	0.98	0.06	0.31
<i>Qforecast 9 days</i>	266	47	6	685	0.95	0.85	0.01	0.98	0.06	0.31
<i>Qforecast 10 days</i>	264	49	7	684	0.94	0.84	0.01	0.97	0.07	0.31

Table 4.11: Contingency tables (with number of hits h , number of misses m , number of false-alarms f and number of correct rejections c) of the 1 up to 10 days ahead forecasted discharges and the reference simulated discharges and their accuracy A , hit rates H , false-alarm rates F , hit ratios H' , miss rate F' and the base rate B of the event type 1 with threshold of $3,900 \text{ m}^3/\text{s}$ for the validation period.

Event type 1 Flood level	Contingency tables				A	H	F	H'	F'	B
	h	m	f	c						
<i>Qsim</i>	168	19	44	773	0.94	0.90	0.05	0.79	0.02	0.19
<i>Qforecast 1 day</i>	183	4	2	815	0.99	0.98	0.00	0.99	0.00	0.19
<i>Qforecast 2 days</i>	179	8	4	813	0.99	0.96	0.00	0.98	0.01	0.19
<i>Qforecast 3 days</i>	171	16	7	810	0.98	0.91	0.01	0.96	0.02	0.19
<i>Qforecast 4 days</i>	162	25	11	806	0.96	0.87	0.01	0.94	0.03	0.19
<i>Qforecast 5 days</i>	155	32	11	806	0.96	0.83	0.01	0.93	0.04	0.19
<i>Qforecast 6 days</i>	144	43	12	805	0.95	0.77	0.02	0.92	0.05	0.19
<i>Qforecast 7 days</i>	140	47	8	809	0.95	0.75	0.01	0.95	0.05	0.19
<i>Qforecast 8 days</i>	137	50	8	809	0.94	0.73	0.01	0.94	0.06	0.19
<i>Qforecast 9 days</i>	136	51	7	810	0.94	0.73	0.01	0.95	0.06	0.19
<i>Qforecast 10 days</i>	133	54	6	811	0.94	0.71	0.01	0.96	0.06	0.19

Table 4.10 shows that the accuracy A of the forecasted discharges 1 to 10 days ahead ($A \geq 0.94$) is higher than the accuracy of the simulated discharges ($A = 0.87$), for events type 1 with a high water level threshold. This difference is caused by the relatively low number of correct rejections of *Qsim* compared to the *Qforecasts*. This is confirmed by the False-Alarm rates of *Qsim* and *Qforecasts*: F of *Qsim* is 0.12 and the F of *Qforecasts* ≤ 0.02 . In terms of hit rates for the high water threshold, the *Qforecasts* up to 7 days ahead perform better than *Qsim*, see table 4.10. The probabilities of a correct warning H' , are high for *Qforecasts* (H' is close to 1). Although the probability of a correct warning H' is less high for *Qsim*, compared to *Qforecasts*, it is much higher than the base rate B . The probability of a miss F' is low for *Qsim* and the *Qforecasts* ($F' \leq 0.07$), which is partly caused by the high number of correct rejections.

Table 4.11 shows that the accuracy A of the *Qforecasts* ($A \leq 0.94$) is at least as good as the accuracy of *Qsim* ($A = 0.94$) for events type 1 with a flood level threshold. Notice the difference in formation of A : *Qsim* has a relatively low number of correct rejections (thus a high number of false alarms), but a relatively high number of hits (thus a low number of misses) compared to the *Qforecasts*. By the determination of A , no distinctions are made between one hit and one correct rejections. Otherwise, a miss has an equal weight as a false-alarm in determining accuracy A , where in reality a miss of an event causes more damage than an false-alarm. The difference in performance between *Qsim* and *Qforecasts* is noticeable when looking at the hit rate H . From forecasts 4 days ahead to 10 days ahead, *Qsim* performs better in terms of hit rates H and miss rates F' . The false-alarm rates F of event type 1 with a flood level threshold are low, due to the small number of false alarms and the high number of correct rejections, where *Qsim* performs the worst compared to the *Qforecasts*.

In general for event type 1 for both thresholds applies that as the number of forecasting days ahead increase, the accuracy A and the hit rates H decrease. For both thresholds for event type 1 applies that hit ratios are higher for the *Qforecasts* compared to *Qsim*, nevertheless for both *Qsim*s are applies that the hit ratios are above the base rate B .

The contingency tables of event type 1 of the 1 to 10 days ahead forecasts, with as reference the simulated discharge without updating, are shown in table 4.10 and 4.11, together with the hit rates, false-alarm rates and odds. Table 4.12 shows the results of the event type 2 for high water with a threshold of 3,000 m³/s and table 4.13 shows the results of the event type 1 for floods with a threshold of 3,900 m³/s as described in section 3.3.2.

Table 4.12: Contingency tables (with number of hits *h*, number of misses *m*, number of false-alarms *f* and number of correct rejections *c*) of the 1 up to 10 days ahead forecasted discharges and the reference simulated discharges and their accuracy *A*, hit rates *H*, false-alarm rates *F*, hit ratios *H'*, miss rate *F'* and the base rate *B* of the event type 2 with threshold of 3,000 m³/s for the validation period.

Event type 2 High water level	Contingency tables				A	H	F	H'	F'	B
	h	m	f	c						
<i>Qsim</i>	0	6	8	990	0.99	0	0.01	0.00	0.01	0.01
<i>Qforecast 1 day</i>	0	6	10	988	0.98	0	0.01	0.00	0.01	0.01
<i>Qforecast 2 days</i>	0	6	9	989	0.99	0	0.01	0.00	0.01	0.01
<i>Qforecast 3 days</i>	0	6	9	989	0.99	0	0.01	0.00	0.01	0.01
<i>Qforecast 4 days</i>	0	6	8	990	0.99	0	0.01	0.00	0.01	0.01
<i>Qforecast 5 days</i>	0	6	8	990	0.99	0	0.01	0.00	0.01	0.01
<i>Qforecast 6 days</i>	0	6	10	988	0.98	0	0.01	0.00	0.01	0.01
<i>Qforecast 7 days</i>	1	5	7	991	0.99	0.17	0.01	0.13	0.01	0.01
<i>Qforecast 8 days</i>	1	5	10	988	0.99	0.17	0.01	0.09	0.01	0.01
<i>Qforecast 9 days</i>	0	6	8	990	0.99	0.01	0.01	0.00	0.01	0.01
<i>Qforecast 10 days</i>	0	6	8	990	0.99	0.01	0.01	0.00	0.01	0.01

Table 4.13: Contingency tables (with number of hits *h*, number of misses *m*, number of false-alarms *f* and number of correct rejections *c*) of the 1 up to 10 days ahead forecasted discharges and the reference simulated discharges and their accuracy *A*, hit rates *H*, false-alarm rates *F*, hit ratios *H'*, miss rate *F'* and the base rate *B* of the event type 2 with threshold of 3,900 m³/s for the validation period.

Event type 2 Flood level	Contingency tables				A	H	F	H'	F'	B
	h	m	f	c						
<i>Qsim</i>	0	2	5	997	0.99	0	0.01	0.00	0.00	0.00
<i>Qforecast 1 day</i>	1	1	3	999	1.00	0.5	0.00	0.25	0.00	0.00
<i>Qforecast 2 days</i>	0	2	5	997	0.99	0	0.01	0.00	0.00	0.00
<i>Qforecast 3 days</i>	0	2	10	992	0.99	0	0.01	0.00	0.00	0.00
<i>Qforecast 4 days</i>	0	2	9	993	0.99	0	0.01	0.00	0.00	0.00
<i>Qforecast 5 days</i>	0	2	10	992	0.99	0	0.01	0.00	0.00	0.00
<i>Qforecast 6 days</i>	0	2	10	992	0.99	0	0.01	0.00	0.00	0.00
<i>Qforecast 7 days</i>	0	2	9	993	0.99	0	0.01	0.00	0.00	0.00
<i>Qforecast 8 days</i>	0	2	12	990	0.99	0	0.01	0.00	0.00	0.00
<i>Qforecast 9 days</i>	0	2	11	991	0.99	0	0.01	0.00	0.00	0.00
<i>Qforecast 10 days</i>	0	2	13	989	0.99	0	0.01	0.00	0.00	0.00

In general, for event type 2 the number of events (hits+misses) are small, 6 and 2 for the high water level threshold and flood level threshold respectively. The amount of hits of event type 2 of the simulated discharges and forecasted discharges is very low; 3 hits out of 88 events. Due to the high correct rejections of both thresholds, the accuracy *A* is high ($A \geq 0.98$), the false-alarm rates are low ($F \leq 0.01$) and the miss rates are low ($F' \leq 0.01$). Due to the rarity of the occurrence of events and the

even rarer occurrence of a hit, table 4.12 and 4.13. The contingency table gives the clearest insight in the performance of *Qsim* and the *Qforecasts* of event type 2. The analyses by the rates, ratio are of less importance since they are biased by the small amount of events.

Despite the fact that the performance of the forecast presented by the objective function NS_H , see table 4.9, is very promising, they are barely able to forecast the beginning of a flood. An explanation for this could be that the objective function used in the calibration procedure was not sufficient enough for the goal of the evaluation of the model performance. Calibrating with a combined objective function with the hit rate and false-alarm rate embedded should perhaps lead to better results in forecasting the start of a flood.

5 Conclusions and recommendations

The conclusions of the study are the answers to the research questions stated in section 1.3. In section 5.1 the conclusions of the research are summed up. After that, in section 5.2, some recommendations for further research are listed.

5.1 Conclusions

The objective of this study is *to set up and evaluate the hydrological HBV-model to simulate discharges and forecast floods of the Mamoré River at the city of Trinidad*. This is to be able to warn the people in the area of Trinidad when the Mamoré River water level will reach alarming levels, so people can evacuate and take action to limit the flood damage.

This research contains three research questions in order to reach the research objective. The first question forms the foundation in order to answer the second research question and the second research question itself forms the foundation in order to answer the third research question.

The first research question is:

1. *What is the best HBV configuration for the Mamoré River basin given the available data?*

A data analysis has been executed to select the meteorological stations which are used in the research to determine the input data and to determine the sub basins with corresponding discharge stations. This data analysis showed that the Mamoré basin for this study can be divided best into two sub basins: sub basin Grande with outflow at discharge station Abapo and sub basin Mamoré with outflow at discharge station Camiaco. Grande is the upstream basin with its outflow into the downstream basin Mamoré.

The areal mean precipitation is determined with Thiessen polygons. Four approaches to deal with the elevation differences between the measuring stations and the areal mean elevation are considered (Appendix B) and the approach with no correction factor for elevation turned out to be the most suitable for this study.

The discharge of upstream sub basin Grande goes through sub basin Mamoré to become the combined outflow of the total basin at Camiaco. The lag time of the discharge of Grande through Mamoré is determined by a correlation study and resulted in a lag time of 17 days.

Inundation maps of recent floods show that inundations occur within the sub basin Mamoré around the tributary Grande. This is confirmed by the fact that the peak discharges of sub basin Grande exceed the peak discharges of the outflow of the total basin at Camiaco. Therefore, a reservoir has been added in the HBV model in sub basin Mamoré, to deal with the floods within the sub basin Mamoré due to the contribution of the discharge from sub basin Grande. Further it the outflow of the reservoir can be described by the same non-linear equation as for the fast runoff component of the HBV-model.

Research question 2 stated:

2. *How well does the HBV-model perform with the available data for the Mamoré River basin in simulating discharges?*

For sub basin Grande the model parameters FC , $BETA$, $ALFA$ and $PERC$ were found to be the most sensitive to the objective function and thus are varied in the final calibration step in order to obtain the optimum parameter set. The Y value of the optimum parameter set after the first calibration step was 0.31 and the Y value of the optimum parameter set after the final calibration step was 0.39. This improvement of the Y value after the final calibration step shows that the parameter values have been improved.

For sub basin Mamoré the model parameters $BETA$, LP , $ALFA$, k_F and k_S were found to be the most sensitive to the objective function and thus are varied in the final calibration step in order to obtain the optimum parameter set. The NS_H value of the optimum parameter set after the first calibration step was 0.69 and the NS_H value of the optimum parameter set after the final calibration step was 0.72. Also this improvement of the objective function after the final calibration step shows that the parameter values have been improved.

The shapes of the scatter plots of parameter $BETA$, $PERC$ and $ALFA$ of sub basin Grande and parameter k_S , k_F and $ALFA$ of sub basin Mamoré give confidence that their values of the optimum values are actually the global optimum values.

In the validation procedure, sub basin Grande performs even better, in terms of its objective function, for the validation period compared to the calibration period: 0.54 vs 0.39. Sub basin Mamoré performs for the validation period worse than for the calibration period. In terms of their objective function values: 0.51 vs 0.72.

The third and final research question is:

3. *How well does the HBV model perform in forecasting floods of the Mamoré River?*

The forecasted discharges of 1 to 10 days ahead performed quite well considering the objective function. The NS_H values of the forecasts lie between 0.99 for one day ahead and 0.69 for 10 days ahead. These performances are an improvement compared to the simulated discharge, which had a NS_H value of 0.51. The overall accuracy of the HBV model in forecasting discharges, using perfect forecasts, is high and the forecasts up to 10 days ahead are more accurate than the simulated discharges.

The accuracies A of the forecasts up to 10 days ahead ($A \geq 0.94$) are at least higher than the accuracies of the simulated discharges in forecasting event type 1 '*the exceedance of a discharge threshold at time step t'* ' for the high water level and the flood level threshold. Accuracy A has a value between 0 and 1, with 1 as optimum value, thus the performance of the forecasts in terms of accuracy are considered as good for the event type 1.

The skill of the model in forecasting high water and flood levels up to 10 days ahead in terms of False-alarm rates F is better than the skill of the model in simulating high water and flood levels. Partly due to the high number of correct rejections the false-alarm rates F , which have a value between 0 and 1, of the forecasts are ≤ 0.02 . The skill of the model in forecasting high water and flood levels up to 10 days ahead in terms of hit rate H are decreasing as the forecasting days ahead are increasing. Nevertheless, hit rates H of the high water level of the forecasts up to 7 days ahead are higher than the hit rate of the simulated discharges and the hit rates H of the flood level of the

forecasts up to 3 days ahead are higher than the hit rate of the simulated discharges. At least the forecasts up to 3 days ahead perform well in terms of skill for the event type 1 for both thresholds.

The reliability of the forecasts up to 10 days ahead for event type 1 in terms of the probability of a correct warning H' is high ($H' \geq 0.92$) for the high water and flood level threshold. The reliabilities of simulated discharges are 0.76 and 0.79 for the high water level and the flood level respectively. These values are much higher than the base rates, which has a value of 0.31 and 0.19 for the high water level and the flood level respectively. The reliability of the forecasts up to 10 days ahead for event type 1 in terms of probability of an incorrect non-warning (miss rate F'), decreases sharply as the forecasting days ahead are increasing for the high water and flood level thresholds. This is not directly visible in the miss rate F' , because the number of correct rejections is high.

When looking at the contingency table of event type 2 '*the exceedance of a discharge threshold at time step t, with the condition that at time step t-1 this threshold was not exceeded*', the performance of the forecasts is very poor for the high water and flood level thresholds. In other words, event type 2 is the start of a high water or flood period. In the validation period, 6 high water periods and 2 flood periods occurred. Out of all the 80 events (2 events for flood threshold plus 6 events for high water threshold times 10 forecasts) the model was able to forecast 2 events and missed 78 events. Due to the small number of event (and thus the small number of hits and misses) and the large number of correct rejections the evaluation in terms of accuracy, skill and reliability is not meaningful.

In conclusion, the overall accuracy of the forecasts increase as the prediction days decrease and is higher than accuracy of the simulated discharges. The accuracy A , skills F and H and reliabilities F' and H' of the forecasts up to 3 days ahead of event type 1 are higher than the simulated discharges for both the high water and flood level. However, as a decision maker, you are also interested in ability of a model to forecast the start of a high water or flood level threshold exceedance, event type 2. This to give a high water or flood warning to the people in the area, so they are able to evacuate and limit the flood damage. Unfortunately, the model is barely able to forecast and simulate events of type 2 for both high water and flood level thresholds.

5.2 Recommendations

There are several recommendations for further research which are derived from the discussion and the conclusions of this research:

First of all the meteorological input data of the HBV model in this study have been determined using measuring stations in the basin area and Thiessen polygons. The measuring stations are unevenly distributed over the area and given that the area is spatially variable in terms of annual mean temperature, annual mean precipitation, elevation and climate classification to Köppen-Geiger, the method used in this study to determine areal mean precipitation and potential evapotranspiration has large uncertainties. Further research should be aimed at increasing the quality of the meteorological input data. For example, remote sensing could be applied to increase the quality of the model input.

The number of sub basins of this study is small compared to other HBV studies with similar total basin size. Therefore, in combination with the spatially variability of the basin, more discharge

measuring stations should be set up in the study area at strategic locations in the study area to be able to simulate and forecast the discharges at Camiaco.

To cope with the fact that the peak discharges of sub basin Grande exceeds the peak discharges of the outflow of the total basin, some assumptions are made. The assumption is made that inundations take place inside sub basin Mamoré and therefore, a reservoir has been added to the HBV model. Some assumptions are made concerning the discharge threshold above which the inflow of the reservoir is generated and assumptions are made concerning the outflow of the reservoir. Further research should be aimed on finding out what actual happens in the area and how this could be modelled.

The aim of this research was to forecast floods of the Mamoré River. The results presented in section 4.5.2., showed that the model used and the methodology followed was barely able to forecast floods. The objective function of the calibration of the downstream basin was the Nash-Sutcliffe coefficient for high flows NS_{H_t} with the objective of *'a good agreement of the peak flows with respect to timing, rate and volume'*. This study showed that this objective function for this study area was not adequate to forecast beginning of high water and floods. Further research should be aimed at calibrating with another objective function which is aimed at beginning of high water and floods, like skill measure hit rate H .

This study showed that the travel time of the discharge of sub basin Grande through sub basin Mamoré is quite long, compared to the forecast time ahead. In order to better forecast discharges at Camiaco, the basin should be decreased in size and more discharge measuring stations at strategically locations should be set up, to be able to use the observed inflows into the adjusted basin. This approach can be seen as a combination of a neural network model and the HBV model.

References

- Abebe, N. A., Ogden, F. L., Pradhan, N. R., 2010. Sensitivity and uncertainty analysis of the conceptual HBV rainfall–runoff model: Implications for parameter estimation. *Journal of Hydrology* 389, 301-310
- Akhtar, M., Ahmad, N., and Booij, M. J., 2009. Use of regional climate model simulations as input for hydrological models for the Hindukush-Karakorum- Himalaya region." *Hydrology and Earth System Sciences*, 13, 1075
- Bartholmes, J.C., Thielen, J., Ramos, M.H., and Gentilini, S., 2009. The European flood alert system EFAS – Part 2: Statistical skill assessment of probabilistic and deterministic operational forecasts. *Hydrol. Earth Syst. Sci.*, 13, 141–153
- Beven, K. and Freer, J., 2001. Equifinality, data assimilation, and uncertainty estimation in mechanistic modelling of complex environmental systems using the GLUE methodology. *Journal of Hydrology* 249.
- Booij, M.J., 2002. Appropriate modelling of climate change impacts on river flooding. Ph.D. thesis, University of Twente, Enschede.
- Booij, M.J., 2005. Impact of climate change on river flooding assessed with different spatial model resolutions, *J.Hydr.*, 303(1-4), 176-198
- Booij, M.J. and Krol, M.S., 2010. Balance between calibration objectives in a conceptual hydrological model. *Hydrological Sciences Journal*, 55, 1017.
- Brutsaert, W., 1982. *Evaporation Into the Atmosphere: Theory, History, and Applications*, 299, Kluwer Acad., Norwell, Mass., ISBN: 978-90-481-8365-4.
- Centro de Investigaciones Fitosociológicas. Bolivia-Trinidad" (in Spanish). Retrieved December 24, 2012. <http://pendientedemigracion.ucm.es/info/cif/station/bo-trini.htm>
- Cloke, H., Pappenberger, F., 2008. Evaluating forecasts of extreme events for hydrological applications: an approach for screening unfamiliar performance measures. *Meteorological Applications* 15 (1), 181.
- Cloke, H.L., Pappenberger, F., 2009. Ensemble flood forecasting: A review. *Journal of Hydrology* 375, 613-626
- Deckers, D.L.E.H., 2006. Predicting discharge at ungauged basins, parameter estimation through the method of regionalization, Universiteit Twente, Enschede, The Netherlands.
- Deltares, 2012. Early warning systeem voor Bolivia. 29 November, 2012. Visited on 29-10-2013 <http://www.deltares.nl/nl/actueel/nieuwsbericht/item/14865/early-warning-systeem-voor-bolivia>
- Demirel, C.M., Booij, M.J., Hoekstra, A.Y., 2013. Effect of different uncertainty sources on the skill of 10 day ensemble low flow forecasts for two hydrological models. *Water resources research* 49, 4035-4053

- De Roo, A., et al., 2003. Development of a European flood forecasting system. *International Journal of River Basin Management* 1, 49-59
- Fundel, F., Zapp, M., 2011. Hydrological ensemble forecasting in meso-scale basins: Sensitivity to initial conditions and value of reforests. *Water Resources* 47, W09520
- Grant, W., 2007. Crisis talks over Bolivian floods. *BBC News*. Visited on 9 October, 2013 <http://news.bbc.co.uk/2/hi/americas/6384267.stm>
- Gurtz, J., Baltensweiler, A., Lang, H., 1999. Spatially distributed hydrotope-based modeling of evapotranspiration and runoff in mountainous basins. *Hydrological Processes* 13, 2751-2768
- Jensen, M.E., Burman, R.D., Allen, R.G., 1990. Evapotranspiration and irrigation water requirements, *ASCE Manuals and Reports on Engineering Practice No. 70*, ASCE, Stockholm, Sweden
- Kang, E., Cheng, G., Lan, Y., Jin, H., 1999. A model for simulating the response of runoff from the mountainous watersheds of inland river basins in the arid area of northwest China to climatic changes. *Science in China Series D: Earth Sciences* 42, 52-63
- Knoben, W.J.M., 2013. Estimation of non-stationary hydrological model parameters for the Polish Welna catchment. MSc. Thesis, University of Twente, Enschede.
- Lidén, R., Harlin, J., 2000. Analysis of conceptual rainfall-runoff modeling performance in different climates. *Journal of Hydrology* 238, 231-247
- Lindström, G., Johansson, B., Persson, M., Gardelin, M., Bergström, S., 1997. Development and test of the distributed HBV-96 hydrological model. *Journal of Hydrology* 201, 272-288
- Madsen, H., 2000. Automatic calibration of a conceptual rainfall-runoff model using multiple objectives. *Journal of Hydrology* 235.
- Madsen, H., Wilson, G., Ammentorp, H.C., 2002. Comparison of different automated strategies for calibration of rainfall-runoff models, *Journal of Hydrology* 261, 48-59
- Martina, M.L.V., Todini, E., and Libralon, A., 2006. A Bayesian decision approach to rainfall thresholds based flood warning. *Hydrol. Earth Syst. Sci.*, 10, 413-426
- Mason, I. B., 1982: A model for the assessment of weather forecasts. *Aust. Meteor. Mag.*, 30, 291-303
- Ministerio de Desarrollo Rural Agropecuario y Medio Ambiente, Viceministerio de Tierras, Instituto Nacional de Reforma Agraria, 2007. Proyecto; Espaciograma de zonas afectadas por las inundaciones en los departamentos (Beni, Santa Cruz y Cochabamba). La Paz, March 2007.
- Molinari, D., Menomi, S., Ballio, F., 2013. *Flood Early Warning Systems – Knowledge and tools for their critical assessment*. WITPRESS Southampton, Boston. ISBN: 978-1-84564-688-2
- Moore, R. J., Bell, V. A., Jones, D. A., 2005. Forecasting for flood warning. *Comptes Rendus Geoscience* 337

- Murphy, A.H., 1993. What Is a Good Forecast? An Essay on the Nature of Goodness in Weather Forecasting. *Wea. Forecasting*, 8, 281-293
- Nash, J.E., and J.V. Sutcliffe. 1970. River flow forecasting through conceptual models part I — A discussion of principles. *Journal of Hydrology* 10.
- Oudin, L., Hervieu, F., Michel, C., Perrin, C., Andreassian, V., Anctil, F., Loumagne, C., 2005. Which potential evapotranspiration input for a lumped rainfall-runoff model? Part 2-Towards a simple and efficient potential evapotranspiration model for rainfall-runoff modeling. *Journal of Hydrology* 303, 290-306
- Patrick, S., 2002. The future of flood forecasting. *Bulletin of the American Meteorological Society*, p. 183
- Peel, M.C., Finlayson, B.L., McMahon, T.A., 2007. Updated world map of the Köppen-Geiger climate classification. *Hydrology & Earth System Sciences Discussions*. Vol. 4.
- Penman, H.L., 1948. Natural evaporation from open water, bare soil and grass. *Proceedings, Royal Society of London* 193: 120–145.
- Penning-Rowsell, E., Tunstall, S., Tapsell, S., Parker, D., 2000. The benefits of flood warnings: real but elusive, and politically significant. *Journal of the Chartered Institution of Water and Environmental Management* 14, 7-14
- Perrin, C., Michel, C., Andréassian, V., 2001. Does a large number of parameters enhance model performance? Comparative assessment of common basin model structures on 429 basins. *Journal of Hydrology* 242
- Rodal, H.E.R., 2008. *Hidrologia y Dinámica Fuvial de la Cuenca del Rio Mamoré. Evento Extraordinario Inundación 2008. Planteamientos de Solución*. ISBN: 978-99954-731-1-2
- Roulin, E., Vannitsem, S., 2005. Skill of medium-range hydrological ensemble prediction. *Journal of Hydrometeorol*, 6, 729-744
- Roulin, E., 2007. Skill and relative economic value of medium-range hydrologic ensemble predictions. *Hydrology Earth Systems Science*, 11, 725-737
- Schellekens, J., 2013. *Wflow Documentation Release 0.91*. Open Streams, August 28, 2013
- Seibert, J., 1999. Regionalisation of parameters for a conceptual rainfall-runoff model. *Agricultural and Forest Meteorology*, 279-293
- Seibert, J., 2005. *HBV light version 2 User's Manual*. Stockholm University, Department of Physical Geography and Quaternary Geology
- Silberstein, R.P. and Vertessy, R.A., 1999. Topog_Scenario: A tool for exploring hydrologic possibilities. *Second Inter-Regional Conference on Environment-Water* 99
- Singh, V.P., 2005. *Computer Models of Watershed Hydrology*. Water Resource Publications, Baton Rouge, U.S.A., ISBN 0-918334-91-8

- Shrestha, D.L., Kayastha, N. and Solomatine, D.P., 2009. A novel approach to parameter uncertainty analysis of hydrological models using neural networks. *Hydrol. Earth Syst. Sci.* 13, 1235-1248.
- Shuttleworth, W.J., 1993. Evaporation. Chapter 4. In *Handbook of Hydrology*, Maidment DR. McGraw-Hill: New York, USA.
- Stephenson, D. B.: Use of the “odds ratio” for diagnosing forecast skill, *Weather and Forecasting*, 15, 221–232, 2000.
- Thorntwaite CW. 1948. An approach toward a rational classification of climate. *Geographical Review* 38: 55–94.
- Tillaart, van den S.P.M., 2010. Influence of uncertainties in discharge determination on the parameter estimation and performance of a HBV model in Meuse sub basins. MSc. Thesis, University of Twente, Enschede.
- Uhlenbrook, S., Seibert, J., Leibundgut, C. and Rodhe, A., 1999. Prediction uncertainty of conceptual rainfall-runoff models caused by problems in identifying model parameters and structure. *Hydrological Sciences Journal*, 44:5, 779-797
- UNISDR: The United Nations Office for Disaster Risk Reduction, 2007. <http://www.unisdr.org/we/inform/terminology> visited on 9-3-2015
- Velázquez, J.A., Anctil, F., and Perrin, C., 2010. Performance and reliability of multimodel hydrological ensemble simulations based on seventeen lumped models and a thousand basin *Hydrol. Earth Syst. Sci.*, 14 (11), 2303-2317
- Viviroli, D., Zappa, M., Gurtz, J., Weingartner, R., 2009. An introduction to the hydrological modelling system PREVAH and its pre- and post-processing-tools. *Environmental Modelling & Software* 24, 1209-1222
- Werner, M., 2005. FEWS NL Version 1.0 - Report Q3933, Delft Hydraulics, Delft
- Wöling, Th., Lennartz, F., and Zappa, M., 2006. Technical Note: Updating procedure for flood forecasting with conceptual HBV-type models. *Hydrol. Earth Syst. Sci.* 10, 783-788
- Xu, C.-Y., Singh, V. P., 2001. Evaluation and generalization of temperature-based methods for calculating evaporation. *Hydrological Processes*. 15.

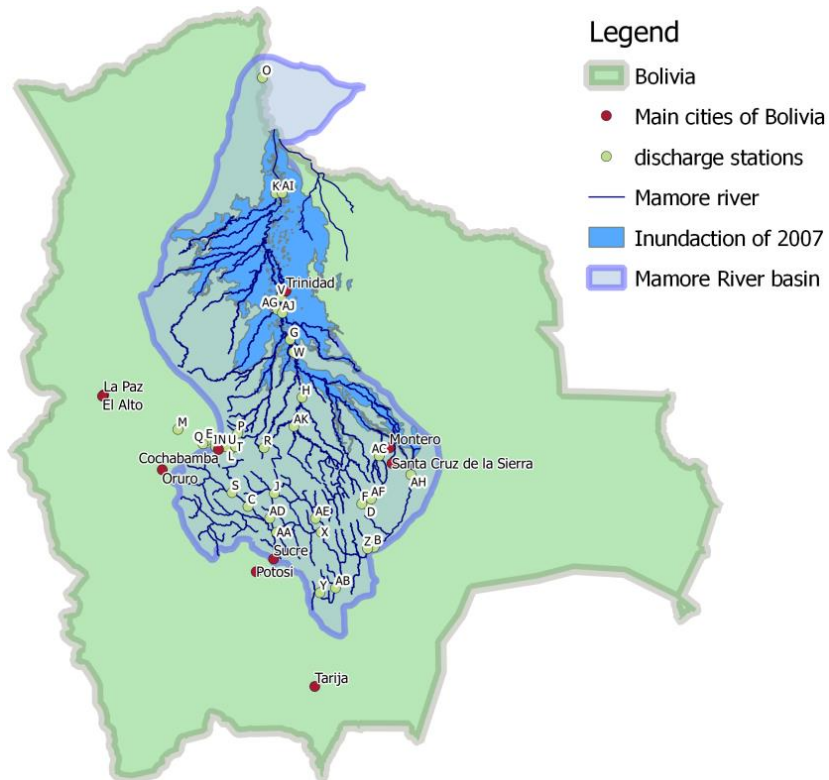


Figure A.1: Map of the Mamoré River basin, the Mamoré River, the inundated area of the 2007 floods and the locations of the discharge stations and main cities of Bolivia [QGIS data provided by Centro Agua Bolivia].

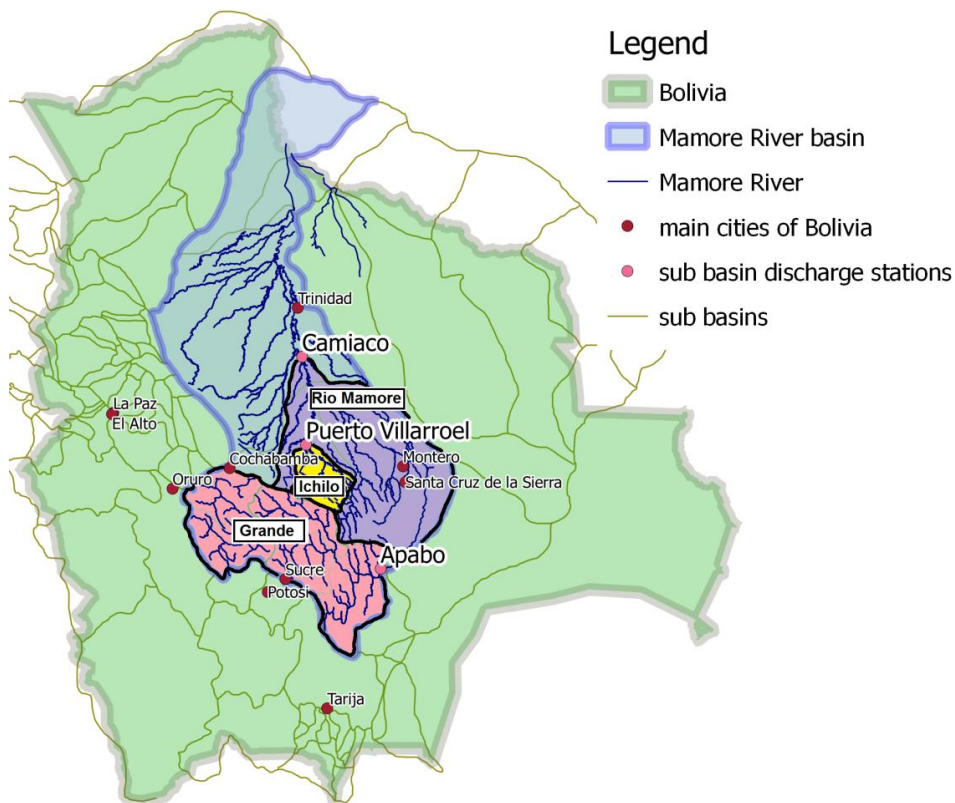


Figure A.2: Map of Bolivia with the Mamoré River basin, Mamoré River, sub basins and their discharge stations and main cities of Bolivia. The pink area is the sub basin Grande with discharge station Apabo, the yellow area is sub basin Ichilo with discharge station Puerto Villarroel and the purple area is sub basin Rio Mamore with discharge station Camiaco.

Meteorological stations

The locations meteorological stations which held records of the weather data are presented in figure A.3. It is clear that the stations are not spread evenly over the area of Bolivia and there are large areas without stations and small areas where the stations are grouped together. Further, the data analysis showed that a small amount stations kept records of daily humidity, atmospheric pressure, wind speed and direction. But they all recorded daily precipitation and mean temperature.

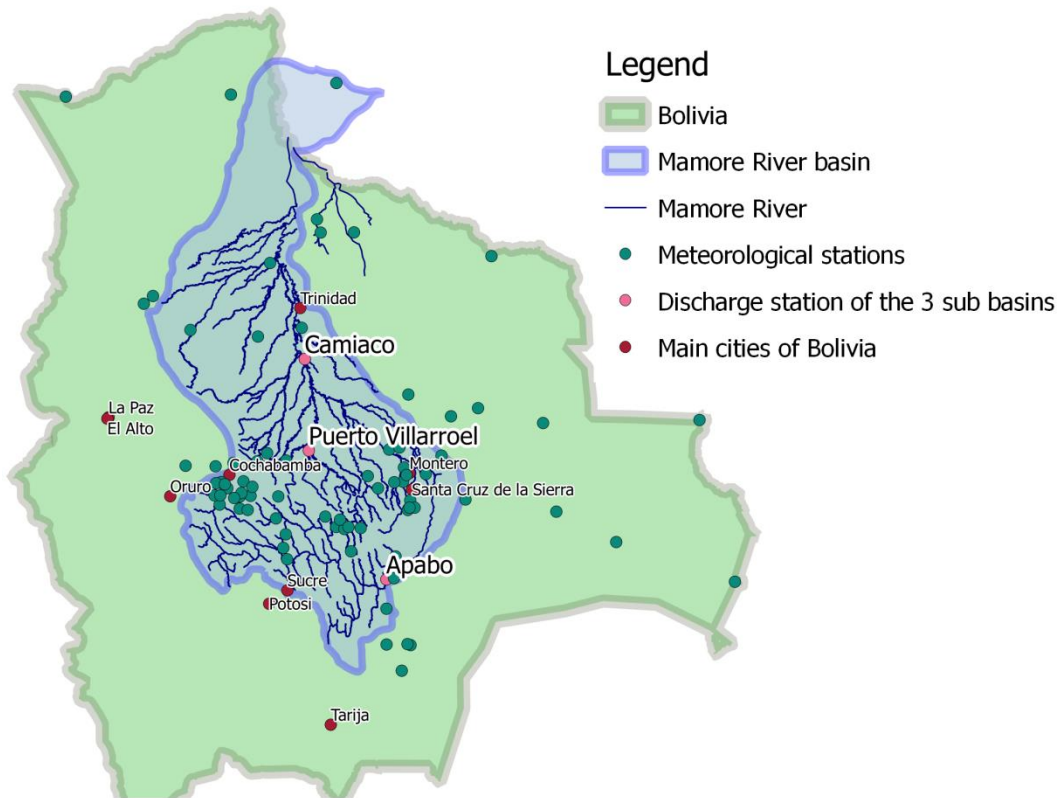


Figure A.3: Map of Mamoré River basin, Mamoré River, the locations of the discharge stations of the three sub basins, the locations of the hydrological stations in Bolivia and the main cities of Bolivia [QGIS data provided by Centro Agua Bolivia].

Appendix B: Areal mean precipitation: 4 different approaches

To generate the areal mean precipitation a couple of different approaches have been executed. All approaches use the Thiessen polygons method as basis. The area of each sub basin is divided into several areas which is represented by a precipitation and temperature measure station. Precipitation varies over the area and will increase with the increase of height. The measure stations are commonly situated a populated area or valley, which leads to a difference between the areal mean elevation and the elevation of the measure station. The areal mean elevation for each Thiessen polygon is determined in QGIS with a Digital Elevation Map (DEM) of the area.

Next, three approaches to coop with the height difference and one approach without any elevation correction for precipitation are presented. To check whether the approach is suitable for each sub basin a volume check is executed in which each sub basin have to meet two boundary conditions:

- the observed discharge q_{obs} [mm] needs to be smaller than the precipitation P [mm] [$q_{obs} < P$].
- the precipitation needs to be smaller than the summation of the potential evapotranspiration et_p [mm] and the observed discharge [$P < et_p + q_{obs}$].

The assumption is made that the determination of the precipitation is the factor with the highest uncertainty compared to the potential evapotranspiration and the observed discharge. The potential evapotranspiration et_p [mm] has been determined following the Thornthwaite method, as described in mm. The data of the observed discharges is given by the Bolivian government and the method which is used to determine the values is unknown. The volume check is measured in mm/y and is executed for five hydrological years, which all start on the 1st of August and end on the 31st of October. The records of the observed discharge q_{obs} are converted from a value in m³/s to mm/y. This to adequately perform a volume check and the daily precipitation and et_p are summed for each hydrological year. The observed discharge of the Mamore sub basin is calculated by subtracting the q_{obs} [mm/y] of the two upper sub basins Grande and Ichilo from the total q_{obs} [mm/y] of the whole basin.

1. +10%/ 100m - approach

The first approach assumes that the precipitation increases with 10% for every 100 meter increase in elevation. This is a common rule with is used more often in other research studies. The results for each sub basin of this approach are shown in the table below. If the approach does not meet the condition, the value is shown in red.

Grande [+10 % P / +100 m]					
meteorological year	et_p [mm/y]	q_{obs} [mm/y]	P [mm/y]	$q_{obs} < P$	$P < et_p + q_{obs}$
aug 2002 - jul 2003	793	123	984	861	-68
aug 2003 - jul 2004	776	115	905	790	-14
aug 2004 - jul 2005	727	98	862	764	-37
aug 2005 - jul 2006	672	155	1081	926	-254
aug 2006 - jul 2007	714	166	982	816	-102
Ichilo [+10 % P / +100 m]					
meteorological year	et_p [mm/y]	q_{obs} [mm/y]	P [mm/y]	$q_{obs} < P$	$P < et_p + q_{obs}$
aug 2001 - jul 2002	1121	2397	2356	-41	1162
aug 2002 - jul 2003	112	2624	2097	-527	639
aug 2003 - jul 2004	1127	2023	2059	36	1091
aug 2004 - jul 2005	1222	1762	1955	193	1029
aug 2005 - jul 2006	1181	2135	2001	-134	1315

Mamore [+10 % P / +100 m]					
<i>meteorological year</i>	et_p [mm/y]	q_{obs} [mm/y]	P [mm/y]	$q_{obs} < P$	$P < et_p + q_{obs}$
aug 2002 - jul 2003	1432	719	1790	1071	361
aug 2003 - jul 2004	1393	601	1697	1096	297
aug 2004 - jul 2005	1436	468	1636	1168	268
aug 2005 - jul 2006	1369	757	1906	1149	220
aug 2006 - jul 2007	1271	698	2069	1371	-100

As shown in the table, in particular the sub basins Grande and Ichilo do not meet the conditions. For sub basin Grande the precipitation is overestimated with this approach, because the summation of the et_p and discharge are smaller than the P for each hydrological year. With this approach the precipitation for the Ichilo basin is underestimated, because for 60% of the hydrological years the observed discharge exceeds the precipitation.

2. Correction factor per sub basin - approach

For the second approach first a correlation between height and precipitation is made for each sub basin. With a more annually mean isohyets map and a DEM in QGIS, a couple of points for each sub basin are examined. With these points the trend line is obtained and a correction factor for each sub basin is made. This correction factor is used for all of the Thiessen polygons of that specific sub basin to calculate the areal mean precipitation. The results are shown in the table below.

Grande [P correction factor obtained per sub basin]					
<i>meteorological year</i>	et_p [mm/y]	q_{obs} [mm/y]	P [mm/y]	$q_{obs} < P$	$P < et_p + q_{obs}$
aug 2002 - jul 2003	793	123	1630	1507	-714
aug 2003 - jul 2004	776	115	1444	1329	-553
aug 2004 - jul 2005	727	98	1475	1377	-650
aug 2005 - jul 2006	672	155	1779	1624	-952
aug 2006 - jul 2007	714	166	1541	1375	-661
Ichilo [P correction factor obtained per sub basin]					
<i>meteorological year</i>	et_p [mm/y]	q_{obs} [mm/y]	P [mm/y]	$Q_{obs} < P$	$P < et_p + q_{obs}$
aug 2001 - jul 2002	1121	2397	1927	-470	1591
aug 2002 - jul 2003	112	2624	1742	-882	994
aug 2003 - jul 2004	1127	2023	1722	-301	1428
aug 2004 - jul 2005	1222	1762	1544	-218	1440
aug 2005 - jul 2006	1181	2135	1686	-449	1630
Mamore [P correction factor obtained per sub basin]					
<i>meteorological year</i>	et_p [mm/y]	q_{obs} [mm/y]	P [mm/y]	$q_{obs} < P$	$P < et_p + q_{obs}$
aug 2002 - jul 2003	1432	719	1756	1037	395
aug 2003 - jul 2004	1393	601	1707	1106	287
aug 2004 - jul 2005	1436	468	1621	1153	283
aug 2005 - jul 2006	1369	757	1931	1174	195
aug 2006 - jul 2007	1271	698	2009	1311	-40

Similar to the +10% correction factor approach, the sub basins Grande and Ichilo do not meet the boundary conditions. The areal mean precipitation is overestimated for sub basin Grande and underestimated for sub basin Ichilo. The results of the volume check of sub basin Grande and Ichilo with this approach are even worst compared to the +10% correction factor approach.

3. Correction factor per Thiessen polygon - approach

This approach is similar to the 'correction factor per sub basin approach', but instead of a height correction factor for each sub basin, a height correction is made for each Thiessen polygon in the three sub basins. The results are shown in the table below.

Grande [P correction factor obtained per Thiessen polygon]					
<i>meteorological year</i>	et_p [mm/y]	q_{obs} [mm/y]	P [mm/y]	$q_{obs} < P$	$P < et_p + q_{obs}$
aug 2002 - jul 2003	793	123	568	445	348
aug 2003 - jul 2004	776	115	511	396	380
aug 2004 - jul 2005	727	98	495	397	330
aug 2005 - jul 2006	672	155	617	462	210
aug 2006 - jul 2007	714	166	564	398	316
Ichilo [P correction factor obtained per Thiessen polygon]					
<i>meteorological year</i>	et_p [mm/y]	q_{obs} [mm/y]	P [mm/y]	$q_{obs} < P$	$P < et_p + q_{obs}$
aug 2001 - jul 2002	1121	2397	1778	-619	1740
aug 2002 - jul 2003	112	2624	1614	-1010	1122
aug 2003 - jul 2004	1127	2023	1599	-424	1551
aug 2004 - jul 2005	1222	1762	1428	-334	1556
aug 2005 - jul 2006	1181	2135	1567	-568	1749
Mamore [P correction factor obtained per Thiessen polygon]					
<i>meteorological year</i>	et_p [mm/y]	q_{obs} [mm/y]	P [mm/y]	$q_{obs} < P$	$P < et_p + q_{obs}$
aug 2002 - jul 2003	1432	719	3046	2327	-895
aug 2003 - jul 2004	1393	601	2951	2350	-957
aug 2004 - jul 2005	1436	468	2756	2288	-852
aug 2005 - jul 2006	1369	757	3322	2565	-1196
aug 2006 - jul 2007	1271	698	3378	2680	-1409

The results show an underestimation of the yearly areal mean precipitation for the sub basin Ichilo. This underestimation is even larger than the results of the two previous approaches shown above. The results of sub basin Grande shows values within both boundary conditions. Sub basin Mamore shows results with an overestimation of the yearly areal mean precipitation.

4. No correction factor - approach

This approach does not use a correction factor for height for the areal mean precipitation. This means the area of each Thiessen polygon will just be represented by its measure station. The results of this approach are shown in the table below.

Grande [P no correction]					
<i>meteorological year</i>	et_p [mm/y]	q_{obs} [mm/y]	P [mm/y]	$q_{obs} < P$	$P < et_p + q_{obs}$
aug 2002 - jul 2003	793	123	546	423	370
aug 2003 - jul 2004	776	115	497	382	394
aug 2004 - jul 2005	727	98	485	387	340
aug 2005 - jul 2006	672	155	605	450	222
aug 2006 - jul 2007	714	166	549	383	331
Ichilo [P no correction]					
<i>meteorological year</i>	et_p [mm/y]	q_{obs} [mm/y]	P [mm/y]	$q_{obs} < P$	$P < et_p + q_{obs}$
aug 2001 - jul 2002	1121	2397	1968	-429	1550
aug 2002 - jul 2003	112	2624	1778	-846	958
aug 2003 - jul 2004	1127	2023	1754	-269	1396
aug 2004 - jul 2005	1222	1762	1572	-190	1412
aug 2005 - jul 2006	1181	2135	1716	-419	1600
Mamore [P no correction]					
<i>meteorological year</i>	et_p [mm/y]	q_{obs} [mm/y]	P [mm/y]	$q_{obs} < P$	$P < et_p + q_{obs}$
aug 2002 - jul 2003	1432	719	1784	1065	367
aug 2003 - jul 2004	1393	601	1699	1098	295
aug 2004 - jul 2005	1436	468	1636	1168	268
aug 2005 - jul 2006	1369	757	1920	1163	206
aug 2006 - jul 2007	1271	698	2054	1356	-85

The results show once again an underestimation of the areal mean precipitation for sub basin Ichilo. An explanation for these underestimations could be that the calculations of the observed discharge for this sub basin is systematically done wrong. Another aspect which could have led to the failure of meeting the boundary conditions is the fact that none of the meteorological measure stations are location within the borders of sub basin Ichilo. Data of measure stations outside sub basin Ichilo needs to be extrapolated to calculate the areal mean precipitation, which means that the sources are less related to the area they represent.

From 3 to 2 sub basins

Because sub basin Ichilo failed to meet the boundary conditions for all four approaches, the decision is merge sub basin Ichilo and sub basin Mamore, which off course leads to one sub basin less.

A volume check is executed for this new sub basin following the two areal mean precipitation approaches for with sub basin Grande met the boundary conditions: ‘no correction factor’-approach and ‘correction factor per Thiessen polygon’ approach. The results of these volume checks are shown in the table below.

Mamore			P no correction			P corre. per polygon		
<i>meteorological year</i>	et_p [mm/y]	q_{obs} [mm/y]	P [mm/y]	$q_{obs} < P$	$P < et_p + q_{obs}$	P [mm/y]	$q_{obs} < P$	$P < et_p + q_{obs}$
aug 2002 - jul 2003	1267	1071	1783	712	555	3146	2075	-808
aug 2003 - jul 2004	1233	872	1706	834	399	3064	2192	-959
aug 2004 - jul 2005	1268	704	1629	925	343	2819	2115	-847
aug 2005 - jul 2006	1214	1043	1896	853	361	3400	2357	-1143
aug 2006 - jul 2007	1120	1132	2057	925	195	3478	2346	-1226

The results of new, larger, sub basin Mamore shows a failure of meeting the boundary conditions with ‘correction factor per Thiessen polygon’-approach. The areal mean precipitation is overestimated with this approach.

In conclusion, to meet the boundary conditions in the volume checks the sub basins Ichilo and Mamore need to merge. Further, out of the four approaches described, ‘no correction factor’-approach seems to be the best approach to determine the areal mean precipitation for this basin.

Appendix C

Tables copied from Rodal (2008) showing characteristics of the sections of river Mamoré and its tributaries.

CANAL TRAPEZOIDAL (RIOS COMPONENTES DE LA CUENCA DEL MAMORÉ)													
Nº	RÍO	Qmax-normal (m3/s)	Pend (%)	coef rugos. (-)	Base-inf Canal (m)	Base-sup Canal (m)	Acc (m2)	Pm (m)	m (-)	Y (m)	Rmax (m)	Vmax (m/s)	Qcap-max (m3/s)
1	Ichilo-01	404.4	1.0482	0.025	50.00	56.00	79.50	54.24	1.00	3.00	1.47	5.28	420.1
2	Chimore-01	177.9	2.4875	0.04	50.00	54.00	52.00	52.83	1.00	2.00	0.98	3.90	202.9
3	Choré-01	137.2	1.0503	0.04	50.00	54.40	57.42	53.11	1.00	2.20	1.08	2.70	155.0
4	Ichilo-02	748.9	0.0143	0.02	168.00	181.60	594.32	177.62	1.00	6.80	3.35	1.34	794.6
5	Mamorecillo-01	811.9	0.0290	0.02	145.00	158.00	492.38	154.19	1.00	6.50	3.19	1.85	909.3
6	Chapare-01	351.4	1.7115	0.04	80.00	85.00	103.13	83.54	1.00	2.50	1.23	3.76	388.1
7	Mamoré-01	1,172.8	0.0238	0.02	160.00	176.00	672.00	171.31	1.00	8.00	3.92	1.92	1,289.5
8	Piray-01	59.7	0.5851	0.025	80.00	82.00	40.50	81.41	1.00	1.00	0.50	1.92	77.8
9	Yapacani-01	336.0	0.6435	0.025	80.00	85.00	103.13	83.54	1.00	2.50	1.23	3.69	380.8
10	Yapacani-02	446.6	0.0058	0.02	250.00	261.00	702.63	257.78	1.00	5.50	2.73	0.74	520.1
11	Grande-01	476.6	0.3278	0.02	180.00	184.00	182.00	182.83	1.00	2.00	1.00	2.85	519.5
12	Grande-02	943.1	0.0084	0.02	250.00	265.00	965.63	260.61	1.00	7.50	3.71	1.10	1,058.3
13	Mamoré-02	2,287.7	0.0163	0.02	310.00	328.00	1,435.50	322.73	1.00	9.00	4.45	1.73	2,480.8
14	Ichoa-01	281.5	0.2559	0.025	100.00	105.00	128.13	103.54	1.00	2.50	1.24	2.33	298.9
15	Isiboro-01	490.3	0.1185	0.025	180.00	186.00	274.50	184.24	1.00	3.00	1.49	1.80	493.0
16	Isiboro-02	843.6	0.0093	0.02	335.00	346.00	936.38	342.78	1.00	5.50	2.73	0.94	884.5
17	Sécure-01	222.7	0.0689	0.025	150.00	155.00	190.63	153.54	1.00	2.50	1.24	1.21	231.2
18	Sécure-02	1,091.8	0.0169	0.02	282.00	294.00	864.00	290.49	1.00	6.00	2.97	1.34	1,159.9
19	Mamoré-03	3,463.6	0.0081	0.02	585.00	605.00	2,975.00	599.14	1.00	10.00	4.97	1.31	3,897.4
20	Ibare-01	323.6	0.0126	0.02	95.00	107.00	303.00	103.49	1.00	6.00	2.93	1.15	348.6
21	TRINIDAD	3,463.6	0.0081	0.02	585.00	605.00	2,975.00	599.14	1.00	10.00	4.97	1.31	3,897.4
22	Mamoré-04	3,863.8	0.0067	0.02	730.00	750.00	3,700.00	744.14	1.00	10.00	4.97	1.19	4,400.4
23	Tijamuchi-01	210.2	0.0144	0.02	50.00	64.00	199.50	59.90	1.00	7.00	3.33	1.34	267.4
24	Mamoré-05	4,149.4	0.0050	0.02	965.00	985.00	4,875.00	979.14	1.00	10.00	4.98	1.03	5,031.8
25	Apere-01	594.8	0.0116	0.02	165.00	178.00	557.38	174.19	1.00	6.50	3.20	1.17	652.2
26	Rapulo-01	278.7	0.0727	0.02	50.00	60.00	137.50	57.07	1.00	5.00	2.41	2.42	333.1
27	Yacuma-01	336.8	0.0219	0.02	98.00	108.00	257.50	105.07	1.00	5.00	2.45	1.35	346.7
28	Mamoré-06	5,399.4	0.0049	0.02	1,282.00	1,302.00	6,460.00	1,296.14	1.00	10.00	4.98	1.02	6,593.0
29	SANTA ANA	5,399.4	0.0049	0.02	1,282.00	1,302.00	6,460.00	1,296.14	1.00	10.00	4.98	1.02	6,593.0

CÁLCULO HIDRÁULICO (CUENCA RIO MAMORÉ)											
Nº	RÍO	L-DIS (KM)	FACT-CURVAS	LARGO (KM)	ÁREA (KM2)	ÁREA (KM2) ACUMULADA	PERIMET. (KM)	ANCHO MEDIO (KM)	COTA INI (M)	COTA FIN (M)	PEND-MEDIA (%)
1	Ichilo-01	133.30	1.45	193.29	7,952.00	7,952.00	408.30	59.10	2,220.00	194.00	1.0482
2	Chimore-01	132.10	1.25	165.13	2,275.20	10,227.20	334.70	15.30	3,480.00	194.00	2.4875
3	Choré-01	164.90	1.40	230.86	2,979.00	13,206.20	308.30	26.50	1,924.00	192.00	1.0503
4	Ichilo-02	35.00	1.45	50.75	514.20	13,720.40	109.00	13.80	194.00	189.00	0.0143
5	Mamorecillo-01	58.60	1.50	87.90	1,332.70	15,053.10	232.00	21.50	189.00	172.00	0.0290
6	Chapare-01	235.00	1.50	352.50	4,748.90	19,802.00	497.00	20.10	4,194.00	172.00	1.7115
7	Mamoré-01	16.80	1.20	20.16	254.00	20,056.00	85.60	7.30	172.00	168.00	0.0238
8	Piray-01	374.80	1.05	393.54	6,519.70	26,575.70	672.60	22.80	2,368.00	175.00	0.5851
9	Yapacani-01	367.50	1.05	385.88	12,631.50	39,207.20	653.40	48.50	2,540.00	175.00	0.6435
10	Yapacani-02	69.50	1.00	69.50	1,359.30	40,566.50	189.20	22.50	175.00	171.00	0.0058
11	Grande-01	1,042.00	1.00	1,042.00	72,978.20	113,544.70	2,105.20	99.50	3,587.00	171.00	0.3278
12	Grande-02	35.80	1.00	35.80	1,456.20	115,000.90	244.30	24.60	171.00	168.00	0.0084
13	Mamoré-02	79.60	1.20	95.52	4,428.10	119,429.00	449.20	34.60	168.00	155.00	0.0163
14	Ichoa-01	159.80	1.45	231.71	4,143.10	123,572.10	347.40	31.40	580.00	171.00	0.2559
15	Isiboro-01	172.20	1.40	241.08	6,244.30	129,816.40	516.20	31.50	375.00	171.00	0.1185
16	Isiboro-02	42.80	1.15	49.22	1,628.00	131,444.40	285.40	16.00	171.00	167.00	0.0093
17	Sécure-01	251.20	1.15	288.88	4,770.00	136,214.40	438.40	29.90	340.00	167.00	0.0689
18	Sécure-02	71.20	1.15	81.88	687.70	136,902.10	143.00	13.20	167.00	155.00	0.0169
19	Mamoré-03	123.40	1.00	123.40	2,259.30	139,161.40	328.10	18.70	155.00	145.00	0.0081
20	Ibare-01	261.10	1.15	300.27	9,601.10	148,762.50	488.90	55.00	178.00	145.00	0.0126
21	TRINIDAD										
22	Mamoré-04	60.00	1.00	60.00	2,270.00	151,032.50	232.40	29.80	145.00	141.00	0.0067
23	Tijamuchi-01	235.40	1.25	294.25	5,663.30	156,695.80	419.30	38.00	175.00	141.00	0.0144
24	Mamoré-05	119.70	1.00	119.70	2,285.00	158,980.80	302.60	23.50	141.00	135.00	0.0050
25	Apere-01	378.80	1.25	473.50	16,277.30	175,258.10	639.30	78.70	178.00	134.00	0.0116
26	Rapulo-01	394.20	1.25	492.75	7,719.70	182,977.80	641.90	24.50	420.00	133.50	0.0727
27	Yacuma-01	293.90	1.25	367.38	9,446.30	192,424.10	525.40	34.30	198.00	133.50	0.0219
28	Mamoré-06	61.30	1.00	61.30	1,263.90	193,688.00	202.90	28.50	135.00	132.00	-0.0049
29	SANTA ANA										